Stony Brook University

Provenance and Weathering of Holocene Ganges-Brahmaputra Sediments: Applications of Sr Geochemistry to Late Quaternary Delta Evolution

A Dissertation Presented

by

Penny Marie Paolo

to

The Graduate School

In Partial Fulfillment of the

Requirements

For the Degree of

Doctor of Philosophy

in

Marine and Atmospheric Science

Stony Brook University

December 2010

Stony Brook University

The Graduate School

Penny Marie Paolo

We, the dissertation committee for the above candidate for the Doctor of Philosophy degree, hereby recommend acceptance of this dissertation.

Steven Goodbred, Jr. – Dissertation Advisor
Adjunct Associate Professor, School of Marine and Atmospheric Science
Stony Brook University
Associate Professor, Vanderbilt University

Roger D. Flood – Chairperson of Defense
Professor, School of Marine and Atmospheric Sciences
Stony Brook University

Gilbert N. Hanson
Professor and Distinguished Service Professor, Department of Geosciences
Stony Brook University

Troy Rasbury
Associate Professor, Department of Geosciences
Stony Brook University

Steven A. Kuehl
Professor, Department of Physical Sciences
Virginia Institute of Marine Science

This dissertation is accepted by the Graduate School

Lawrence Martin
Dean of the Graduate School

Abstract of the Dissertation

Provenance and Weathering of Holocene Ganges-Brahmaputra Sediments: Applications of Sr Geochemistry to Late Quaternary Delta Evolution

by

Penny Marie Paolo

Doctor of Philosophy

in

Marine and Atmospheric Science

Stony Brook University

2010

The Ganges and Brahmaputra drainage systems make up one of the largest source-to-sink systems in the world. Together, the rivers carry >1Gt of sediment annually from the Himalayas to the continental margin where approximately two-thirds of this enormous load is presently sequestered to the Ganges-Brahmaputra delta (GBD), with the remaining third deposited on the Bengal Fan via the Swatch of No Ground canyon. There has been extensive work to characterize Himalayan lithologies and the sediments of the Bengal Fan, but surprisingly little focus on the geochemistry of deltaic deposits where the majority of sediments have been deposited in the Holocene. Here we demonstrate the use of geochemical signatures of provenance and weathering in Holocene sediments to understand how internal and external forcing mechanisms such as short-term climate change and river migration and avulsions have contributed to the shaping of the GBD. This study uses $^{87}Sr/^{86}Sr$ and Sr concentrations ([Sr]) of bulk sediments to

track sediment provenance and major elemental and clay assemblages to characterize alteration of sediments due to weathering. We find that unique $^{87}Sr/^{86}Sr$ and [Sr] signatures persist throughout the Holocene and allow for tracing of individual river deposition patterns. Further, the Brahmaputra is responsible for the bulk of sediments preserved on the delta, dominating eastern and central delta deposition and mixing with Ganges sediments only in the western part of the delta. In the modern, the two rivers carry roughly equal sediment loads which raises the question of whether this proportion has remained stable through the Late Quaternary or if there is preferential sequestration of Brahmaputra sediments on the delta, which could affect the erosional signals preserved on the fan. With regard to weathering, deltaic deposits preserve weathering signals embedded in the sediments from processes in the catchment, but undergo very little post-depositional alteration during the Holocene due to rapid burial. There are no trends in weathering or provenance that can be definitively linked to climate change such as variations in summer monsoon intensity, suggesting that these signals are either not preserved in the delta, or are dwarfed by the magnitude of fluvial processes. This study is one step in unraveling the complex history of sedimentation in this large and dynamic system.

Table of Contents

List of Figures

List of Tables

Acknowledgments

It is impossible for me to thank all the people who have supported me in my graduate career, or in my life beforehand that led to this accomplishment, but I'll do my best to acknowledge the few who have had the greatest influence.

I must of course first thank my advisor, Steve Goodbred whose energy, enthusiasm and promise of world-travel drew me back to Stony Brook in the first place. He has been an advisor in every sense of the word, and without his unwavering energy and support (and countless pep talks) I would certainly not have been able to muster my own energy to overcome these last hurdles. His guidance as well as the times he let go of the reins and let me pursue my own avenues of interest have allowed me to build confidence and grow as a scientist in ways I'm not sure would have happened with another advisor.

I also need to thank Troy Rasbury and Gil Hanson at the top of this list, who are committee members, but who have both been like co-advisors. Together they have taught me more science than I can ever really comprehend, instilled a love of mass spectrometry and pushed me to achieve much more than I ever thought I was capable of. They adopted me into the Isotope Lab and gave me a home in the Geology Department. I only hope the rest of my career will do their efforts justice.

Roger Flood was instrumental in ensuring a successful defense and his input into this manuscript has been invaluable. I only wish I had consulted him earlier in my writing process!

Rounding out my committee is Steve ("Papa") Kuehl, who has graciously opened both his home and his lab to me during the course of this research for which I thank him, as well as many great conversations about clays and Bangladesh in general. I've been so happy to have him on my committee, even if only for a short time. I also need to thank Christian France-Lanord for his input and interest in this project over the years. And while not a committee member, I am also indebted to Sidney Hemming for sharing her vast knowledge of mass spectrometry and cation exchange chromatography, and inspiring me along with Gil and Troy.

So many fellow students and colleagues have supported me over the years whether in the lab, in the office, or on long commutes from the city. Beth Weinman, Lenaye Gray, Andy Winslow, Doug Escribano, Kristal Kallenburg, Alex Kolker, Paula Rose, Gillian Stewart, Vesna Kundic and Jennie Munster are just a few of the very special people who have shared their time with me and whose friendship I will always treasure. I'm sure I'm forgetting so many people, and I hope they'll forgive me. If I've ever hugged you, you belong on this list too. I also can't thank Carol Dovi enough for her assistance, especially in these past two years.

My family is large and all have helped me get to this point in one way or another. I thank my Mom for always encouraging my love of learning and being probably the strongest force in making me the person I am today. I thank my Dad and Cheryl for titling a picture in my high school senior yearbook "The future Dr. Youngs." It seems such a silly thing, but at times when I most wanted to give up, that was a token I held on to in order to push through. Jessica Ryan may as well be family for all her love and support since 5th grade. My mother-in-law Pat has also provided tremendous support emotionally as well as countless hours of free childcare. I wouldn't have been able to finish writing without her! I thank my cats Mattingly and Harlie for being constant companions when I was sequestered away in the guest room writing for what seemed like days on end.

There have been many teachers over the years who have inspired and encouraged me. I thank Mr. Armstrong for not only teaching me Chemistry and Physics, but for making them

really, really cool, and showing me the charm in real science geekery. I thank Dan Davis for insisting that I pursue a research project in geophysics as an undergraduate. I also need to acknowledge Hannah Nekvasil who was the first professor to suggest I pursue a graduate career and who gave me invaluable career advice.

I thank Abby, who is only two years old and won't remember any of this, but who has been very patient while her Mommy was often preoccupied with writing over the past year. Abby, I could never have anticipated what a phenomenal, beautiful force you have been in my life. While I am proud of this achievement, it will never match the pride I feel to be your Mom.

And last, but farthest from least, is Bill, my husband, best friend, and partner in every aspect of life. I am at a loss for words to express how much love and gratitude I feel. You have been there through every single step, from the first suggestion of graduate school that day in the Air and Space Museum to an unbelievably exhausting middle-of-the-night drive to get me to my defense on time. You have sacrificed more than anyone else to help me pursue this goal. These are just a few measly sentences to acknowledge you, but your contribution has been immeasurable. Thank you for every single day of the past 12 years and for the lifetime of years ahead.

Chapter 1: Introduction and Background

I. Introduction

The Ganges-Brahmaputra (G-B) river system is one of the largest in the world. The location of these two large rivers along a tectonically active margin allows for the generation of tremendous sediment loads, the largest carried by any river system on Earth (Milliman and Syvitski, 1992). The G-B river system has proven to be a valuable source of information in unraveling the long-term history of Himalayan development and subsequent erosion thanks to the tremendous sedimentary deposits contained in the Bengal Fan. The Himalayan mountains are responsible for 25% of the annual global sediment budget, and are therefore of interest to geologists for their potential role in climate change over the past 65 million years, as well as the effects of this erosion on the evolution of ocean chemistry (e.g. Raymo and Ruddiman, 1992; Galy et al., 1996; Bouquillon et al.,1990; Derry and France-Lanord, 1996; Edmond, 1992). Using geochemical data from Bengal Fan deposits as well as estimates of modern and historic suspended and dissolved loads, researchers have attempted to quantify the history of Himalayan contribution to global climate via CO_2 drawdown through silicate weathering and carbon burial, as well as the impacts on various aspects of global ocean chemistry such as strontium (Sr) concentrations and alkalinity (e.g. Singh et al., 2006; Galy and France-Lanord, 1999; France-Lanord and Derry, 1994; Harris 1995; Edmond, 1992; Höhndorf et al., 2003; etc.).

These studies represent an important effort in understanding long-term, large-scale changes in the Himalayan development and erosion, but work in the last decade has shown that such a large is also worthwhile to studies of shorter-term (millennial time scale) and regional variations in erosion, weathering and deposition of Himalayan sediments. Research from the Ganges-Brahmaputra Delta shows that delta formation and sediment sequestration in the late Quaternary has been controlled by eustasy, tectonics, and sediment supply from the Himalayas (Goodbred and Kuehl, 2000a). Of particular note is the speed with which erosional signals from the Himalayas and foreland basins are received and recorded in the deltaic stratigraphic record. More specifically, short term climate signals such as the peak in SW monsoon intensity approximately 9ka resulted in a concurrent 2.3-fold increase in river discharge between 7- and

11-ka, illustrating the G-B system's rapid response to short-term, regional climate change (Goodbred and Kuehl, 2000b). These short-term changes in sediment flux have been documented on the Bengal Fan as well, along with changes in the geochemical character of sediments deposited (e.g. Colin et al, 1999). These studies illustrate the rapid response time and wide range of sedimentary characteristics (provenance, weathering, load, deposition) that are affected by climatic variation in the Himalayas. However, the extent to which geochemical fluctuations are caused by variations in sediment provenance or the degree of chemical weathering is not clear at this time.

Recent work on the Indus drainage basin along the western Himalayas suggests that changes in sediment character corresponding to monsoon intensity are a result of changing provenance with increased erosion from the Lesser Himalayas during times of enhanced monsoon strength (Clift et al., 2008). Similar studies from the Bengal Fan have interpreted such signals as fluctuations in weathering intensity (Colin et al., 1999). The thick sedimentary sequences in the G-B delta allow for further high-resolution studies on the geochemical character of sediments eroded from the Himalayas. Not only will comparison of G-B delta studies with Indus Delta studies further the understanding of how the Eastern and Western portions of the Himalayan Range respond to climate change, but the fact that these short-term signals are recorded in the Bengal Fan allow for comparison between the onshore and offshore deposition of sediments. Are changes in geochemical nature of sediments primarily the result of provenance changes corresponding to regional Himalayan erosion or changes in the chemical weathering of sediments associated with climate change? While there have been several in-depth studies of the geochemistry of Bengal Fan sediments that have determined that provenance is the primary control on sediment character on million year timescales (e.g. Bouquillon et al., 1990; Derry and France-Lanord, 1996; Yokoyama et al. 1990; France-Lanord et al., 1993), the sediments preserved in the delta throughout the late Quaternary have been largely unstudied.

The purpose of this dissertation research is to determine the provenance and chemical weathering history of sediments in the Ganges-Brahmaputra delta of Bangladesh. This information is then used to consider a variety of questions. The previous in-depth sedimentological studies that have been performed on the Holocene sediments of the delta were aimed at reconstructing quantitative Holocene sediment budgets, stratigraphic evolution of the delta, and identifying tectonic and climatic controls on sediment delivery to the margin and delta

formation (Goodbred and Kuehl, 1998; Goodbred and Kuehl, 1999; Goodbred and Kuehl, 2000a; Allison et al., 2003). These studies focused on the delta as a single unit due to the difficulty of distinguishing sediments derived specifically from the Ganges, Brahmaputra, or other local tributary rivers (e.g. Tista). Previous efforts to sort out these mixed inputs have relied on clay mineralogy and heavy mineral assemblages (Heroy et al., 2003; Allison et al., 2003; Datta and Subramanian 1997; Segall and Kuehl 1992; Huizing, 1971) and have met with limited success due to the intensity of mixing and potentially sorting in the complex deltaic environment. Closer inspection of the geochemical nature of these sediments in this study using radiogenic isotopes ($^{87}Sr/^{86}Sr$), [Sr], major elemental data, and clay mineralogy allows for an understanding of where these sediments are sourced from in the varied units of Himalayan lithology as well as which of the major rivers or tributaries have carried and deposited these sediments. This allows for the reconstruction of the position, timing, and inferred behavior of the rivers in the Holocene and latest Pleistocene.

Understanding the role of the individual rivers in delta development serves several purposes. First, it will help to highlight which regions of the Himalayas are the primary contributors to sediment sequestered in the delta. This data can then be used to reconstruct more specific, detailed sedimentary and geochemical budgets of Himalayan erosion. In terms of delta formation, this data can then be used to reconstruct river avulsion histories, and will allow for a better understanding of how the basin responds to short-term, millennial scale climatic shifts. These data may then be compared to late Quaternary Bengal Fan deposits to see how the geochemical nature of sediments may be altered by their passage through the delta. Finally, recent work suggests that provenance of aquifer sands may be critical to understanding the heterogeneity of arsenic contamination in South Asian groundwater, and that river migration and avulsion history may play a role as well (Weinman, 2010). Since As contamination of groundwater is a critical and widespread public health concern in the region, mapping sedimentary deposits and river migration patterns may assist in the location of uncontaminated drinking water for millions of people.

1.1 Organization of this dissertation

Chapter 1 (this chapter) presents the pertinent background information necessary to understand and put the data from this study into context. Bengal Basin, G-B delta, and Ganges and Brahmaputra fluvial histories are presented. In addition, the major goals of this dissertation are outlined along with the analytical methods used to collect the data. More detailed analysis and specific discussion of the data are presented in the individual chapters.

Chapter 2 addresses the chemical weathering of Holocene and latest Pleistocene sediments that were analyzed for this study. An in-depth discussion of the major elemental data is presented along with a review and re-analysis of previously collect clay mineralogy data. Understanding the weathering history of the deltaic sediments is an important part of understanding overall morphological development and the fate of sediments that are sequestered on the delta. In addition, characterizing the weathering of sediments is important in assessing confidence in the geochemical provenance proxies discussed in the following chapter.

Chapter 3 discusses the use of Sr isotopes and Sr concentration of bulk sediments in determining the provenance of Holocene and latest Pleistocene deltaic sediments. These data are then used to track the individual as well as the combined depositional histories of the Ganges and Brahmaputra rivers in an effort to better understand G-B delta development.

Chapter 4 summarizes the findings of this dissertation and presents this new information from the delta in light of a full source-to-sink picture for the G-B drainage system. The response of deltaic sedimentation to short-term climatic shifts is discussed and directions for future work are presented.

II. Study Area

2.1 Geological history of basin formation

The modern G-B delta overlies thick sedimentary sequences that have been accumulating in the Bengal Basin since at least the Oligocene (Lindsay et al., 1991). The delta is surrounded by active tectonic structures, and also contains intra-basinal topographic structures within that exert control on the location of river channels, the distribution of sediments, and delta formation. First order controls on basin morphology are exerted by the collision of the Indian plate with the Eurasian plate resulting in the uplift of the Himalayas and Tibet, and the additional subduction of the Indian oceanic crust beneath the Burma plate in the east, resulting in the Indo-Burman mountains and the Chittagong-Tripura fold belt. In the west, the delta is bounded by the Rajmahal Hills, a region of Jurassic to early Cretaceous basalts overlying the Precambrian basement of the Indian Shield at average elevations between 150 and 250m (Morgan and McIntire 1959; Alam et al., 2003) (Figure 1). The hills of the Chittagong-Tripura fold belt rise along the eastern border of the delta. These northward-plunging anticlines are composed of Paleocene-Pliocene oceanic sediments scraped from the plunging Indian oceanic plate (Morgan and McIntyre 1959; Johnson and Alam, 1991; Alam et al., 2003). The Shillong Plateau rises 2 km above the northeastern portion of the G-B delta along the Dauki Fault. The plateau is composed of Archaen quartzite basement with granitic intrusions overlain by Eocene sandstones and limestones (Morgan and McIntyre, 1959; Srivastava et al., 2005). These high-elevation structures represent the complex tectonics of the region and constrain the delta to its current boundaries. In addition to delineating the deltaic borders, the active tectonism of the region continues to create additional accommodation through varying rates of subsidence throughout the basin (Goodbred and Kuehl, 2000a; Alam, 1996; Johnson and Alam, 1991). Estimates of subsidence vary from 1-2mm/year in the southern portions of the delta, to 2-4mm/year and perhaps higher in the Sylhet basin (Goodbred and Kuehl, 2000a; Alam, 1996). This subsidence exerts control on the courses of the Ganges and Brahmaputra rivers through the delta and also provides locations for sediment deposition (Goodbred and Kuehl, 2000a).

Within the delta, further control on river behavior and delta morphology is exerted by several regions of uplifted Pleistocene deltaic sediments. These sediments are characterized by

their highly oxidized and intensely chemically weathered nature as well as their clear fluvial origin noted by evidence of former stream scars (Morgan and McIntyre, 1959; Coleman, 1969). The largest of these are the Barind tracts in the northwestern delta. The Barind tracts are composed of several distinct bodies through which several small rivers flow (Atrai, Lower Purnabhaba and Little Jamuna) covering an area of approximately 9300km^2 with elevations up to 40 m (Morgan and McIntyre, 1959; Coleman, 1969; Brammer, 1996). The exact cause and timing of the uplift of these terraces are unknown, though the presence of a 65 km-long fault along the northeastern edge clearly indicates the tectonic nature of the uplift (Morgan and McIntyre, 1959; Coleman, 1969). Along with the Rajmahal hills to the southeast, the Barind tracts confine the entrance of the Ganges River to the delta along a rather narrow corridor. The Madhupur Terrace is another region of raised Pleistocene sediments located in the center of the delta. The character of the sediments is similar to the Barind tracts, suggesting a formerly continuous surface that has been uplifted in several regions (Morgan and McIntyre, 1959). The Madhupur Terrace dips eastward, with elevations ranging from a maximum of ~30m in the west where the terrace is cut by several faults or erosional features, to 6m in the southern and eastern portions (Morgan and McIntyre, 1959; Coleman, 1969). This feature has played an important role in the migration and avulsion of the Brahmaputra river in recent times, either as one of the confining mechanisms keeping the Brahmaputra in the Sylhet basin when it follows its eastern path, or as the easternmost barrier when the Brahmaputra follows its modern western path along the Jamuna course. Less is known about the Comilla terrace, which abuts the Chittagong Hills in the southeastern portion of the delta (referred to as the Tippera surface in Morgan and McIntyre, 1959 and Coleman, 1969). The sediments appear more oxidized and chemically weathered than recent alluvial deposits, but not to the extent seen in the Barind and Madhupur regions (Morgan and McIntyre, 1959; Coleman, 1969). Initially thought to be alluvial deposits, the terrace is instead composed of sediments deposited in either estuarine or brackish marine environments (Morgan and McIntyre, 1959; Coleman, 1969). The location of several faults around the terrace indicates that like the Barind and Madhupur, the Comilla terrace is a result of local tectonics (Morgan and McIntyre, 1959; Coleman, 1969). The Meghna River is confined to its present flow path by the Comilla Terrace to the south, and partially by the Madhupur Terrace in the north.

2.2 Himalayan lithologies

The source for the vast majority of sediments entering the G-B delta is the Himalayan mountains (e.g. Wasson, 2003; Sinha et al., 2005; Singh and France-Lanord, 2002; Garzanti et al., 2004; Galy and France-Lanord, 2001). There are several distinct lithologic units that contribute to the geochemical character of basin sediments. A detailed review of Himalayan geology is available from Najman (2006) and summarized here (Figure 2). The Trans-Himalaya Plutonic Belt (THB), Tibetan or Tethyan Sedimentary Series (TSS), High Himalayan Crystalline Series (HHC) and Lesser Himalayas (LH) are the primary source lithologies for Bengal Basin sediments. Ophiolites from the Indus-Tsangpo Suture Zone (ITSZ) and Siwaliks or Sub-Himalaya are of minor consequence to overall sediment loads. Beginning in the north are the units of the Trans-Himalaya (THB). This is a plutonic complex formed from the melting slab of subducting Tethyan oceanic crust containing granites, diorites and gabbros. The TSS rocks are mainly of Paleozoic to Mesozoic age, and consist of mostly pelitic sediments that were deposited on a shallow, gradually sinking Tethys Sea platform. The Mesozoic sections are composed of plastic shales, thick limestones, and dolomites. The TSS rocks overlie the HHC, which consist primarily of gneisses derived from quartzo-pelitic sediments. This region is also characterized by migmatites and highly metamorphosed marbles. The LH unit contains metamorphosed Precambrian sediments dominated by quartzo-pelitic schists, and containing minor dolomitic carbonates. These Himalayan lithologies combined provide the vast majority of sediment to the Bengal Basin. Minor sedimentary inputs come from outlying topography, including the Indo-Burman Range, the Shillong Plateau, and the Indian Craton. The Deccan Traps, located on the Indian Craton are a minor source of sediment to the Ganges via southern tributaries (Wasson, 2003; Singh et al., 2008). These are flood basalts of approximately Cretaceous-Tertiary age. The rocks of the Indo-Burman range consist of marine turbidites, shales, and ophiolites of Cretaceous and Oligocene age. Finally, the Shillong Plateau is composed primarily of Archean gneisses and porphyritic granites, with Cretaceous-Tertiary aged sedimentary rocks outcropping in the south (Morgan and McIntyre, 1959; Srivastava et al., 2005).

2.3 Rivers: History and modern characteristics

2.3.1 Ganges

The Ganges drainage basin covers an area of 1.086×10^6 km^2 and drains the front ranges of the Himalayas and portions of the northern Indian Craton as well as the Ganges alluvial plain (Figure 3). Positioned south of the active India/Asia collision zone, the drainage basin represents a diversity of geomorphic features ranging from strong incised valleys and megafan deposits in the upper plains to the more sinuous, gently sloping southern tributaries (Sinha et al., 2005; Singh et al., 2007). The Ganges River is sourced high in the Himalayas (~3800m elevation) from the Gangotri glacier in Northern India near the Tibetan border. After draining the front slopes of the Himalayas, the Ganges exits the Himalayan foothills and begins its west-east flow along the tectonic depression created between the still uplifting Himalayan mountains to the North and the Indian Craton in the South. Here it is joined by its largest tributary, the Yamuna which has drained the same southern Himalayan slopes and also gathered the Chambra and Betwa rivers draining the Indian Craton, composed of Archaen gneiss and schists and the Cretaceous age Deccan Trap Basalts.

Continuing eastward along its more than 2500 km path to the Bay of Bengal, the Ganges gathers water and sediments from tributaries either sourced from the Himalayas, the Ganges alluvial plain, or the northern Indian craton. Himalayan tributaries carry predominantly fine to very fine sands, while the cratonic tributaries are characterized by higher content of coarse- and medium-grained sands. Fine sands, recycled from the Himalayan sediments are contributed by the alluvial plain tributaries. As the Ganges reaches Farraka, approaching the Indian border with Bangladesh, it carries a suspended sediment load of approximately 729 million tons/year, the vast majority of which has been supplied by the higher relief Himalayan tributaries (Wasson, 2003; Singh et al., 2008; Singh et al., 2007). As the Ganges enters the G-B delta, less than 10% of the suspended sediment load can be attributed to sediments derived from the Indian Craton (Wasson, 2003). Along the western margin of the G-B delta, a portion of the Ganges flow is diverted to its major distributary, the Hooghly, which flows southward into the Bay of Bengal taking approximately 45% of the suspended sediment load, leaving the Ganges carrying 400-440 $\times 10^6$ tons/y of suspended sediment as it approaches the confluence with the Brahmaputra River at Aricha.

The Ganges basin is characterized by a subtropical climate and is heavily influenced by the annual summer SW monsoon system. Annually, an average of about 1 x 10^6 m^3/km^2 of rain falls throughout the basin, 70-80% of which occurs during the summer monsoon months of June to September (Singh et al., 2007). This precipitation is not equally distributed, with the eastern portions of the basin receiving higher annual rainfall (up to 160 cm) as compared to the 40-50 cm averages in the western portion of the basin (Singh et al., 2007; Sinha et al., 2005). As a result of this seasonal variation in precipitation, the majority of the annual water and sediment discharge (70-90%) occurs during the SW monsoon (Singh et al., 2007).

2.3.2 Brahmaputra

The Brahmaputra River begins in the Chema Yundung glacier in Tibet, and flows eastward along the northern slopes of the Himalayas as the Tsangpo River (Figure 4). At the eastern termination of the Himalayan orogenic belt (the eastern as), the Tsangpo traverses Namche Barwa and enters India through one of the deepest gorges on earth (Finlayson et al., 2002). Though this narrow region around the syntaxis represents only 4% of the drainage basin area, sediment contribution to the total Brahmaputra load as it enters the G-B delta are estimated at 45%, highlighting the heterogeneity of erosional patterns in the Brahmaputra basin (Singh and France-Lanord, 2002; Garzanti et al., 2004). In the Assam plains of India (figure 4), the Brahmaputra is known as the Siang and begins collecting water and sediment from several prominent tributaries. The largest of these tributaries in Assam is the Lohit, draining the Mishmi Hills, a region where the eastern-most outcrops of the Transhimalayan lithologies are juxtaposed with the northern extent of the Indo-Burman range (Singh and France-Lanord, 2002). Continuing through Assam, the Brahmaputra takes water and sediment discharge from eastern tributaries, Himalayan tributaries draining the southern slopes of the Himalayas, and southern tributaries draining the Shillong Plateau, of which the Himalayan tributaries carry the most significant portion of water and sediment discharge (Garzanti et al., 2004, Singh and France-Lanord, 2002). As the Brahmaputra river turns southward around the western margin of the Shillong Plateau and enters the G-B delta, approximately 30% of the sediment load is derived from a combination of the eastern and southern tributaries, with an almost equal portion attributed to the Himalayan tributaries, and the remaining load from the Tsangpo, eastern syntaxis and sediments picked up along the Assam plains (Garzanti et al., 2004). After entering

the G-B delta, the Brahmaputra collects water and sediment from its last major tributary, the Tista which drains the Lesser Himalayas and portions of the Siwaliks present in the eastern portion of the range. The current course of the Brahmaputra on the delta is to the west of the Madhupur terrace along the Jamuna path before the confluence with the Ganges at Aricha, approximately 150 km north of the Bay of Bengal.

The Brahmaputra drainage basin is significantly smaller than the Ganges basin at 0.68 x 10^6 km^2 (Hay, 1998), however its elevation is higher with a mean modal elevation of 2734 m compared with 890 m for the Ganges. This significantly higher elevation combined with shorter flow path leads to steeper gradients and accounts for the larger sediment load carried by the Brahmaputra as it approaches its confluence with the Ganges on the G-B delta estimated at between 540 and 608 x 10^6 tons per year (Coleman, 1969; Milliman and Syvitski, 1992; Wasson, 2003).

Throughout the mid to late Holocene, it has been estimated that approximately 30% of the combined 1Gt suspended sediment load of the two rivers has been sequestered on the delta (Goodbred and Kuehl, 1999), with modern sequestration estimates of 30- 50% (Milliman and Syvitski, 1992; Goodbred and Kuehl, 1998; Wasson, 2003). Reliable bedload data is not available at this time for the combined G-B rivers. For many rivers in the world, a bedload estimate of 10% of the suspended load is reasonable, but more specific studies of the G-B system have placed bedload estimates at anywhere between 60% and 100% of the suspended load (Coleman, 1969; Hay, 1998; Galy and France-Lanord, 2001; Wasson, 2003).

III. Methods

3.1 Sampling

Samples for this study were taken from six boreholes collected from the G-B delta and described by Goodbred and Kuehl (2000a) and Heroy et al., (2003). Figure 1 shows the locations of these boreholes. Sediments were recovered at 1.5 m intervals from a 2.5 cm hollow-stem pipe with a split-spoon sampler to depths between 85 and 107 meters. BH-1, as the

westernmost borehole was selected to represent a Ganges end-member based on mineralogical studies previously performed on the same borehole (Heroy et al 2003). In addition, this borehole represents a variety of depositional environments from early Holocene channel fill to a transgressive marine intertidal/mangrove environment, to progradational sands representing later Holocene progradation and channel migration (Goodbred and Kuehl, 2000a). To reconstruct a Brahmaputra history, BH-8 located in the Sylhet basin was selected as previous geomorphological and mineralogical studies have indicated that the Brahmaputra is the only major river to have flowed through this region in the late Quaternary (Heroy et al., 2003; Coleman, 1969; Bristow, 1999). Boreholes 7 and 9 (BH-7, BH-9), also located in the Sylhet basin were selected to confirm results from BH-8 and to represent a variety of Brahmaputra depositional environments. The coarser grained stratigraphy of BH-7 has been attributed to active channel fill, while the finer, silt-dominated stratigraphy of BH-8 and BH-9 represents distal deposition from minor distributaries and/or regional flooding (Goodbred and Kuehl, 2000a). To reconstruct a history of combined Ganges and Brahmaputra sediment geochemistry, BH-2 was selected for its position downstream of the modern confluence, but far enough from the coast to have avoided significant impact by marine processes (Goodbred and Kuehl, 2000a). This borehole contains early-mid Holocene fine sand channel fill, capped by late Holocene overbank mud deposits. Finally, BH-5 was selected for its close location to the modern confluence for the purpose of capturing geochemical signals to reconstruct a history of Brahmaputra avulsions in the Quaternary.

3.2 Grain size

Grain-size analysis was performed by Goodbred (2000a) by first separating sands by wet sieving a weighed portion of each sample through a 63μm sieve. The sand fractions were analyzed for different size fractions based on settling velocity in a settling tube. Sodium-hexametaphosphate was added to the remaining fine-grained (silt and clay) fraction and samples were placed in an ultrasonic bath in order to disaggregate the clay minerals. These samples were then washed into a 1000mL graduated cylinder to which deionized water was added up to the 1000mL mark and samples were well-mixed. A sample was taken just after mixing and again after a designated period of time (based on settling velocity of silt particles) with a pipette, then

dried in aluminum pans to determine the weight proportion of the silt and clay fractions. Figure 5 displays the textural profiles for all the boreholes used in this study.

3.3 Clay analyses

Clay mineralogical analyses were performed by Heroy et al. (2003) and Tennant (2005). Analyses were performed on the <2μm size fraction, separated by a combination of gravity settling and centrifuging techniques. Clay samples were mounted on glass slides in preferred orientation and analyzed on a Scintag ADS X-ray diffractometer (XRD) with Cu-Kα radiation. Samples were analyzed in three states in order to best differentiate between different mineral peaks: air dried, after exposure to ethylene glycol at 60°C to expand smectite layers, and after heating at 550°C to reduce overlap between air-dried illite and chlorite peaks. Peak analysis was performed on DMNST version 1.39-1 software from ThermoARL. Background signals were removed and peak areas were calculated and weighted in order to calculate relative abundance of the clay minerals smectite, chlorite, illite, kaolinite and interlayered illite/smectite clays. Clay mineralogy data is available for BH-1, BH-2, BH-5, BH-7 and BH-8 and is listed in Table 1.

For the purposes of this study, the illite crystallization index (or illite crystallinity) was calculated to determine if the illite found in samples was of physical or diagenetic origin. Illite crystallinity was calculated following the method of Kübler described in Jaboyedoff et al. (2001). The Kübler Index (or illite crystallinity index) is defined by the FWHM (full width at half maximum) height of the illite 10Å peak. These calculations were made using the same XRD data files of Heroy et al (2003) and Tennant (2005) using the air-dried clay samples. The same computer program was used. Background was moved with a Boxcar Curve fit with a filter width of 1.5°, a Pearson 7 curve was fit to the data and all steps received the same weigh factor (1/Intensity). As with the clay mineralogy data, illite crystallinity indexes were calculated for all the boreholes in this study with the exception of BH-9.

Illite crystallinity index (Ix) values calculated in 2007 from the original XRD data files of Heroy et al. (2003) and Tennant (2005) are presented in Table 2 and plotted in Figure 6. Heroy et al. (2003) report crystallinity values for the samples included in that study, however no explanation is given with regard to which stage of sample preparation was analyzed (e.g. air-

dried, hot glycolated, etc.), nor is any detail given regarding technique used for the calculation of the actual index (e.g. curve fitting and filtering as described in the methods section of this dissertation). As a result, the calculated values between the two studies show a marked discrepancy for the same samples analyzed. For example, the average Ix calculated for BH-2 in this study is 0.29, whereas the data in Heroy et al. show an average for the same borehole of 0.17. For boreholes 2, 5, 7, and 8, that data calculated in this study will be used as there are more samples analyzed than were published in the previous study, and this will allow for consistent calculation within each borehole. However, for the purposes of BH-1, the data reported in Heroy et al (2003) will be used, since the raw data was not available for re-analysis in this study, despite the discrepancy in calculation method. This is acceptable because application of Ix in this study is to compare samples and analyzed trends within a given borehole, not to draw comparisons between different boreholes.

3.4 Sr Isotope analysis

Samples analyzed in this study for Sr isotopes and major and trace elemental data were prepared for chemical analysis in the same manner. 30-50 g of bulk sediment was taken from each sample to ensure representative sample. Bulk sediments were first ashed at 600°C for 72 hours to ensure the removal of all organic material and to destabilize refractory carbonate minerals. Carbonates were removed by leaching sediments with ~15% acetic acid at 80°C. Following carbonate removal, samples were rinsed and dried, then crushed into a fine powder using a Shatterbox agate mill. Aliquots of these prepared samples were then taken for their separate chemical analyses. In the case of BH-8, bulk samples were wet sieved through a 63μm sieve prior to ashing, and the two separate grain-size fractions, sand and silt+clay were prepared using the above steps.

For Sr analysis, ~50mg of prepared bulk sample were weighed into 7 ml Savillex® Teflon vials and dissolved using a series of acid steps. First 2 ml of 28N HF and 0.5 ml of 14N HNO_3 were added to each vial to remove silica. Vials were then tightly capped and placed on a hotplate at 100°C for 48 hours. Samples were uncapped and dried down before adding 2 ml of 6N HCl. Samples were recapped and placed on the hotplate at 100°C for 24 hours. Following drying after HCl, 2 ml of 14N HNO_3 was added to each vial, capped, and again placed on a

hotplate at 100°C for 24 hours. After final drying, samples were taken up in 50 µl of 3N HNO_3 for Sr separation using cation exchange chromatography. Dissolved samples were placed into quartz columns prepared with SrSPEC® resin with a resin bed volume of 63 µl. All other elements were eluted with 3N HNO_3, and Sr was collected using 0.02N HNO_3.

Separated Sr samples were loaded onto outgassed W filaments using a combination of Ta_2O_5 slurry with H_3PO_4 for analysis on a Finnigan MAT 262 multi-collector thermal ionization mass spectrometer (TIMS) in dynamic mode. $^{87}Sr/^{86}Sr$ values were normalized to $^{86}Sr/^{88}Sr$ of 0.1194. Rubidium interference was monitored using ^{85}Rb to correct ^{87}Sr for the presence of ^{87}Rb; however it should be noted that in all cases, ^{85}Rb was negligible if present at all. Several values were measured for the National Institute of Standards (NIST) Sr Standard Reference Material (SRM) 987 over the time period that $^{87}Sr/^{86}Sr$ data was collected. However, Sr isotope data was collected over a period of nearly 5 years, during which time the source was disassembled and cleaned on several occasions, and the mass spectrometer also underwent a period of repair. As a result, average SRM 987 values varied over this time. Table 3 reports the average SRM 987 values for each time period during which $^{87}Sr/^{86}Sr$ data was collected for this study, along with average error, reported as 2σ. Data collected during each time interval has been normalized to the corresponding SRM 987 value, assuming an accepted NIST SRM 987 value of $^{87}Sr/^{86}Sr = 0.710250$. Overall, $^{87}Sr/^{86}Sr$ averages for SRM 987 varied between 0.710222 and 0.710253, a difference of 0.000031, and 2σ varied between 0.000016 and 0.000064. Data values were only accepted for those samples with an in run precision of <0.000025 2se (standard error). Table 4 lists the $^{87}Sr/^{86}Sr$ data collected for this study, and depth profiles for each borehole are shown in Figure 7.

3.5 Major and trace elements

Elemental analysis was performed at the Washington State University GeoAnalytical Laboratory in Pullman, WA using X-ray fluorescence (XRF) and inductively-coupled argon plasma mass spectrometry (ICP-MS). Samples were submitted for analysis after undergoing the same ashing, leaching, and crushing procedure described above. Two separate batches of samples were sent, one in 2002, the other in 2007. Blind duplicates were sent with each batch. Major and trace elemental data are presented in Tables 5 and 6. In the Summer of 2009, further

Sr concentration data was collected at CUNY Queens College using an Innov-X Alpha handheld XRF. Samples were analyzed in duplicate and periodically normalized to three different standards: NIST 1646a, USGS BCR-2, and USGS GSP-2 with an overall error of less than ±5 ppm. All Sr data is compiled in Table 7.

Major elemental oxide data was collected at Washington State University was received in weight percent of the bulk sample and was converted to percent molar abundance, as that is what is necessary for calculating weathering indices such as CIA which are discussed in Chapter 2. Mole percent was calculated by dividing each oxide by its molecular weight to determine the number of moles of each oxide in each sample, assuming a sample size of 100 g, then dividing by the total number of moles in the entire sample to determine proportion. This conversion is not necessary for calculation of the W index (Ohta and Arai, 2007) but neither does it affect the calculated outcomes, so mole % is used in all cases throughout this study. Some major and trace elemental data is used for comparison from other published studies, and in these cases major elemental data reported in weight % has also been converted to mole %. Trace elemental data is reported in ppm (parts per million).

3.6 Calculation of mixing curves

In Chapter 3, mixing several mixing curves are calculated on plots of $^{87}Sr/^{86}Sr$ vs. [Sr]. Curves are calculated between two end-members, End-member A ($[Sr]_A$, $^{87}Sr/^{86}Sr_A$) and End-member B ($[Sr]_B$, $^{87}Sr/^{86}Sr_B$), where the proportion of each end-member at a given point on the mixing curve is represented by F_A and F_B respectively, with both proportions summing to 1 at each point along the curve.

The equation for calculating the x-axis ([Sr]) values along the curve is:

$$[Sr] = ([Sr]_A \times F_A) + ([Sr]_B \times F_B)$$

The equation for calculating the y-axis ($^{87}Sr/^{86}Sr$) values along the curve is:

$$^{87}Sr/^{86}Sr = \frac{(^{87}Sr/^{86}Sr_A \times [Sr]_A \times F_A) + (^{87}Sr/^{86}Sr_B \times [Sr]_B \times F_B)}{([Sr]_A \times F_A) + ([Sr]_B \times F_B)}$$

References

Alam, M., 1996. Subsidence of the Ganges-Brahmaputra delta of Bangladesh and associated drainage, sedimentation, and salinity problems. In: Milliman, J.D., Haq, B.U. (Eds). Sea-Level Rise and Coastal Subsidence. Kluwer Academic Publishers, Dordrecht, 169-192.

Alam., M., Alam, M.M., Curray, J.R., Chowdhury, M.L.R., Gani, M.R., 2003. An overview of the sedimentary geology of the Bengal Basin in relation to the regional tectonic framework and basin-fill history. Sedimentary Geology 155, 179-208.

Allison, M.A., Khan, S.R., Goodbred Jr., S.L., Kuehl, S.A., 2003. Stratigraphic evolution of the late Holocene Ganges-Brahmaputra lower delta plain. Sedimentary Geology 155, 317-342.

Bouquillon, A., France-Lanord, C., Michard, A., Tiercelin, J.J.,1990. Sedimentology and isotopic chemistry of the Bengal Fan sediments: the denudation of the Himalaya. Proceedings of the Ocean Drilling Program. Scientific Results, vol. 116, 43– 58.

Brammer, H., 1996. The Geography of the Soils of Bangladesh. University Press, Ltd. Dhaka, 287 pp.

Bristow, C.S., 1999. Gradual avulsion, river metamorphosis and reworking by underfit streams: a modern example from the Brahmaputra River in Bangladesh and possible ancient example in the Spanish Pyrenees. In: Smith, N., Rogers, J., (Eds.), Fluvial Sedimentology VI. Special Publication of International Association of Sedimentologists, vol. 28, 221-230.

Clift, P.D., Giosan, L., Blusztajn, J., Campbell, I.H., Allen, C., Pringle, M., Tabrez, A.R., Danish, M., Rabbani, M.M., Alizai, An., Carter, A., Lückge, A., 2008. Holocene erosion of the Lesser Himalaya triggered by intensified summer monsoon. Geology 36, 79-82.

Coleman, J.M., 1969. Brahmaputra river: channel processes and sedimentation. Sedimentary Geology 3, 129-239.

Colin, C., Turpin, L., Bertaux, J., Desprairies, A., Kissel, C., 1999. Erosional history of the Himalayan and Burman ranges during the last two glacial-interglacial cycles. Earth and Planetary Science Letters 171, 647-660.

Derry, L.A., France-Lanord, C., 1996. Neogene Himalayan weathering history and river $^{87}Sr/^{86}Sr$: impact on the marine Sr record. Earth and Planetary Science Letters 142, 59-74.

Edmond, J.M., 1992. Himalayan Tectonics, Weathering Processes, and the Strontium Isotope Record in Marine Limestones. Science 258, 1594-1597.

English, N.B., Quade, J., DeCelles, P.G., Garzione, C.N., 2000. Geologic control of Sr and major elemental chemistry in Himalayan Rivers, Nepal. Geochimica et Cosmochimica Acta 64, 2549-2566.

Finlayson, D.P., Montgomery, D.R., Hallet, B., 2002. Spatial coincidence of rapid inferred erosion with young metamorphic massifs in the Himalayas. Geology 30, 219-222.

France-Lanord, C., Derry, L.A., 1994. $\delta^{13}C$ of organic carbon in the Bengal fan: source evolution and transport of C3 and C4 plant carbon to marine sediments. Geochimica et Cosmochimica Acta 58, 4809-4814.

Galy, A, France-Lanord, C, Derry, L.A., 1996. The Late Oligocene-Early Miocene Himalayan belt Constraints deduced from isotopic compositions of Early Miocene turbidites in the Bengal Fan. Tectonophysics 260, 109-118.

Galy, A., France-Lanord, C., Derry, L.A., 1999. The strontium isotopic budget of Himalayan Rivers in Nepal and Bangladesh. Geochimica et Cosmochimica Acta 63, 1905-1925.

Galy, A., France-Lanord, C., 2001. Higher erosion rates in the Himalaya: Geochemical constraints on riverine fluxes. Geology 29, 23-26.

Galy, V., France-Lanord, C., Peucker-Ehrenbrink, B., Huyghe, P., 2010. Sr-Nd-Os evidence for a stable erosion regime in the Himalaya during the past 12 Myr. Earth and Planetary Science Letters 290, 474-480.

Garzanti, E., Vezzoli, G., Andò, S., France-Lanord, C., Singh, S.K., Foster, G., 2004. Sand petrology and focused erosion in collision orogens: the Brahmaputra case. Earth and Planetary Science Letters 230, 157-174.

Goodbred Jr., S.L., Kuehl, S.A., 1998. Floodplain processes in the Bengal Basin and the storage of Ganges-Brahmaputra river sediment: an accretion study using ^{137}Cs and ^{210}Pb geochronology. Sedimentary Geology 121, 239-258.

Goodbred Jr., S.L., Kuehl, S.A., 1999. Holocene and modern sediment budgets for the Ganges-Brahmaputra river system: Evidence for highstand dispersal to flood-plain, shelf, and deep-sea depocenters. Geology 27, 559-562.

Goodbred Jr., S.L., Kuehl, S.A., 2000a. The significance of large sediment supply, active tectonism, and eustasy on margin sequence development: Late Quaternary stratigraphy and evolution of the Ganges-Brahmaputra delta. Sedimentary Geology 133, 227-248.

Goodbred Jr., S.L., Kuehl, S.A., 2000b. Enormous Ganges-Brahmaputra sediment discharge during strengthened early Holocene monsoon. Geology 28, 1083-1086.

Harris, N., 1995. Significance of weathering Himalayan metasedimentary rocks and leucogranites for the Sr isotope evolution of seawater during the early Miocene. Geology 23, 795-798.

Harris, N., Bickle, M., Chapman, H., Fairchild, I., Bunbury, J., 1998. The significance of Himalayan rivers for silicate weathering rates: evidence from the Bhote Kosi tributary. Chemical Geology 144, 205-220.

Hay, W.W., 1998. Detrital sediment fluxes from continents to oceans. Chemical Geology 145, 287-323.

Heroy, D.C., Kuehl, S.A., Goodbred Jr., S.L., 2003. Mineralogy of the Ganges and Brahmaputra Rivers: implications for river switching and Late Quaternary climate change. Sedimentary Geology 155, 343-359.

Höhndorf, A., Kudrass, H.R., France-Lanord, C., 2003. Transfer of the Sr isotopic signature of the Himalayas to the Bay of Bengal. Deep-Sea research II 50, 951-960.

Huizing, H.G.J., 1971. A reconnaissance study of the mineralogy of sand fractions from East Pakistan sediments and soils. Geoderma 6, 109-133.

Jacobson, A.D., Blum, J.D., Walter, L.M., 2002a. Reconciling the elemental and Sr isotope composition of Himalayan weathering: Insights from the carbonate geochemistry of stream waters. Geochimica et Cosmochimica Acta 66, 3417-3429.

Jacobson, A.D., Blum, J.D., Chamberlain, C.P., Poage, M.A., Sloan, V. F., 2002b. Ca/Sr and Sr isotope systematics of a Himalayan glacial chronosequence: Carbonate versus silicate weathering rates as a function of landscape surface age. Geochimica et Cosmochimica Acta 66, 13-27.

Jaboyedoff, M., Bussy, F., Kübler, B., Thelen, Ph., 2001. Illite "crystallinity" revisited. Clays and Clay Minerals 49, 156-167.

Johnson, A.Y., Alam, A.M.N., 1991. Sedimentation and tectonics of the Sylhet trough, Bangladesh. Geological Society of America Bulletin 103, 1513-1527.

Lindsay, J.F., Holiday, D.W., Hulbert, A.G., 1991. Sequence stratigraphy and the evolution of the Ganges-Brahmaputra complex. American Association of Petroleum Geologists Bulletin 75, 1233-1254.

Milliman, J.D., Syvitski, J.P.M., 1992. Geomorphic/tectonic control of sediment discharge to the ocean: The importance of small mountainous rivers. Journal of Geology 100, 525-544.

Morgan, J.P., McIntire, W.G., 1959. Quaternary geology of the Bengal basin, East Pakistan and India. Geological Society of America Bulletin 70, 319-342.

Najman, Y., 2006. The detrital record of orogenesis: A review of approaches and techniques used in the Himalayan sedimentary basin. Earth-Science Reviews 74, 1-72.

Raymo, M.E., Ruddiman, W.F., 1992. Tectonic forcing of late Cenozoic climate. Nature 359, 117-122.

Segall, M.P., Kuehl, S.A., 1992. Sedimentary processes on the Bengal shelf as revealed by clay-size mineralogy. Continental Shelf Research 12, 517-541.

Singh, M., Singh, I.R., Müller, G., 2007. Sediment characteristics and transportation dynamics of the Ganga River. Geomorphology 86, 144-175.

Singh, S.K., France-Lanord, C., 2002. Tracing the distribution of erosion in the Brahmaputra watershed from isotopic compositions of stream sediments. Earth and Planetary Science Letters 6341, 1-18.

Singh, S.K., Santosh, K.R., Krishnaswami, S., 2008. Sr and Nd isotopes in river sediments from the Ganga Basin: Sediment provenance and spatial variability in physical erosion. Journal of Geophysical Research 113, F03006, 18pp.

Sinha, R., Tandon, S.K., Gibling, M.R., Bhattacharjee, P.S., Dasgupta, A.S., 2005. Late Quaternary geology and alluvial stratigraphy of the Ganga basin. Himalayan Geology 26, 223-240.

Srivastava, R.K., Heaman, L.M., Sinha, A.K., Shihua, S., 2005. Emplacement age and isotope geochemistry of Sung Valley alkaline-carbonatite complex, Shillong Plateau, northeastern India: Implications for primary carbonate melt and genesis of the associated silicate rocks. Lithos 81, 33-54.

Tennant, E., 2005. Late Quaternary climate and provenance signals of the Ganges-Brahmaputra Delta Plain, Bangladesh. Honors Thesis, William and Mary, Williamsburg, VA.

Wasson, R.J., 2003. A sediment budget for the Ganga-Brahmaputra catchment. Current Science 84, 1041-1047.

Weinman, B., 2010. The evolution of aquifers and arsenic in Asia: A study of the fluvio-deltaic processes leading to aquifer formation and arsenic cycling and heterogeneity in Bangladesh, Vietnam, and Nepal. Ph.D. Dissertation, Vanderbilt University, Nashville, TN, 220pp.

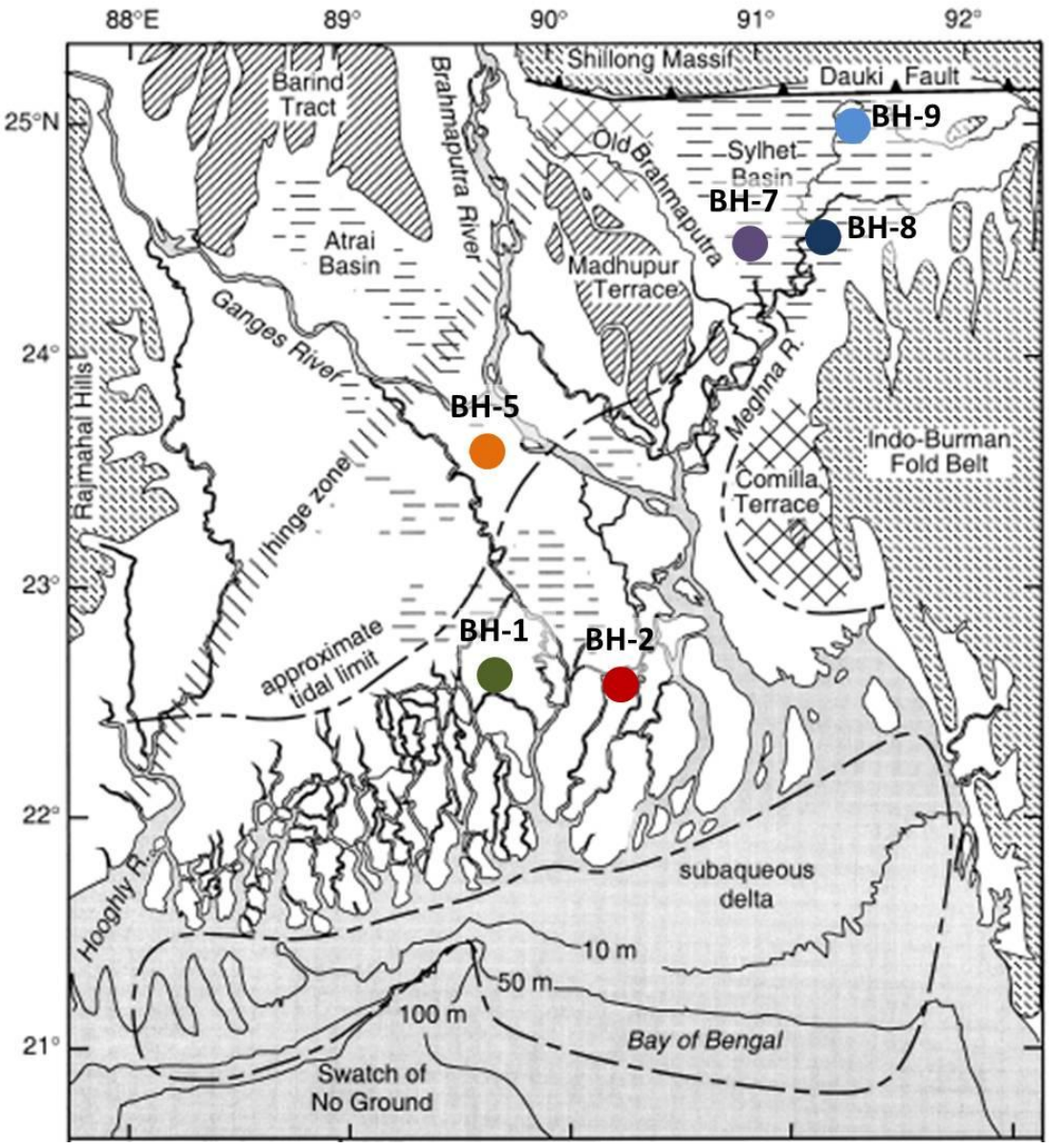

Figure 1. Generalized map of Ganges-Brahmaputra Delta adapted from Goodbred and Kuehl (2000a) indicating the location of boreholes used in this study.

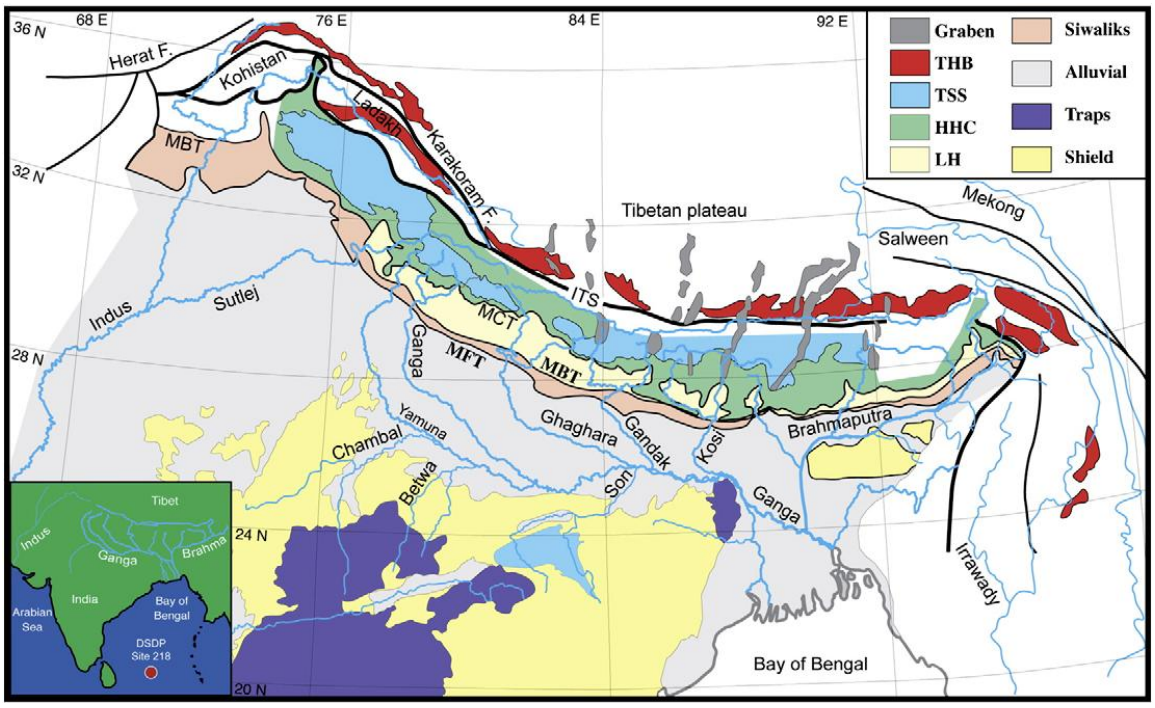

Figure 2. Lithologic provinces of the Himalayas (From Galy et al., 2010). Each lithology is unique in mineralogical and geochemical character. The Trans-Himalayan Plutonic Belt (THB), the Tibetan Sedimentary Series (TSS), the High Himalayan Crystalline (HHC), and the Lesser Himalayas (LH) are the lithologies discussed in this study as important sources of sediment. Other provinces shown on this map provide only minor contributions.

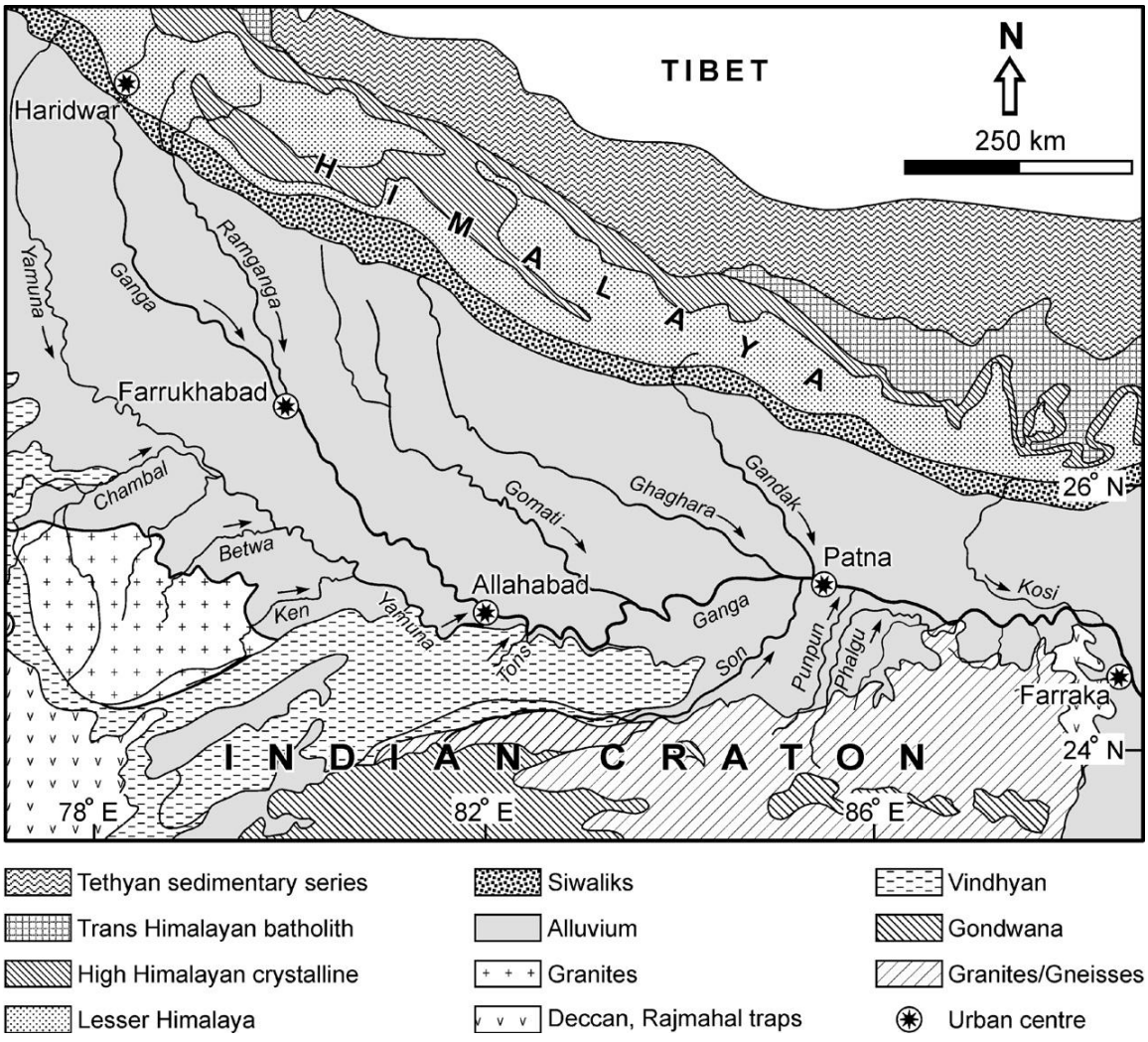

Figure 3. Map of Ganges drainage basin taken from Singh et al. (2007) indicating major tributaries and their component lithologies.

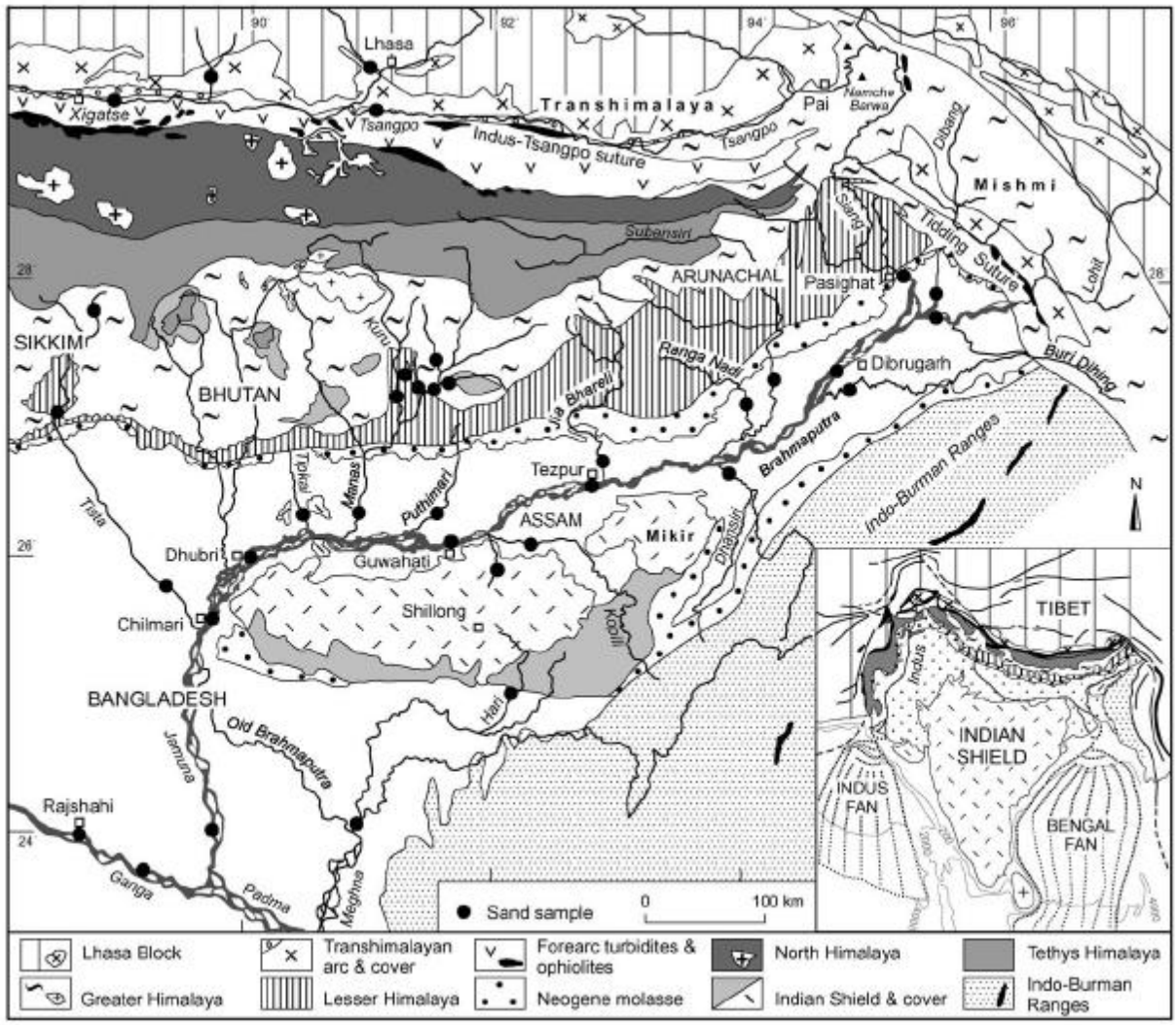

Figure 4. Map of Brahmaputra drainage basin taken from Garzanti et al. (2004) indicating major tributaries and lithologic regions drained.

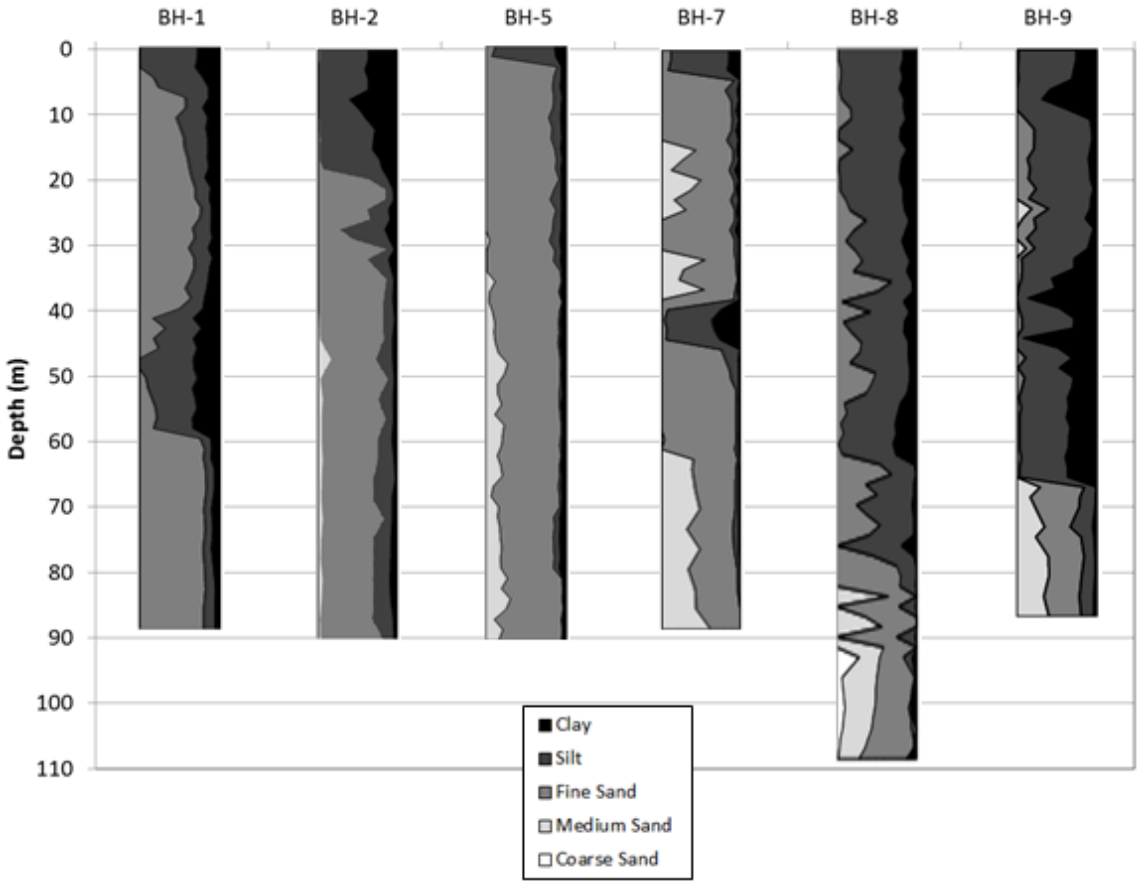

Figure 5. Relative grain-size data from Goodbred and Kuehl (2000a) for boreholes used in this study.

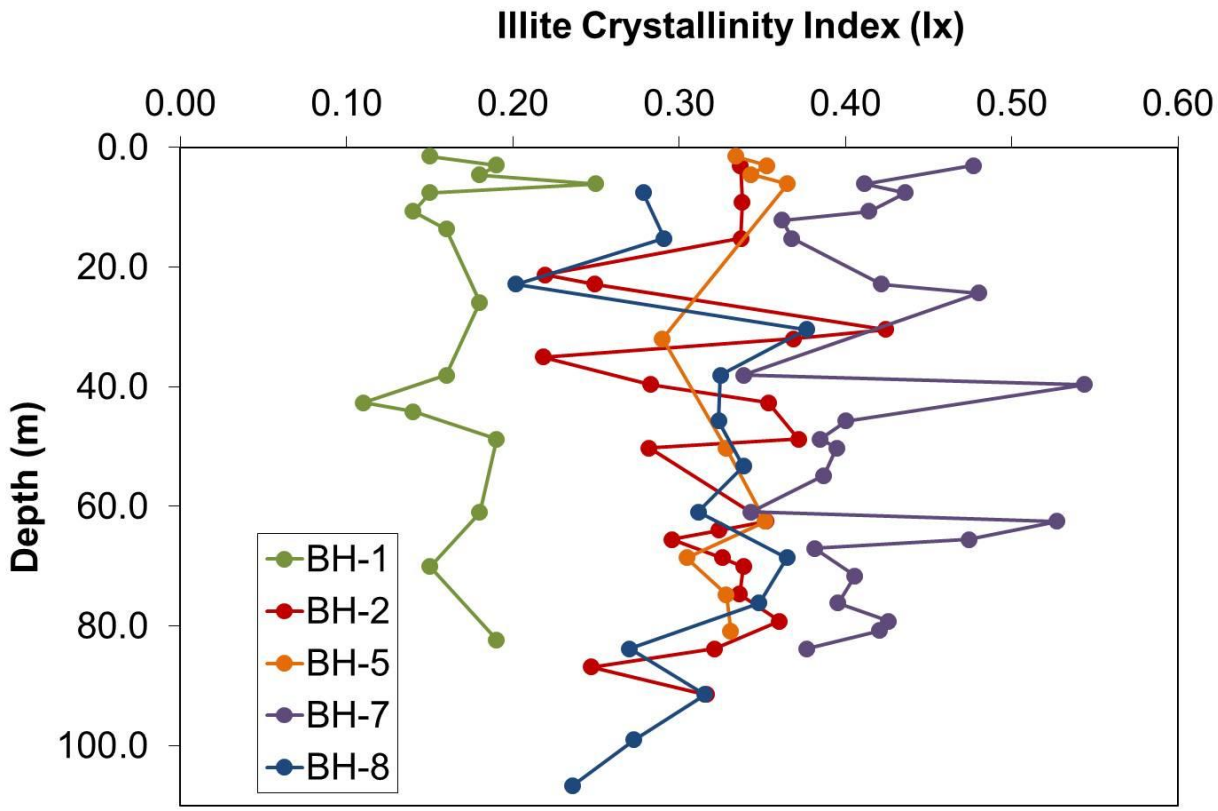

Figure 6. Profiles of illite crystallinity index (Ix) with depth for the boreholes used in this study. Note that Ix for BH-1 was calculated using different parameters which explains the offset from the other boreholes.

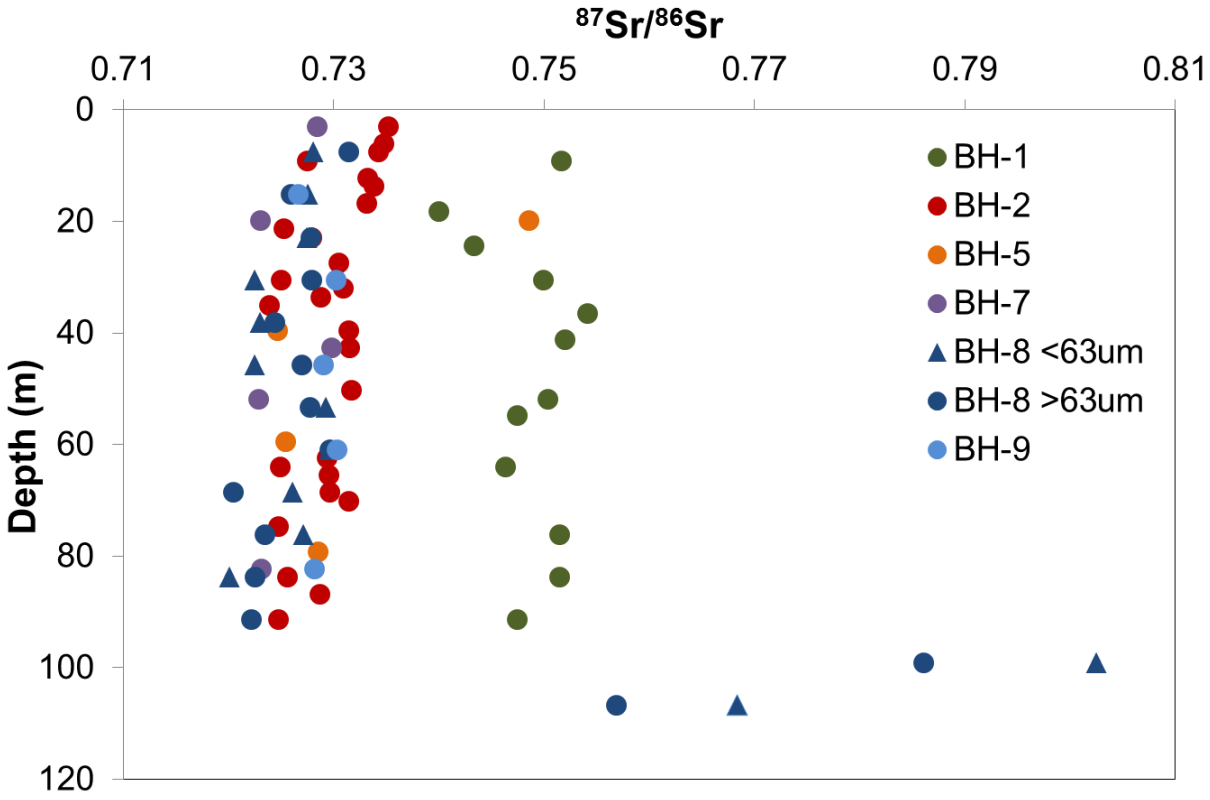

Figure 7. $^{87}Sr/^{86}Sr$ values with depth for each borehole used in this study.

	Depth (m)	%S	%K	%I	%C
BH-1	1.5	8	26	59	5
	3.0	15	23	56	4
	4.6	10	24	58	5
	6.1	15	23	56	5
	7.6	5	23	71	1
	10.7	3	22	68	5
	13.7	12	22	58	6
	25.9	6	15	72	5
	38.1	7	20	66	6
	42.7	5	23	67	4
	44.2	5	22	67	5
	48.8	4	20	68	7
	61.0	2	14	75	9
	70.1	4	18	73	4
	82.3	5	15	69	9
BH-2	3.0	4	37	58	1
	9.1	5	21	61	12
	21.3	4	22	63	12
	22.9	0	20	68	12
	30.5	7	24	65	4
	32.0	6	24	61	9
	35.1	5	23	64	9
	39.6	0	21	68	10
	42.7	7	24	62	7
	50.3	4	29	65	3
	62.5	4	31	64	1
	64.0	4	29	64	3
	65.5	2	34	61	3
	68.6	7	32	59	2
	70.1	4	19	66	11
	74.7	6	17	66	11
	83.8	3	23	64	10
	86.9	7	24	69	0
	91.4	11	35	54	0
BH-5	1.5	17	17	66	0
	3.0	10	16	74	0
	4.6	8	18	74	0
	6.1	21	12	67	0
	15.2	7	23	69	3
	24.4	3	23	74	2
	32.0	9	21	70	1
	50.3	13	18	68	1
	62.5	6	22	71	1
	68.6	7	23	69	1
	74.7	4	19	73	5
	80.8	21	21	56	2

	Depth (m)	%S	%K	%I	%C
BH-7	3.0	13	30	55	2
	6.4	1	15	82	2
	7.6	0	28	67	5
	10.7	1	35	63	2
	12.2	1	61	28	10
	13.7	5	9	81	6
	16.8	1	29	68	2
	18.3	3	43	50	4
	19.8	0	35	64	2
	22.9	1	33	63	3
	24.4	2	37	58	3
	25.9	0	10	85	5
	27.4	2	49	45	5
	29.0	0	27	69	3
	30.5	0	27	66	7
	32.0	0	39	61	0
	35.1	12	56	32	0
	38.1	0	29	64	7
	39.6	4	30	63	2
	41.2	0	45	52	3
	42.7	0	42	52	7
	45.7	3	35	60	3
	47.3	0	25	72	3
	48.8	0	34	62	4
	50.3	0	33	65	2
	51.8	0	26	72	2
	53.4	0	29	70	2
	54.9	0	36	63	1
	56.4	0	29	67	4
	57.9	0	27	70	3
	61.0	3	33	58	5
	62.5	0	30	66	4
	64.0	0	63	30	7
	65.5	0	31	65	3
	67.1	2	27	66	5
	68.6	0	26	69	5
	70.1	0	54	39	7
	71.6	0	32	66	3
	73.2	4	45	47	4
	74.7	0	33	64	3
	76.2	0	21	74	5
	77.7	0	23	71	6
	79.3	0	29	67	4
	82.3	0	27	66	7
	83.8	0	28	68	4
	85.4	0	29	60	12
	86.9	0	30	65	4

	Depth (m)	%S	%K	%I	%C
BH-8	7.6	6	38	56	0
	15.2	7	36	57	0
	22.9	2	43	55	0
	30.5	11	37	50	2
	38.1	6	37	57	0
	45.7	8	35	57	1
	53.4	12	43	45	0
	61.0	10	42	48	0
	68.6	0	32	67	1
	76.2	12	35	53	0
	83.8	0	36	64	0
	91.4	0	27	59	14
	99.1	0	41	59	0
	106.7	4	40	56	1

Table 1. Compilation of relative clay mineral abundance data from Heroy et al (2003) and Tennant (2005). S = smectite, K = kaolinite, I = illite, C = chlorite.

	Depth (m)	Ix
BH-1	1.5	0.15
	3.0	0.19
	4.6	0.18
	6.1	0.25
	7.6	0.15
	10.7	0.14
	13.7	0.16
	25.9	0.18
	38.1	0.16
	42.7	0.11
	44.2	0.14
	48.8	0.19
	61.0	0.18
	70.1	0.15
	82.3	0.19
BH-2	3.0	0.34
	9.1	0.34
	15.2	0.34
	21.3	0.22
	22.9	0.25
	30.5	0.42
	32.0	0.37
	35.1	0.22
	39.6	0.28
	42.7	0.35
	48.8	0.37
	50.3	0.28
	62.5	0.35
	64.0	0.32
	65.5	0.30
	68.6	0.33
	70.1	0.34
	74.7	0.34
	79.2	0.36
	83.8	0.32
	86.9	0.25
	91.4	0.32

	Depth (m)	Ix
BH-5	1.5	0.33
	3.1	0.35
	4.6	0.34
	6.1	0.37
	32.0	0.29
	50.3	0.33
	62.5	0.35
	68.6	0.30
	74.7	0.33
	80.8	0.33
BH-7	3.0	0.48
	6.1	0.41
	7.6	0.44
	10.7	0.41
	12.2	0.36
	15.2	0.37
	22.9	0.42
	24.4	0.48
	38.1	0.34
	39.6	0.54
	45.7	0.40
	48.8	0.38
	50.3	0.39
	54.9	0.39
	61.0	0.34
	62.5	0.53
	65.5	0.47
	67.1	0.38
	71.6	0.41
	76.2	0.40
	79.2	0.43
	80.8	0.42
	83.8	0.38

	Depth (m)	Ix
BH-8	7.6	0.28
	15.2	0.29
	22.9	0.20
	30.5	0.38
	38.1	0.32
	45.7	0.32
	53.3	0.34
	61.0	0.31
	68.6	0.36
	76.2	0.35
	83.8	0.27
	91.4	0.32
	99.1	0.27
	106.7	0.24

Table 2. Illite crystallinity (Ix) for boreholes used in this study calculated from original data files collected by Heroy et al (2003) and Tennant (2005).

Dates	Average $^{87}Sr/^{86}Sr$ value for NIST SRM 987	Error (2σ)	n
July - September 2002	0.710222	0.000024	11
June 2003	0.710236	0.000029	6
September-October 2003	0.710235	0.000016	11
July - August 2004	0.710241	0.000031	11
November 2004 - February 2005	0.710224	0.000028	56
November - December 2006	0.710232	0.000031	14
January - March 2007	0.710253	0.000064	32

Table 3. Average values of $^{87}Sr/^{86}Sr$ for Standard Reference Material 987 during the time periods for which data were collected for this study. The number of standard runs for each time period is represented by n.

Borehole	Depth (m)	$^{87}Sr/^{86}Sr$
BH-1	9.1	0.751630
	18.3	0.739991
	24.4	0.743384
	30.5	0.749974
	36.6	0.754179
	41.1	0.751990
	51.8	0.750390
	54.9	0.747451
	64.0	0.746365
	76.2	0.751477
	83.8	0.751521
	91.4	0.747483
BH-2	3.0	0.735219
	6.1	0.734792
	7.6	0.734305
	9.1	0.727529
	12.2	0.733266
	13.7	0.733860
	16.8	0.733189
	21.3	0.725266
	22.9	0.727907
	27.4	0.730474
	30.5	0.724987
	32.0	0.730929
	33.5	0.728784
	35.1	0.723885
	39.6	0.731421
BH-2 (cont.)	42.7	0.731536
	50.3	0.731659
	62.5	0.729405
	64.0	0.724915
	65.5	0.729525
	68.6	0.729607
	70.1	0.731463
	74.7	0.724731
	83.8	0.725655
	86.9	0.728736
	91.4	0.724760
BH-5	19.8	0.748585
	39.6	0.724655
	59.4	0.725449
	79.2	0.728568
BH-7	3.0	0.728432
	19.8	0.723084
	42.7	0.729804
	51.8	0.722874
	82.3	0.723115
BH-8 (<63um)	7.6	0.728130
	15.2	0.727561
	22.9	0.727482
	30.5	0.722566
	38.1	0.723085
	45.7	0.722503
BH-8 (<63um) (cont.)	53.3	0.729326
	61.0	0.729624
	68.6	0.726143
	76.2	0.727121
	83.8	0.720122
	99.1	0.802525
	106.7	0.768353
BH-8 (>63um)	7.6	0.731412
	15.2	0.725959
	22.9	0.727859
	30.5	0.727922
	38.1	0.724393
	45.7	0.726966
	53.3	0.727751
	61.0	0.729632
	68.6	0.720452
	76.2	0.723457
	83.8	0.722543
	91.4	0.722165
	99.1	0.786102
	106.7	0.756852
BH-9	15.2	0.726676
	30.5	0.730231
	45.7	0.729079
	61.0	0.730340
	82.3	0.728170

Table 4. $^{87}Sr/^{86}Sr$ values for individual samples with depth in the boreholes used for this study.

		Major Elements (mole %)							
Boreholes	**Depth (m)**	**SiO_2**	**Al_2O_3**	**TiO_2**	**FeO***	**CaO**	**MgO**	**K_2O**	**Na_2O**
BH-1	9.1	83.5	6.3	0.40	3.02	1.65	1.96	1.53	1.65
	18.3	84.0	6.3	0.36	2.89	1.53	1.78	1.53	1.69
	24.4	84.7	6.3	0.25	2.47	1.34	1.62	1.63	1.74
	36.6	80.7	7.3	0.42	4.06	1.50	2.65	1.80	1.58
	51.8	74.0	10.3	0.56	5.50	1.60	3.96	2.40	1.65
	64.0	86.2	5.6	0.30	2.06	1.50	1.30	1.39	1.68
	76.2	85.6	5.8	0.31	2.24	1.51	1.40	1.44	1.69
BH-2	9.1	71.1	12.3	0.64	6.05	1.41	4.66	2.41	1.43
	13.7	72.3	11.2	0.65	6.09	1.60	4.26	2.28	1.66
	21.3	84.6	6.2	0.26	2.05	2.12	1.44	1.40	2.00
	39.6	82.5	6.9	0.31	2.86	1.95	1.93	1.66	1.93
	68.6	82.9	6.8	0.33	2.57	2.13	1.83	1.53	1.95
	83.8	83.0	6.7	0.32	2.56	2.16	1.79	1.51	1.96
BH-5	19.8	86.6	5.4	0.25	1.96	1.50	1.17	1.36	1.70
	39.6	83.1	5.9	0.39	3.02	2.67	1.71	1.27	1.85
	79.3	84.2	6.2	0.29	2.33	2.10	1.51	1.46	1.90
BH-8	15.2	74.0	9.9	0.67	5.30	2.58	3.91	1.87	1.80
(<63um)	30.5	75.2	9.7	0.67	5.37	2.22	3.51	1.74	1.63
	45.7	73.8	9.8	0.68	5.32	2.68	4.01	1.85	1.83
	76.2	84.1	6.7	0.54	3.17	1.15	1.59	1.32	1.42
	80.8	76.5	6.8	1.86	6.76	3.53	2.09	1.03	1.39
BH-8	15.2	76.9	8.0	0.45	4.88	2.35	3.73	1.81	1.87
(>63um)	30.5	79.8	7.6	0.36	3.61	2.16	2.90	1.69	1.92
	45.7	76.9	8.1	0.42	4.88	2.15	3.76	1.87	1.95
	61.0	91.0	4.3	0.16	1.06	0.44	0.49	1.47	1.06
	83.8	83.4	5.8	0.50	2.73	2.97	1.76	1.12	1.67
	91.5	85.2	5.7	0.28	2.11	2.18	1.28	1.40	1.83
	99.1	87.2	5.7	0.18	1.66	1.02	1.04	1.57	1.61
	106.7	87.0	5.9	0.18	1.47	1.19	0.99	1.50	1.73

Table 5. Major elemental data collected for this study and converted to mole % for use in calculating weathering proxies. FeO* combines Fe measured in both FeO and Fe_2O_3 oxide states.

Borehole	Depth (m)	Ni	Cr	Sc	V	Ba	Rb	Sr	Zr	Y	Nb	Ga	Cu	Zn	Pb	La	Ce	Th	Nd	U	Cs
BH-1	9.1	16	44	9	54	355	118	107	350	34	12	12	8	42	18	48	98	20	39	4	7
	18.3	16	42	9	52	357	111	109	332	31	10	12	11	51	19	46	87	19	36	3	5
	24.4	14	34	7	46	370	118	114	150	20	7	12	5	38	20	25	50	10	22	2	8
	36.6	23	53	10	69	406	148	101	286	30	13	15	15	64	22	43	83	17	36	4	9
	51.8	39	83	14	104	538	180	116	215	33	15	20	33	86	25	42	90	18	36	4	14
	64.0	8	35	7	39	324	95	109	316	30	8	10	3	38	18	40	82	18	36	5	5
	76.2	10	34	7	46	340	101	109	307	30	9	11	5	42	19	43	83	19	38	3	6
BH-2	9.1	63	116	16	136	505	194	125	173	34	17	23	44	101	31	52	94	18			
	13.7	54	108	16	118	476	175	131	224	36	16	22	38	92	28	47	98	21	41	4	12
	21.3	17	37	8	35	339	84	161	227	26	8	14	3	27	16	32	61	13			
	39.6	23	42	10	49	385	121	152	205	23	9	14	5	46	20	32	57	13			
	68.6	21	49	8	52	375	100	159	250	28	10	13	5	35	15	37	83	16			
	83.8	20	44	15	52	362	98	162	276	31	9	10	7	39	18	45	87	16			
BH-5	19.8	8	33	6	39	310	89	113	227	25	8	10	3	42	18	34	65	16	29	2	4
	39.6	10	60	9	62	303	72	166	372	39	10	11	2	45	20	58	117	25	47	2	1
	79.3	10	45	8	51	345	88	156	212	24	7	11	5	33	19	33	70	15	28	3	3
BH-8	15.2	54	108	20	118	455	138	162	352	45	18	19	31	82	24	57	125	25			
(<63um)	30.5	55	113	19	118	420	127	144	361	44	17	18	23	76	23	52	108	22			
	45.7	54	106	20	119	461	136	163	374	45	18	20	31	82	30	62	119	26			
	76.2	38	100	16	71	315	86	109	490	38	14	13	10	48	16	39	87	19			
	80.8	16	110	12	74	279	63	161	865	54	15	10	3	34	16	73	146	34	61	4	1
BH-8	15.2	43	79	20	78	423	140	152	206	26	13	17	20	71	18	22	54	11			
(>63um)	30.5	32	59	14	80	413	121	152	116	21	10	14	8	60	16	27	51	7			
	45.7	43	69	14	88	436	145	151	135	22	12	17	19	76	17	29	44	9			
	61.0	16	24	4	24	377	80	85	52	9	4	8	4	18	17	6	26	5	8	0	3
	83.8	20	80	9	68	274	65	164	323	43	14	11	2	31	12	57	112	23			
	91.5	9	46	8	46	327	78	168	178	25	7	11	1	25	17	32	68	15	27	3	2
	99.1	4	24	5	28	331	109	77	141	23	6	11	2	24	23	28	51	13	23	2	4
	106.7	9	15	5	23	333	107	86	173	27	6	10	1	22	20	36	81	16			

Table 6. Concentration of trace elements in parts per million collected for this study. Values left blank were not measured for.

Borehole	Depth (m)	[Sr] (ppm)
BH-1	9.1	107
	18.3	109
	24.4	114
	30.5	104
	36.6	101
	41.1	101
	51.8	116
	54.9	108
	64.0	109
	76.2	109
	83.8	113
	91.4	106
BH-2	3.0	131
	6.1	126
	7.6	121
	9.1	125
	12.2	141
	13.7	131
	21.3	161
	30.5	158
	32.0	150
	35.1	163
	39.6	152
	42.7	148
	62.5	160
	64.0	155
	68.6	159
	70.1	150
	74.7	159
	83.8	162
	91.4	164
BH-5	19.8	113
	39.6	166
	59.4	165
	79.2	156

Borehole	Depth (m)	[Sr] (ppm)
BH-7	3.0	122
	19.8	164
	42.7	115
	51.8	156
	82.3	163
BH-8 (<63um)	7.6	135
	15.2	162
	22.9	150
	30.5	144
	38.1	138
	45.7	163
	53.3	105
	61.0	82
	68.6	107
	76.2	109
	99.1	97
	106.7	97
BH-8 (>63um)	7.6	122
	15.2	152
	22.9	148
	30.5	152
	38.1	126
	45.7	151
	53.3	119
	61.0	85
	68.6	143
	83.8	164
	91.4	168
	99.1	77
	106.7	86
BH-9	15.2	151
	30.5	126
	45.7	95
	61.0	117
	82.3	83

Table 7. Sr concentration data compiled for this study, compiled from analyses from Washington State University and CUNY Queens College.

Chapter 2: Weathering and sorting of Holocene sediments in the Ganges-Brahmaptura delta and effects on [Sr] and $^{87}Sr/^{86}Sr$

I. Introduction

There are three primary controls on the geochemical nature of sediments: the rocks from which the sediments are derived (provenance), the amount of weathering or chemical alteration the sediments have undergone, and mineral sorting due to differences in density and grain size. The purpose of this chapter is to characterize the level of alteration due to chemical weathering experienced by Holocene sediments in the Ganges-Brahmaputra delta, and to determine whether or not hydraulic sorting has affected the geochemistry of the bulk sediments. Samples that have been extensively weathered or have undergone a high degree of sorting may not be geochemically representative of provenance lithologies, which would make them less useful in tracing patterns of erosion, deposition, and river migration on the delta throughout the Holocene. Sediment provenance and delta development are discussed in the following chapters using geochemical proxies such as Sr isotopes and Sr concentration ([Sr]), the usefulness of which may be affected by weathering and sorting processes. In addition, characterizing the weathering history of deltaic sediments is an important component of reconstructing river avulsion and migration patterns and morphological development. Clay mineralogy and geochemical weathering proxies calculated from major and trace elemental data are examined in order to address the issue of weathering in sediments used in this study. Major and trace elemental data are used to address the issue of sorting as well.

II. Background

2.1 Effects of weathering on $^{87}Sr/^{86}Sr$ and [Sr] of sediments

Strontium readily substitutes for calcium and is found most commonly in common Ca-bearing minerals such as plagioclase feldspars, apatite, and carbonates. In addition, radiogenic

strontium (^{87}Sr) can be found in rubidium (Rb)-bearing minerals such as potassium feldspars (e.g. orthoclase, microcline) and in the interlayers of micaceous minerals such as muscovite and biotite due to the decay of ^{87}Rb to ^{87}Sr. These minerals are common in the igneous and metamorphic rocks of the major Himalayan lithologies drained by the Ganges and Brahmaputra rivers, and are therefore a significant component of the sedimentary material that makes up the Ganges-Brahmaputra delta. The unique [Sr] and $^{87}Sr/^{86}Sr$ ratios of the different Himalayan lithologies make these good proxies for tracing the provenance of deltaic sediments (discussed further in Chapter 3 of this thesis). However, these minerals are subject to varying degrees of chemical alteration that could impact the usefulness of these proxies. Studies have shown that $^{87}Sr/^{86}Sr$ of river water and soils can be affected by denudation rates, and that mineral weathering is heterogeneous on both spatial and temporal scales even for constant parent material (e.g. Blum and Erel, 1997 and references therein). Therefore, it is important to understand how weathering affects the $^{87}Sr/^{86}Sr$ and [Sr] of bedload and suspended sediments in order to recognize any limitations of using these proxies as provenance tracers.

2.1.1 Effects of preferential feldspar and mica weathering on $^{87}Sr/^{86}Sr$ and [Sr] signatures

In a comprehensive study of several types of rock lithology (e.g. granite, basalt, gneiss) and their resulting weathering and soil formation profiles, Dasch (1969) found that the [Rb]/[Sr] of weathered material increased along with the intensity of chemical alteration. This result is explained by the fact that Sr concentrations are highest in the more readily decomposed primary minerals such as plagioclase, so the preferential weathering of these minerals over more Rb-rich minerals such as micas results in the relative decrease in concentration of Sr with respect to Rb over time. In addition, the Rb^{+} ion sorbs more readily onto clay exchange sites than Sr^{2+}. However, such a consistent effect was absent for Sr isotopes. Some weathering profiles did show a slight increase in $^{87}Sr/^{86}Sr$, again attributed to the preferential dissolution of Sr-bearing minerals over Rb-bearing minerals which tend to have more radiogenic isotopic signatures. However, the number of samples analyzed was small, and not all samples were de-carbonated making it difficult to fully quantify the effect of silicate mineral weathering on the $^{87}Sr/^{86}Sr$ ratio. The study concludes that except in the case of ancient granitic and metamorphosed material, chemical alteration of most continental rocks does not result in a significant increase in $^{87}Sr/^{86}Sr$ of the resultant secondary material (Dasch 1969). Applying this generalized conclusion to the

deposits of the Ganges-Brahmaputra delta would suggest that there would be little expected effect of weathering on $^{87}Sr/^{86}Sr$ in these sediments. However, this thesis will examine new data presented for evidence of preferential plagioclase weathering in the G-B deltaic deposits that could influence $^{87}Sr/^{86}Sr$ ratios and Sr concentrations of bulk sediments.

While feldspars contain higher concentrations of Sr, the extremely radiogenic nature of micaceous minerals such as biotite ($^{87}Sr/^{86}Sr > 0.9$; Blum and Erel, 1997) and muscovite warrant inspection for the effects of their weathering on the $^{87}Sr/^{86}Sr$ signature of bulk sediments. Biotite need not undergo complete or even partial dissolution for weathering to impact the $^{87}Sr/^{86}Sr$ of soils and stream waters (Blum and Erel, 1997). Even in freshly weathered, C-horizon soils, biotite may undergo partial alteration to vermiculite in which the interlayer K^+ cations (and ^{87}Rb and ^{87}Sr associated therewith) are replaced with Fe and Mg cations. This release of radiogenic Sr without dissolution or complete alteration of the biotite mineral itself can have rather significant impacts on the $^{87}Sr/^{86}Sr$ of exchangeable Sr and associated stream waters (Blum and Erel, 1997). However, the impact on the isotopic character of the bulk soil samples is much less dramatic, and it must also be noted that this effect is seen most in the incipient weathering of fresh biotites in glacial soils and is absent in downstream alluvium (Blum and Erel, 1997). Therefore, while this type of weathering may be of concern in the headwater streams, the effect on overall weathering and geochemistry of sediments downstream that have already experienced a minor degree of weathering will be negligible. However, with modern floodplain deposits containing mica fractions of up to 30% in sandy sediments and up to 80% in some silty deposits (Huizing, 1971; Derry and France-Lanord, 1996), even small amounts of preferential biotite weathering have the potential to impact bulk sediment strontium chemistry. For this reason, even the possibility of significant biotite weathering in the delta must be considered.

While Dasch (1969) investigated the effects of weathering on $^{87}Sr/^{86}Sr$ within several soil profiles of several rock types, Blum and Erel (1997) investigated several soil profiles of varying ages (9.4 kyr to $\geq$297 kyr) all derived from the same parent material. Like Dasch, they found that within a given soil profile, the effects of weathering on $^{87}Sr/^{86}Sr$ of bulk samples were inconsistent, increasing slightly in some profiles, and decreasing slightly in others. However, overall $^{87}Sr/^{86}Sr$ and [Sr] did vary between profiles of different ages. For the three soil profiles with ages between 0.4 and 11.7 kyr, $^{87}Sr/^{86}Sr$ averaged 0.726486 and Rb/Sr was 0.204, both values higher than the unweathered whole rock values of 0.722577 and 0.182 respectively. For

the older profiles ranging from 21.7 to ≥297 kyr, $^{87}Sr/^{86}Sr$ averaged 0.714265 and Rb/Sr 0.144, both values lower than the unweathered parent values. These results show that $^{87}Sr/^{86}Sr$ and [Sr] can be significantly altered from parent material in old, well-developed soils (≥21.7kyr in this case). It is therefore important that the sediments utilized in this study for tracing provenance first be analyzed for weathering intensity of the silicate fraction.

2.1.2 Effects of clay mineralogy on $^{87}Sr/^{86}Sr$ and [Sr] signatures

Clay mineralogy is also of concern for the direct affect some secondary minerals, namely smectite, can have on $^{87}Sr/^{86}Sr$ of sediments. More specifically, it has been shown for smectites in the <2 μm size fraction that these highly weathered minerals have undergone a complete exchange of Sr from interlayer sites with surrounding water (groundwater, river water) in the location that the silicate weathering takes place (Derry and France-Lanord, 1996). As a result, the $^{87}Sr/^{86}Sr$ signature of these minerals may bear no similarity to the parent material and is instead a representation of meteoric and fluvial waters at the time of formation. For this reason, any sample with high smectite content in this study will warrant further investigation for its use in provenance studies.

2.2 Clays as a weathering proxy

Many clay minerals are formed as a direct result of weathering of primary rock material, and therefore have the potential to provide information about the weathering history of rocks, as well as provenance. In the G-B basin, the most commonly used clay minerals to these ends are smectite, illite, chlorite, and kaolinite. Illite minerals can be formed by the physical grinding of primary micaceous minerals or as secondary minerals from the chemical weathering of muscovite and feldspar minerals. Chlorite is commonly derived from the physical break down of low-grade metamorphic rocks such as those found in the High and Lesser Himalayas. Kaolinite and smectite minerals represent clays that have undergone a higher degree of alteration. Kaolinite is formed from intense chemical weathering of feldspars and micaceous minerals (biotite and muscovite), therefore, the presence of kaolinite indicates that significant alteration has taken place. Smectites form as a result of chemical alteration of more mafic igneous rocks and therefore contain more Fe and Mg.

Since illite may be formed from either physical or chemical weathering processes, a useful tool in examining illite is the illite crystallinity (or the illite crystallization index, Ix). The illite crystallization index is a proxy for how crystallized the illite in a given clay sample is. Hydrolization of illite expands the spacing between the layers and is enhanced under conditions of high rainfall and warmer temperatures, conditions which lead to more chemical weathering overall (Singer, 1984). A lower crystallinity index value indicates a smaller spacing between the illite layers, which in turn indicates a more crystallized, physically sourced illite. A higher crystallinity value indicates less-crystallized illite, and hence illite derived from diagenesis of primary minerals. The actual, specific values of the crystallinity index are different for different rock materials, and therefore are best used in drawing relations between samples rather than as a quantitative characteristic on its own (Jaboyedoff et al., 2001).

2.2.1 Clay mineralogy of the Bengal Basin

Early studies from ODP Leg 116 cores on the distal Bengal Fan (e.g. Bouquillon et al., 1990; Derry and France-Lanord, 1996; Yokoyama et al. 1990; France-Lanord et al., 1993) concluded that smectites and kaolinites found in the distal portions of the Bengal Fan were largely derived from weathering of sediments into soils on the Indo-Gangetic Plain. Isotopic and mineralogical provenance studies on the sediments revealed nearly constant source histories for all sediments in the core, allowing for changes in smectite and kaolinite composition of the clays to be attributed to variations in weathering intensity of soils, and hence serve to reflect changes in climate experienced in the basin (Yokoyama et al. 1990; Derry and France-Lanord, 1996; Bouquillon et al., 1990). The clay mineral proxy SK/IC is used to denote relative weathering intensity based on the abundance of the major clay minerals smectite (S), kaolinite (K), illite (I), and chlorite (C). The abundances for these four minerals are summed to 100%, then the relative abundances are added (S+K and I+C) to calculate the ratio. Higher values of SK/IC indicate an abundance of the chemical weathering products smectite and kaolinite over illite and chlorite, which are a product of physical breakdown of primary minerals such as muscovite and potassium feldspar (e.g. Singer, 1984; Derry and France-Lanord, 1996; Bouquillon et al., 1990; France-Lanord et al., 1993). Comparing SK/IC of the clay fraction within cores and between cores of the Bengal Fan has allowed researchers to identify periods such as times of increased southwest monsoon intensity where chemical alteration of sediments is high, and times when physical

alteration dominates, such as in cooler, drier climates (Derry and France-Lanord, 1996; Bouquillon et al., 1990).

More recent work has applied this proxy to the study of sediment cores throughout the Ganges-Brahmaputra Delta (Heroy et al., 2003) in order to discern millennial-scale variations in weathering intensity of delta sediments, assuming negligible variation in initial sediment provenance. Results of that study indicate that the main control on SK/IC of deltaic sediments is the input of physically weathered IC material driven by climate and sediment load variations rather than changes in weathering intensity due to climate fluctuations. However, comparison of clay mineralogy with EM conductivity in a deep Sylhet basin core suggest that smectite and kaolinite abundances correlate with higher electromagnetic conductance indicating periods of soil formation which would allow for chemical alteration of delta plain sediments (Tennant, 2005).

While clay mineralogy of Holocene deltaic sediments may not provide a powerful record of past weathering changes based on Holocene climatic variations, the clays may still record more localized changes in weathering such as river migration and pedogenic processes. Therefore one objective of this study is to identify samples that may have been altered since deposition. In addition, due to the nature of fine-grained material being more chemically weathered than coarser-grained counterparts, it is possible that some of the other weathering indices based on major elemental data used in this study may be skewed by the relative grain-size of bulk samples. For example, bulk samples with a higher proportion of clays as a result of grain-size sorting may have a higher weathering index, even though the sediments themselves may not have undergone a greater degree of weathering than a similar coarser-grained sample. In these cases, the clay mineralogy can indicate if the weathering signal is due to an increase in chemical alteration or just an increase in the deposition of previously weathered material.

Before using SK/IC ratios as a diagnostic for weathering, it is important to first recognize that the Ganges and Brahmaputra each rivers carry unique clay signatures to begin with based on the different source lithologies through which they flow (Chapter 1 of this thesis). Illite is the dominant clay mineral in both rivers, however the Ganges carries more smectite due in large part to the influence of Deccan Trap sediments as well as pedogenic processes on the Indo-Gangetic plain (Sarin et al., 1989; Bouquillon et al., 1990; France-Lanord et al., 1993). In general,

Brahmaputra clays have greater kaolinite content than the Ganges as a result of the greater relative contribution from upland tributaries (Sarin et al.,1989; Heroy et al., 2003).

For discussion purposes in this thesis, the combined smectite and kaolinite proportion of the clay fraction is presented in lieu of SK/IC. Trends and signals are consistent between the two proxies, however, S+K% is favored here to give a more straightforward representation of how much of the clay fraction is composed of these more chemically weathered products.

2.3 Weathering proxies from major elemental data

Major element geochemistry of rocks and sediments has long been used as a tool to assess chemical weathering history. The main tenet on which these proxies are based is the sequential and preferential leaching of particular elements as chemical alteration progresses in silicate materials. Major elemental oxides can be examined against each other or in proportion to other oxides, or several oxides may be incorporated into one value known as a weathering index (or index of alteration). Typically, weathering indices are applied to soil profiles from a known parent composition to see how the geochemistry of the in situ weathered material changes through various stages of alteration; however they have been applied to a wide range of applications including inferring the weathering history of sediments and unraveling past impacts of climate change (Price and Velbel, 2003 and references therein). Three specific proxies will be used in this study and are described in more detail below.

2.3.1 Chemical Index of Alteration (CIA)

The chemical index of alteration (CIA) is one proxy used to determine the extent of chemical alteration (Nesbitt and Young, 1984; McLennan, 1993). The CIA is defined by the molar proportion of refractory Al_2O_3 against more labile major elements Ca (of the silicate fraction), K, and Na, where:

$$CIA = [Al_2O_3/(Al_2O_3 + CaO^* + Na_2O + K_2O)] \times 100$$

For the application of CIA in silicate systems, the carbonate fraction of bulk sediments is leached out of sediment and rock samples using a weak acid, ensuring that CaO left behind is

representative of the silicate portion. CaO* is used in formulas to represent CaO in only the silicate portion of the bulk sample. Insignificant degrees of weathering are noted by CIA values falling between 45 and 55 whereas values of 100 reflect the most intense chemical weathering (removal of alkali and alkaline earth elements). CIA is meant to track the extent of alteration of feldspar minerals (Nesbitt and Young, 1984; Price and Velbel, 2003), something of specific importance in this study, making it a potentially valuable tool.

2.3.2 Plagioclase Index of Alteration (PIA)

The plagioclase index of alteration (PIA) uses the same four elemental oxides as CIA, however as the name suggests, it is aimed more toward quantifying the effect of plagioclase alteration, specifically with respect to potassium feldspars via processes such as potassium metasomatism (Fedo et al., 1995). While there is no concern that deltaic sediments have been transformed by exposure to hydrothermal fluids or that extensive diagenesis has taken place, the PIA can still be used to monitor preferential weathering of plagioclase (Price and Velbel, 2003), something discussed above as important to the Sr geochemistry of these sediments. The equation for PIA is:

$$PIA = [(Al_2O_3 - K_2O)/(Al_2O_3 + CaO^* + Na_2O - K_2O)] \times 100$$

As with CIA, CaO represents the calcium only in the silicate fraction after carbonate material has been leached away. PIA values ≤ 50 reflect fresh parent material, while a value of 100 represents complete plagioclase weathering (Fedo et al., 1995). Since plagioclase is more easily weathered than potassium feldspars, this index allows inspection of the specific nature of feldspar weathering and can better indicate the state of alteration that is taking place in the deltaic samples.

2.3.3 W index

The W index uses a statistical approach with principal component analysis, and incorporates eight elemental oxides (SiO_2, TiO_2, Al_2O_3, Fe_2O_3, MgO, CaO*, Na_2O, and K_2O) as opposed to the four elements used for CIA and PIA calculation (Ohta and Arai, 2007). Results are plotted on a ternary diagram that maps geochemical variability based on fresh mafic source

material (M), fresh felsic source material (F), and weathered material (Ohta and Arai 2007). Figure 1 is a plot from Ohta and Arai (2007) that illustrates how the weathering of different fresh parent-rock lithologies are expressed by changes in the calculated W index. Some strengths of the W index are that the incorporation of multiple oxides allows for the tracking of multiple minerals in a bulk sample, rather than just the feldspar minerals quantified in CIA and PIA, and that is it applicable to a variety of rock types. For rock types that fall in the mid-range between mafic and felsic material, a W value between 14 and 20 seems to represent unweathered igneous rock, with values increasing as the amount of chemical alteration progresses (personal interpretation from Ohta and Arai (2007) figures – no specific parameters were identified in the publication). While CIA and PIA are used in this study to assess the degree of feldspar alteration for its effects on Sr geochemistry of bulk samples, the W index is applied here to assess the degree of bulk sediment weathering.

2.3.4 Limitations of weathering proxies

Any weathering proxy will be subject to limitations, and major elemental weathering indices are no exception. For instance, the CIA and PIA indices used in this study are both predicated on the immobility of aluminum during weathering, which may not always hold true (Price and Velbel, 2003 and references therein). In addition, while CIA and PIA are useful in tracking the weathering of feldspars, they must make the assumption that all the Al_2O_3, Na_2O, CaO, and K_2O are located solely in feldspar minerals, something that is clearly not reasonable in most multi-mineralic rocks (Ohta and Arai, 2007). Perhaps the most difficult hurdles to overcome in the application of these indices to mixed sedimentary environments are the reliance of these indices on the homogeneity of parent rock material and the assumption that elements will weather in a uniform and consistent manner on both spatial and temporal scales (Price and Velbel, 2003; Ohta and Arai, 2007). The W index (Ohta and Arai, 2007) addresses these issues by incorporating 8 major oxides and reducing the focus on one specific type of mineral weathering reaction. Instead, multiple mineral dissolution is tracked and therefore the W index is most applicable in discerning bulk response to chemical weathering even a broad range of parent rock types. A concern regarding the use of the W index is the incorporation of iron oxides. The mobility of iron during weathering is highly dependent on its oxidation state. Reduced Fe in the form of FeO is more mobile than the oxidized form of Fe_2O_3. An increase in

oxidized Fe indicates a greater degree of weathering; however, the greater molecular weight of Fe_2O_3 may skew an index toward a less weathered result (Price and Velbel, 2003). The effects of the oxidation state of Fe for the samples used in this study will be addressed in the results and discussion sections below.

Despite these limitations, the weathering indices still have a valuable place in unraveling the sedimentary history of the G-B deltaic sediments. CIA and PIA are used in this study because the specific weathering of feldspar minerals is of concern for the effects on bulk Sr geochemistry, while the W index is used to assess the overall weathering of the bulk sample. A multi-proxy approach to weathering will help to overcome some of the limitations of each individual proxy.

2.4 Effects of sediment sorting on $^{87}Sr/^{86}Sr$ and [Sr]

Even from a geochemically homogeneous parent rock, eroded material will not necessarily maintain that chemical homogeneity upon deposition on a floodplain following transport from the source area. Rivers carry a wide variety of sediment grain sizes, the transport and deposition of which depend on sediment parameters such as size, shape, and density of individual particles, and river hydrodynamics. The complexity of fluvial deposits are compounded in a dynamic delta such as the G-B Delta where the Brahmaputra River periodically makes dramatic course shifts to different depositional basins (most likely controlled by the active tectonics of the region; Goodbred and Kuehl, 2000a) and the Ganges has migrated along a wide swath spanning hundreds of kilometers. The seasonal nature of sediment loads, river discharge, and widespread basinal flooding driven by the monsoon climate that has varied in intensity throughout the late Quaternary add further complexity to these fluvial deposits. Of concern to the geochemical study of deposited sediments is the differentiation of minerals based on density and particle shape and size between the bed and suspended loads, as these loads are often deposited separately from one another along a river flow path. Larger, rounder, and denser mineral grains are sequestered in the bedload and are found in main channel deposits left behind as rivers widen and flow velocity slows. Smaller, flatter (such as sheet minerals like micas), and less dense mineral grains remain in the suspended load and are deposited in overbank flood deposits or even carried out to sea.

When it comes to the mineralogy of fluvial deposits, quartz, large feldspar grains (sand-sized and greater) and heavy minerals tend to be enriched in the bedload, while many secondary minerals such as clays and primary minerals such as micas (though large-grained micas can be transported as bedload as well) are enriched in the suspended load. In general, this results in more Si-bearing minerals being found in the bedload while more aluminous minerals are found in the suspended load. The simple oxide ratio of Al_2O_3/SiO_2 can be used to illustrate the effect of this grain-size differentiation on other geochemical parameters in sedimentary deposits. For example, a plot of Fe_2O_3/SiO_2 vs. Al_2O_3/SiO_2 for several modern Ganges and Brahmaputra bedload and suspended load samples shows how higher concentrations of iron and aluminum are found in the suspended load samples supporting the argument that clays and micaceous minerals are enriched there (Galy and France-Lanord, 2001; M. Singh et al., 2005). Knowing how typical grain-size sorting affects geochemical trends allows for the identification of deviations from the trend such as when bulk samples are enriched or depleted in any particular mineral. Figure 2 displays how biotite and muscovite would plot on the Fe_2O_3/SiO_2 vs. Al_2O_3/SiO_2 diagram, illustrating how enrichment in either of these minerals would be recognized in samples plotted on such a diagram. Metals such as magnesium (in an oxide as MgO), titanium (as TiO) and trace elements such as Zr can be used to identify samples enriched or depleted in heavy minerals. Care must be taken in the application of elemental ratios in mineral sorting, as many of these elements such as Mg and Fe may be lost as unstable heavy minerals are dissolved in the early stages of weathering, though it has been shown that Mg loss in a granitic soil profile does not appreciably occur until after all the biotite has been weathered away (Nesbitt et al., 1980). In instances where complete weathering of biotite is not expected, a significant MgO loss could reveal a sample depleted in heavier minerals due to mineralogical sorting. Compatible and less mobile elements such as scandium (Sc) are useful as normalizing agents in this regard (Nesbitt and Markovics, 1997; McLennan et al., 2003), and a plot of Th/Sc vs. Zr/Sc can be useful in identifying heavy mineral enrichment.

With regard to effects of sorting on the Sr geochemistry of bulk sediments, grain-size plays a role insofar as the mineralogical differentiation that occurs between suspended and bed loads during fluvial processes. Finer-grained material such as clays tend to have higher $^{87}Sr/^{86}Sr$ and [Rb]/[Sr] ratios due to the minerals such as micas that are concentrated in that grain size class, while coarser grains tend to be more enriched in Sr relative to Rb and are characterized by

relatively low $^{87}Sr/^{86}Sr$ (e.g. Eisenhauer et al., 1999). The samples analyzed in this study are derived from a variety of depositional environments such as sandy main channel, silty overbank, and distal floodbasin deposits, so it is conceivable that sorting may play a role in the mineralogy and bulk sediment Sr geochemistry of these samples.

2.5 Weathering in the modern Ganges-Brahmaputra Basin

Weathering studies in the Ganges-Brahmaputra basin and catchments have focused primarily on the effects of weathering on the dissolved load of stream waters for the purposes of (i) unraveling G-B influence on global ocean chemistry (Sr) (Krishnaswami et al 1992, Sarin et al 1989, Harris 1995, Höndorf et al, 2003; Harris et al., 1998), (ii) calculating carbon budgets and examining drawdown of atmospheric CO_2 via silicate weathering (e.g. Jacobson et al., 2002b; Galy and France-Lanord, 1999; Harris et al., 1998), and (iii) establishing exhumation rates and sediment budgets of Himalayan erosion (Galy and France-Lanord, 2001; Galy et al., 1996, Galy et al., 2010; Jacobsen et al., 2002a,b). Fewer studies have characterized the effects these processes have had on the geochemical character of the residual sediments. Of the studies that have analyzed basin sediments, most of the focus has been on the composition of clays in modern suspended load and their classification in the marine environments of the Bengal Fan with an aim toward unraveling paleoclimate signatures (e.g. Derry and France-Lanord, 1996; Sarin et al., 1989; Galy et al., 1996; Yokoyama et al. 1990).

2.5.1 Weathering effects on stream waters

On the whole, the stream water chemical compositions of the Ganges and Brahmaputra rivers are dominated by carbonate weathering while the dissolved Sr chemical compositions ([Sr] and $^{87}Sr/^{86}Sr$) in in the rivers are primarily controlled by silicate weathering (M. Singh et al., 2005; Jacobsen et al., 2002a; Jacobsen et al., 2002b; Galy et al., 1999; Krishnaswami et al., 1992). The dissolved $^{87}Sr/^{86}Sr$ flux from the G-B basin is estimated to be between 0.7213 and 0.7295, more radiogenic than the global river mean of 0.7119 (Krishnaswami et al., 1992; Galy et al., 1999). Tethyan rivers are the main source of Sr to the overall basinal flux due to erosion of Sr-rich carbonates and silicates, but the more radiogenic High Himalayan Crystalline rocks are responsible for the characteristic $^{87}Sr/^{86}Sr$ signature (Galy et al., 1999). Strontium isotope

composition is more radiogenic in the Ganges than the Brahmaptura due to the greater relative influence of High Himalayan over Tethyan lithologies (Krishnaswami et al., 1992; Galy et al., 1999). Waters of the Ganges carry a higher concentration of Sr, however the greater discharge from the Brahmaptura results in similar overall dissolved Sr flux from each river to the margin. There is seasonality to both the overall and isotopic fluxes, with an increase in radiogenic Sr but a decrease in overall Sr concentrations during the monsoon (Krishnaswami et al., 1992; Galy et al., 1999).

2.5.2 Regional weathering signature

Physical and chemical erosion is highly variable both between and within the Ganges and Brahmaputra basins (e.g. Sarin et al., 1989; Galy and France-Lanord, 1999; Singh et al., 2002; Garzanti et al., 2004; S. Singh et al., 2005; M. Singh et al., 2005; Singh et al., 2008; Singh et al., 2006; Singh, 2006; Krishnaswami et al., 1992). In the Ganges highland tributaries, carbonate weathering dominates the dissolved flux while in the lower-elevation southern tributaries draining the Indian craton, silicate weathering is more significant. This contributes to a seasonal control on weathering products transported by the mainstem Ganges. During the dry season, Ganges weathering fluxes are characterized by more chemically altered inputs from the southern tributaries and those developed on the Indo-Gangetic Plain, while during the monsoon season, high erosive fluxes from the higher-relief tributary basins cause the chemistry to be dominated by Himalayan signatures (Galy and France-Lanord, 1999; M. Singh et al., 2006). While the Ganges transports a more chemically weathered signature than the Brahmaputra, calculation of CIA in sediments from the Ganges Alluvial Plain reveal that only incipient to moderate weathering is occurring there (M. Singh et al., 2005; P. Singh, 2009). In the Bhote Kosi, the last major Himalayan tributary to the Ganges before flowing into the G-B delta, there is no evidence for incongruent mineral dissolution such as that which would preferentially release radiogenic Sr at a higher ratio the source rock (Harris et al., 1998). Taking the Ganges-Brahmaputra basin as a whole, carbonate weathering provides 76% of Sr to the dissolved load with the other 24% coming from silicate weathering (Jacobsen et al., 2002a).

While the Brahmaputra exhibits greater rates of chemical erosion as a result of greater physical erosion rates (greater average relief and annual rainfall), the intensity of chemical weathering is greater in the Ganges basin (S. Singh et al., 2005; Sarin et al., 1989). The river

floodplains have been identified as the primary location for silicate weathering based on oxygen isotopic studies of Bengal Fan clays (Derry and France-Lanord, 1996) and a comprehensive geochemical study comparing Ganges floodplain sediments to source rocks and tributary fluxes (P. Singh, 2009). The more expansive, well-developed Indo-Gangetic floodplain and influence of southern tributaries allows for greater chemical alteration to take place in the Ganges basin in contrast to the less extensive, more restricted floodplain of the Brahmaputra (Galy et al., 1999).

2.5.3 Effects of weathering on bedload and suspended load geochemistry

A study of the mineralogy of the modern Brahmaputra bedload and major tributaries shows that carbonates in the sand fraction of the sediments begin dissolving in the catchment and are completely dissolved along the Assam reach in India (Garzanti et al., 2004). There is some evidence for selective alteration of clinopyroxenes through Assam, but this should not have a significant impact on Sr geochemistry of the sediments as pyroxene makes up a very small portion of the overall sediment load (Garzanti et al., 2004) and Sr concentrations in pyroxene are typically quite low (Faure and Powell, 1972). Overall, there is only a marginal decrease in the ratio of plagioclase/total feldspar grains between the tributary basins and the Brahmaputra mainstem indicating that there is negligible preferential dissolution of plagioclase. In the heavy mineral fraction, clinopyroxenes are not more weathered than amphiboles indicating that a very low degree of alteration has taken place. CIA calculated from various tributary basins is similar to the source rocks for those basins further underscoring the overall low degree of chemical alteration (S. Singh et al., 2005). The one location where selective alteration does occur is in sediments from the Shillong Plateau. It is estimated that up to 80% of lithic and plagioclase grains are completely dissolved along with 40-45% of orthoclase (Garzanti et al., 2004). The lower relief and warmer temperatures enhance chemical weathering as shown by lower plagioclase/total feldspar ratios, pitted quartz grains, etched clinopyroxene, and greater CIA (up to 82) making the Shillong Plateau the source for the most weathered sediments to the modern Brahmaputra system (Garzanti et al., 2004; S. Singh et al., 2005).

During the monsoon and post monsoon seasons, the Brahmaputra suspended load is dominated by silt with a low proportion of <2μm clays (0.5-3%) which consist of illite and chlorite and lack smectite or kaolinite (Singh and France-Lanord, 2002). These findings imply that [Sr] and $^{87}Sr/^{86}Sr$ of these bulk sediments should not be significantly impacted by chemical

weathering, and indeed the maximum calculated exchange of Sr due to weathering is 1.5% in these modern sediments (Singh and France-Lanord, 2002). However, during the dry season, the clay composition of the suspended load changes significantly with kaolinite making up ~29% of the <4μm fraction (Heroy et al., 2003) highlighting the strong seasonal influence of sediment load composition. This greater relative influence of weathering process relative to Himalayan erosive flux during the dry season is observed in the Ganges basin as well (Galy and France-Lanord, 1999).

While for the most part the sediments carried by the two main rivers are relatively unweathered, the potential influence of Shillong sediments in localized regions such as the Sylhet basin, and the seasonal transport of weathered clays suggest that the deposition of weathered products from the catchment must be considered as well as the in-situ weathering of deltaic sediments when interpreting Holocene deposits.

Samples of river bedload in the G-B delta (including the Meghna river) surface sands throughout the basin are overall unaltered from parent material indicating that very little chemical alteration has taken place in the coarse fraction during transport through the catchment and floodplains (Huizing, 1971; Datta and Subramanian, 1997). The majority of the heavy mineral assemblage in bedload sediments is comprised of unstable minerals such as hornblende, magnetite, and illite (Datta and Subramanian, 1997). Away from the rivers, deltaic soils are considered to be young and have undergone rapid formation (Huizing, 1971). Significant alteration of feldspars and heavy minerals has not occurred in modern soils, however appreciable weather of biotite is noted in the sandy fraction of most soil samples in the delta (Huizing, 1971). Biotite loss is most noted in topsoils that have undergone repeated puddling for rice cultivation. Though rice has most likely been grown in the region for most of the Holocene (Huggan, 2005), it would not have occurred to the extent of modern cultivation so for the purposes of this study this anthropogenic impact is not taken into consideration for the Holocene sediments.

Despite a lack of extensive rice cultivation throughout the Holocene that could lead to extensive deltaic sediment weathering, the seasonal nature of the weathering signal of suspended load sediments and results of Bengal Fan clay studies underscore the importance of climate control on weathering signatures. Since climate has not remained at stable precipitation and temperature conditions throughout the Holocene, the impact of these changes warrants investigation in the deltaic sediments. In addition, there have been no comprehensive studies of

the nature of geochemical alteration in the modern floodplain sediments that are outside the realm of relatively recent active fluvial influence to determine the extent of alteration that takes place and how that affects sediment geochemistry. The extensive migration and avulsion history have allowed for portions of the delta such as the Sylhet basin to experience extended periods without active channel sedimentation (Goodbred and Kuehl, 2000a; Goodbred at al., 2003) which combined with climate variations allows for the possibility for very highly weathered sediments to be preserved in deltaic deposits.

2.6 Weathering in Holocene deltaic sediments

Only one published study has addressed the weathering of Holocene sediments throughout several regions of the Ganges-Brahmaputra delta (Heroy et al., 2003). The clay mineralogy data presented in this study have been analyzed previously as a tool to address both weathering and provenance of historical deltaic sediments (Heroy et al., 2003; Tennant 2005). The results of the previous work show that the unique clay mineralogical signatures between the Ganges and Brahmaputra rivers (as discussed above) persist throughout the Holocene, reaffirming the influence of provenance on clay signatures; however, overarching trends in mineralogy throughout the Holocene in individual boreholes are absent, and evidence for climatic influence on clay weathering mineralogy (such as an increase in IC assemblages during the early Holocene peak in monsoon intensity) is limited at best. This limitation is due in part to the influence of provenance, but another factor involves the preservation of fine-grained, weathered deposits in such a dynamic depositional basin. Neither the Ganges nor the Brahmaptura has remained geomorphically stable throughout the Holocene, with the Ganges migrating along a broad swath of the western delta and the Brahmaptura avulsing in a dramatic fashion numerous times around the Madhupur Terrace (Allison et al., 2003, Heroy et al., 2003; Goodbred and Kuehl, 2000a; Coleman, 1969). The result is that main river and distributary channels are abandoned and re-occupied periodically. Evidence exists both stratigraphically (Goodbred and Kuehl, 2000a; Goodbred et al., 2003) and geochemically (Datta and Subramanian, 1997) that reactivation of an abandoned channel or floodplain results in remobilization of the finer-grained floodplain sediments and the transport of these sediments to

the margin. Therefore, it is possible that many of these more weathered sediments are simply not preserved in portions of the delta.

While the use of clay mineralogy alone has been of limited success in assessing weathering trends associated with climatic variations in these deltaic sediments, when used in conjunction with elemental data it is a useful component of determining a comprehensive weathering history for sedimentary deposits.

III. Methods

A description of sampling and analytical techniques employed in this study are discussed in detail in Chapter 1 of this thesis.

IV. Results

4.1 Clay mineralogy

No new clay mineralogy data was collected during the course of this study, however the results from previous studies are being further interpreted in combination with illite crystallinity and major elemental data, therefore a compilation of previous results are presented here. Relative clay mineral abundances for the boreholes in this study have been compiled from Heroy et al. (2003) and Tennant (2005) and are presented in Table 1. Data was not available for BH-9. In all five boreholes, illite is the most abundant clay mineral with averages in individual boreholes ranging between 56% in BH-8 and 69% in BH-5. Kaolinite is the next most abundant mineral, followed by smectite and chlorite. The higher smectite and illite concentrations found in BH-5 are balanced by a relatively low average kaolinite concentration at ~19% followed by BH-1 at ~21%. The kaolinite composition of the rest of the boreholes averages between 26% and 37%. In all boreholes, chlorite is of low abundance and relatively invariable. The exception

is in BH-8 where there is one relatively large spike in relative chlorite abundance from zero up to 14% at 90m depth associated with a nadir of smectite. Smectite is also found in low abundance in all boreholes presented here, with the highest concentrations found in BH-5. On the whole, none of the boreholes shows any striking overall trends in clay abundance with depth. BH-7 displays the greatest amount of variability in kaolinite and illite in comparison with the other boreholes; however this could be due at least in part to the fact that BH-7 contains 2-4 times the number of data points as the other boreholes.

4.2 Illite crystallinity (Ix)

The overall borehole averages of Ix in these samples range from 0.30 to 0.45, indicating that the illite present is relatively crystallized (Figure 3). BH-1 and BH-7 have the highest averages with 0.45 and 0.42 respectively, though these values are still indicative of illite sourced from the physical weathering of primary materials (Singer, 1984; Jaboyedoff et al., 2001). There are no major overall trends within any of the boreholes with time or depth, with the exception of BH-8. In the shallower depths of BH-8, Ix values are in the range of 0.20 to 0.30 before increasing below 30m to 0.30 to 0.40 before returning to the lower values below 83.8m, indicating that illite is slightly more weathered between 30 and 84 m depth. The other data do not show such broad scale trends, however single samples deviate strongly from the mean in several boreholes. In BH-7, there are spikes in Ix value in the shallowest sample and at depths of 24.4, 39.6, and 62.5 meters. Two of these spikes at 39.6 and 62.5m are followed by lows in Ix, with variations of 0.19 and 0.2 respectively. A similar spike is seen in BH-2 at 30.5m. No such spike is recorded in BH-5, however, Ix data is sparse in the mid-depths of the borehole.

4.3 Major and trace elements

For many plots Al_2O_3/SiO_2 is used along the X-axis as a geochemical representation of grain-size and can indicate partitioning within the fluvial particulate flux with quartz and more silica-rich minerals such as feldspars concentrated in the coarser bed-load fraction, and finer-grained aluminosilicates such as micas and clay minerals concentrated in the suspended load. Al_2O_3/SiO_2 is well correlated with % clay of the bulk sediment (R^2=0.7) demonstrating that in

these samples Al_2O_3/SiO_2 is a good geochemical proxy for grain-size (Figure 4). The samples from the coarse fraction of BH-8 were not included in this figure as the geochemistry represents the sand fraction only. Since % clay has previously been reported for the total bulk sample, it was recalculated for the fine fraction (<63μm) to represent the % clay of the clay + silt fraction only.

A plot of FeO/SiO_2 vs. Al_2O_3/SiO_2 reveals the expected positive correlation with one noticeable outlier (Figure 5a). The samples that fall within the main trend are separated by grain size, showing the mineralogical sorting this type of plot is expected to reflect. The samples with the highest clay content plot with the highest FeO/SiO_2 (>0.07) and Al_2O_3/SiO_2 (>0.11) values as would be expected with the enrichment of phylosilicates in the finer grain-size fractions. The data outlier is in the fine fraction of BH-8 at 84m depth. The corresponding sample in the sand fraction at the same depth falls within the primary trend. A plot of mole % TiO_2 vs. Al_2O_3/SiO_2 reveals the same trend of greater concentrations of Ti associated with greater Al_2O_3, and again the sample at 84m depth in BH-8 is revealed to be an outlier, clearly enriched in TiO_2 Figure 5b). A plot of Th/Sc vs. Zr/Sc reveals the expected positive correlation (Figures 5c and 5d). This plot also reveals the BH-8 84m sample to be an outlier with a 10- fold enrichment in Zr. Together these plots identify this particular sample as enriched in heavy minerals to an extent not accounted for by mineralogical fractionation due to grain-size. The fact that the sand sample at the same depth does not show any signs of heavy mineral enrichment suggests that this is most likely an artifact of sampling in the lab whereby the sediment was not properly homogenized prior to sampling resulting in a non-representative sample.

4.4 Weathering indices

The weathering indices CIA, PIA, and W calculated from the major elemental data (converted to mole %) are presented in Table 5.

On the whole, low CIA values indicate that the bulk sediments in the Holocene deltaic sediments of the G-B delta have experienced a low degree of chemical alteration with most CIA values falling in the range of 50-60. The highest CIA values (67, 70) for the samples analyzed in this study are found in the shallowest portions of BH-2, a core downstream of the modern Ganges-Brahmaputra confluence on the modern flood plain and are among the finest-grained

deposits analyzed in this study. There is a CIA peak of 64 at 52m depth, also associated with a clay-rich (>35% of bulk) deposit. In BH-8 where the sediments were separated into sand and silt+clay size classes, the finer-grained portion displays higher CIA than the sands with average values of 62 and 56 respectively. The exception to this is the silt+clay sample at a depth of 84m with a CIA of 54, however this sample has already been identified as an outlier based on heavy mineral enrichment, most likely an artifact of sampling as discussed above. The correlation of CIA with grain size suggests a first order control of grain size on bulk weathering signature (Figure 6). Of the bulk sediment samples BH-1 has a slightly higher average CIA than BH-2 and BH-5 (58 vs. 54 and 52 respectively) which may reflect the overall greater portion of clay in the bulk sample (with the exception of the surface 18m of BH-2). It should be noted that the highest calculated values of CIA in this study still fall within the range of low-moderate chemical alteration (McLennan, 1993) indicating that even the most weathered sediments have not been significantly altered.

The calculated PIA for samples in this study follows the same trend in CIA which is expected given their similar parameters of calculation and that both indices focus on feldspar weathering. Since plagioclase is more easily weathered than potassium feldspars, a plot of PIA vs. CIA reveals samples in which preferential alteration of plagioclase has taken place. For the data presented here, CIA and PIA are highly correlated ($R^2 = 0.99$) (Figure 7). The exception is one sample at 61m in BH-8, the sand fraction. This sample has a higher PIA with respect to CIA than the other samples. The calculated difference based on the trend with CIA is approximately 4% indicating that some preferential dissolution of plagioclase may have taken place.

4.4.1 Effects of Fe oxidation state on the W index

In order to assess the importance of the oxidation state of iron on the W index, two sets of calculations were made, one assuming all Fe was in the form of FeO and one assuming all Fe was in Fe_2O_3. Both sets of data are plotted in Figure 8. Assuming all iron is in the form FeO yields results that appear ≤ 8% more mafic and up to 8% more weathered than if all Fe is assumed to be in Fe_2O_3. This is most likely an artifact of the greater molecular weight of Fe_2O_3 rather than a true indication of weathering as iron oxidation should increase as weathering of sediments progresses. Since the relative relationships between samples are preserved regardless of the oxidation state used and iron data reported in this study is in the form of reduced Fe, FeO

will be used for total iron in all calculations involving this data and data taken from other studies for comparison purposes will be converted to FeO.

V. Discussion

5.1 Mineralogical sorting

While the Th/Sc vs. Zr/Sc and the heavy metal plots discussed above (Figure 5) are useful in identifying outliers and heavy mineral enrichment, this study is still concerned with assessing the degree of mineralogical sorting of deltaic sediments overall, and the effects that this sorting may play on the Sr geochemistry of the sediments. Plots of Sr concentration against alkali and alkaline earth metals (Figure 9) reveal the strongest correlation between Ca and Sr (Figure 9a). This is not surprising given that they are both alkaline earth elements and that Sr readily substitutes for Ca in silicate minerals. Progressively weaker trends found in plots of [Sr] vs. Na_2O /SiO_2 (Figure 9b) and K_2O/SiO_2 (Figures 9c and 9d) reveal that Sr is less correlated with Na and K plagioclase endmembers, indicating that most Sr is located in the Ca-rich plagioclase endmembers (e.g. anorthite) which is to be expected given the mineralogy of the source regions as discussed in the background section of this chapter. The weakest trend is noted between Sr and K_2O, where the data actually seems to plot in a few distinct groupings with individual trends. Overall, BH-1 displays very little variation in Sr concentration, while BH-2 along with most of the samples in BH-8 (with the exception of samples at 61m, 91.5m, and 107m depth in the coarse fraction and at 76m depth in the fine fraction), and two of the BH-5 samples display a negative trend suggesting the influence of some other factor on the relationship between Sr and K.

A plot of K_2O/SiO_2 vs. Al_2O_3/SiO_2 (Figure 10a) reveals a strong correlation and suggests partitioning of K along grain-size fractions, with higher concentrations in the finer-grained aluminosilicates. Such a strong correlation does not exist with silicate CaO (Figure 10b). Different boreholes seem to exhibit different trends with no correlation apparent in BH-1, a positive correlation in BH-8 with a slight offset between the coarse and fine fractions, and a

seemingly negative correlation in BH-2. While this does not mean that Ca in the deltaic sediments is not affected at all by mineralogical sorting, it does suggest a complexity in calcium distribution (perhaps due to provenance overprinting) beyond aluminum/silica partitioning.

There is no overarching positive or negative trend that encompasses the relationship between Sr and Al_2O_3/SiO_2 (Figure 11). Samples are separated out into three groups based on [Sr] underscoring the first order control of provenance on Sr geochemistry of these sediments. Within the most concentrated group of samples (encompassing all of BH-2 and much of BH-8) a trend of decreasing [Sr] with decreasing grain-size becomes apparent for the finest-grained samples as would be expected based on normal mineral partitioning between bed and suspended loads in an active stream. The data do not indicate that any extensive chemical alteration has taken place, and within the sand fraction, grain-size exerts no control on Sr concentrations. Despite the trend of Sr-depletion in the finest grain-size samples, the provenance signal is preserved, with even the most clay-rich sediments still plotting within initial provenance limits of [Sr]. Furthermore, when taking into account sedimentological facies and even more robust provenance indicators such as $^{87}Sr/^{86}Sr$, these apparently depleted samples are believed to be a mixture of sediments from different provenance sources that would result in an apparent depletion of [Sr] with fining grain-size (discussed in Chapter 3 of this dissertation). In any event, the data here show that any depletion in [Sr] associated with finer grains is likely to be due to typical bedload/suspended load stream sorting, and is not occurring to a degree that would obscure initial provenance signals.

While there may be evidence for some secondary control of sorting on [Sr], this is not true for the isotopic signature of the sediments (Figure 11) which shows no trend at all within each borehole or among the entire dataset used in this study. This illustrates that Sr isotopic signatures of these samples remain stable through the bedload/suspended load partitioning of minerals and are not impacted by fluvial sorting processes in this case.

This dominance of provenance over sorting in controlling geochemical character is seen in Rb/Sr ratios as well. The Rb/Sr ratio increases as the extent of chemical alteration increases, therefore we would expect a positive correlation with Al_2O_3/SiO_2 with higher Rb/Sr in sediments in the suspended load. There is significant variation in Rb/Sr ratio between the different boreholes. The greatest average value of 1.33 is found in the coarse fraction of BH-8 below 92m depth and the lowest average is in the upper 92m of BH-8 with a value of 0.75. The finer

fraction has a slightly higher average of 0.84 excluding the sample at 84m which has been identified as an outlier (Figure 5a). Ratios display a positive correlation to Al_2O_3/SiO_2 within each borehole indicating that grain-size and mineralogical sorting exert control on Rb/Sr in the expected trend of higher ratios reflected in more weathered (Al-rich) material, yet all boreholes do not plot together in a unified trend, illustrating the significant overprint of provenance signature on the Rb/Sr ratio (Figure 12).

5.2 Bulk sediment weathering

For the Brahmaputra River and tributaries, there is a good catalog of modern sedimentary geochemical character that is used for comparison with the Holocene and latest Pleistocene sediments in this study (Singh and France-Lanord, 2002; van Geen et al., 2008). The data are split into different groups based on their geochemistry: the main channel sediments of the Brahmaputra/Siang river, the sediments derived from the Himalayan Tributaries (those draining Himalayan rocks directly), the southern/eastern tributaries which include the Mishmi Hills, the Indo-Burma ranges, and the Shillong Plateau. Because of its unique geochemical character compared to the other Himalayan tributaries, the Tista River is plotted on its own.

Using the MFW plot the main channel sediments are characterized by relatively low-weathered sediments trending toward the mafic axis, M, a result of the influence of mafic material eroded from the Transhimalayan Plutonic Belt (TPB), while the Tista sediments, also relatively unweathered, trend toward the felsic axis, F (Figure 13). The Himalayan tributaries are slightly more weathered (with higher W values) and fall between the mafic main channel sediments and the felsic Tista sediments. The Eastern/Southern tributaries appear to be much more weathered than the other samples with the highest W values over all, which would be expected given the lower relief, high rainfall and warmer temperatures experienced in regions such as the Shillong Plateau. It is not surprising that the mainstem sediments would display a less weathered signature in this case, as 40-50% of the sediments are derived from the relatively young, fresh rocks of the rapidly uplifting eastern syntaxis region (Garzanti et al., 2004; Singh et al., 2006; Galy and France-Lanord, 2001).

On first glance we note that in terms of weathering index, that none of the samples measured in this study have higher values than the samples collected from the modern

Brahmaputra/Siang and tributaries. This information combined with the clay data and other major elemental data tells us that the samples in the delta are likely no more weathered than the sediments coming out of the drainage basins or carried by the river(s). This would suggest no discernible alteration is taking place post deposition and burial. A closer look at how the samples plot with respect to fresh unweathered rock is shown in Figure 14, where different zones of weathering intensity are highlighted based on the parameters outlined in Ohta and Arai (2007). The samples that fall within these two zones have undergone little to no chemical alteration based on the W index (where proportionate W value is less than 25). The samples beyond this region (W>25) have experienced slight to moderate chemical alteration and include all of the fine-grained samples from BH-8 (relative clay composition >15%), and samples from BH-1 and BH-2 with clay contents also ≥15%. These results further underscore the control of grain size on bulk weathering signatures.

5.3 Preferential weathering of biotite

In the coarser-grained bulk sediments there is a positive correlation between MgO/Al_2O_3 and Al_2O_3/SiO_2 (Figure 15) indicating that Mg-rich minerals (such as biotite) become concentrated in the finer grained suspended as expected. However, for samples with Al_2O_3/SiO_2 > 0.11 this correlation breaks down and samples appear depleted in MgO. This significant depletion in MgO, especially in the finest fractions may represent significant loss of biotite, which can have a substantial impact on Sr isotopic signature. However, these same samples do not display any change in isotopic character above an Al_2O_3/SiO_2 value of 0.11 (Figure 12), so preferential weathering of biotite, which may be occurring in the finest grain fractions, is not impacting the Sr isotopic character of the bulk sediment, even when clay concentrations are >20%.

5.4 Weathering of the clay fraction

The clay data presented here serve to draw generalized conclusions about the weathering condition of the fine grained material and the overall extent of chemical alteration that has taken place. Since clays are a by-product of weathering and naturally carry a more chemically altered

signal than the coarser sand and silt fractions of a given bulk sample, it stands to reason that bulk sediments with higher clay content would exhibit a greater degree of chemical weathering signatures using geochemical proxies. Indeed, this trend is evident in the samples presented here.

In all boreholes, there is considerable variation of approximately 20% in S+K%. The exception to this is BH-7 where variation is on the order of 40%, however overall clay abundance in this borehole is significantly less than in other boreholes (an average of 2.2% total clay content in the channel sand deposits). There are no discernable trends however in the clay data that would suggest periods of more intense chemical alteration preserved in the sedimentary deposits. This is true even in the thickest fine-grained deposit analyzed in this study in the upper 18m of BH-2. Here total clay content averages 35.7% of total sediment composition with a peak value of 60% at 7.6m depth. As would be expected with increasing clay content, the weathering indices for the two samples analyzed within this deposit (9.1m and 13.7m depth) are higher than average for the rest of the borehole. The CIA values for these two samples are 70 and 73 whereas that average for other samples in the borehole is 59. Likewise, their proportional W value is 38 compared with 17 for the rest of the borehole. Despite this greater weathering signal, the average S+K is ~30%, which is the same as the rest of the borehole, and Ix is similar with values of 0.34 and 0.32 respectively above and below the 18m depth mark. The same conclusions are drawn from the 20m-thick fine-grained interval centered around 50m depth in BH-1 where no difference is noted in Ix or S+K compared to the rest of the borehole. These data indicate that even over prolonged periods of quiescent deposition there is no discernable formation of secondary minerals taking place within the delta. Instead, apparent weathering trends are a function of overall grain-size (specifically clay content) related to hydrologic sorting, and the delta is simply preserving signatures of weathering that have occurred farther upstream in the catchment.

Though chemical alteration is not occurring within the deltaic sediments, the concern remains that weathering upstream in the catchment may affect the Sr isotope composition of the sediments presenting complications for provenance analysis. For the three boreholes in this study where clay data and Sr geochemical data were available for identical samples, there is no correlation between S+K% and either Sr concentrations or $^{87}Sr/^{86}Sr$ signature of the bulk sample (Figure 16). The lack of trends in these data show that even for sediments that have experienced

a greater degree of alteration and secondary mineral formation, there has not been a measurable loss of Sr from initial whole rock concentrations, nor has the isotopic signature been affected. Therefore provenance signals in sediments transferred from tributary basins are preserved in deltaic sediments with no appreciable alteration.

VI. Conclusions

With regard to mineral partitioning between different grain-size classes due to hydrologic sorting there are no unexpected enrichments or depletions of any major minerals. Mineralogical or grain-size sorting does not affect $^{87}Sr/^{86}Sr$ signatures, and while there is evidence for Sr depletion in finer grained samples, the variation in provenance signatures is great enough that this depletion does not affect source determination. Overall there is no evidence for significant preferential weathering of feldspars. There is evidence to suggest preferential dissolution of biotite in the finest-grained samples, yet there is no discernable effect on sediment Sr geochemistry due to this phenomenon.

Sediments composed primarily of sand and silt do not display any significant weathering signatures that would indicate any type of alteration has taken place either in the catchment or within the delta. Sands preserve unaltered source rock provenance signals. Bulk sediments composed of >15% clay display more weathered values for weathering indices such as CIA and W, but this is not the result of any chemical alteration or secondary mineral formation that is taking place within the delta. Analysis of clay data reveals that these trends are due in fact to hydrologic sorting and the preservation of catchment weathering signals in the delta.

These data presented here show that there is no post-depositional alteration of Holocene deltaic sediments. Any weathering signals that are noted are due to processes that occurred in the catchment or farther upstream on the individual river floodplains. Hydrologic sorting does exert a control on apparent weathering signatures of bulk sediments, but even for the most weathered sediments preserved in Holocene deposits, alteration has not occurred to such a degree as to significantly alter the Sr geochemistry. Therefore, [Sr] and $^{87}Sr/^{86}Sr$ may be confidently used to address the provenance of bulk deltaic sediments.

References

Blum, J.D., Erel, Y., 1997. Rb-Sr isotope systematics of a granitic soil chronosequence: The importance of biotite weathering. Geochimica et Cosmochimica Acta 61, 3193-3204.

Bouquillon, A., France-Lanord, C., Michard, A., Tiercelin, J.J.,1990. Sedimentology and isotopic chemistry of the Bengal Fan sediments: the denudation of the Himalaya. Proceedings of the Ocean Drilling Program. Scientific Results, vol. 116, 43– 58.

Coleman, J.M., 1969. Brahmaputra river: channel processes and sedimentation. Sedimentary Geology 3, 129-239.

Curtis, C.D., 1990. Aspects of climate influence on the clay mineralogy and geochemistry of soils, paleosols and clastic sedimentary rocks. Journal of the Geological Society, London 147, 351-357.

Dasch, E.J., 1969. Strontium isotopes in weathering profiles, deep-sea sediments, and sedimentary rocks. Geochimica et Cosmochimica Acta 33, 1521-1552.

Datta, D.K., Subramanian, V., 1997. Texture and mineralogy of sediments from the Ganges-Brahmaputra-Meghna river system in the Bengal Basin, Bangladesh and their environmental implications. Environmental Geology 30, 181-188.

Derry, L.A., France-Lanord, C., 1996. Neogene Himalayan weathering history and river $^{87}Sr/^{86}Sr$: impact on the marine Sr record. Earth and Planetary Science Letters 142, 59-74.

Egashira, K., Aramaki, K., Yoshimasa, M., Takeda, A., Yamasaki, S., 2004. Rare earth elements and clay minerals of the soils of the floodplains of three major rivers in Bangladesh. Geoderma 120, 7-15.

Eisenhauer, A., Meyer, H., Rachold, V., Tuetken, T., Wiegand, B., Hansen, B.T., Spielhagen, R.F., Lindemann, F., Kassesn, H., 1999. Grain size separation and sediment mixing in Arctic Ocean sediments: evidence from the strontium isotope systematic. Chemical Geology 158, 173-188.

Evans, L.J., 1992. Alteration products at the earth's surface – the clay minerals. In: Martini, I.P., Chesworth, W., (Eds.) Weathering, Soils, and Paleosols (Developments in Earth Surface Processes). Elsevier Science, 107-125.

Faure, G., Powell, J.L., 1972. Strontium isotope geology. Springer-Verlag, New York, 197 pp.

Fedo, C.M., Nesbitt, H.W., Young, Grant, M., 1995. Unraveling the effects of potassium metasomatism in sedimentary rocks and paleosols, with implications for paleoweathering conditions and provenance. Geology 23, 921-924.

France-Lanord C., Derry L.A. and Michard A. (1993). Evolution of the Himalaya since Miocene time: Isotopic and sedimentologic evidence from the Bengal Fan. In: Treloar, P.J., Searle, M. (Eds) Himalayan Tectonics, Geological Society of London Special Publication 74, 605-623.

Galy, A, France-Lanord, C, Derry, L.A., 1996. The Late Oligocene-Early Miocene Himalayan belt Constraints deduced from isotopic compositions of Early Miocene turbidites in the Bengal Fan. Tectonophysics 260, 109-118.

Galy, A., France-Lanord, C., 1999. Weathering processes in the Ganges-Brahmaputra basin and the riverine alkalinity budget. Chemical Geology 135, 31-60.

Galy, A., France-Lanord, C., 2001. Higher erosion rates in the Himalaya: Geochemical constraints on riverine fluxes. Geology 29, 23-26.

Galy, V., France-Lanord, C., Peucker-Ehrenbrink, B., Huyghe, P., 2010. Sr-Nd-Os evidence for a stable erosion regime in the Himalaya during the past 12 Myr. Earth and Planetary Science Letters 290, 474-480.

Gardner, R., Walsh, N., 1996. Chemical weathering of metamorphic rocks from low elevations in the southern Himalaya. Chemical Geology 127, 161-176.

Garzanti, E., Vezzoli, G., Andò, S., France-Lanord, C., Singh, S.K., Foster, G., 2004. Sand petrology and focused erosion in collision orogens: the Brahmaputra case. Earth and Planetary Science Letters 230, 157-174.

Goodbred Jr., S.L., Kuehl, S.A., 2000a. The significance of large sediment supply, active tectonism, and eustasy on margin sequence development: Late Quaternary stratigraphy and evolution of the Ganges-Brahmaputra delta. Sedimentary Geology 133, 227-248.

Goodbred, Jr., S.L., Kuehl, S.A., Steckler, M., and Sarker, M.H., 2003. Controls on facies distribution and stratigraphic preservation in the Ganges-Brahmaputra delta sequence. Sedimentary Geology 155, 301-316.

Harris, N., 1995. Significance of weathering Himalayan metasedimentary rocks and leucogranites for the Sr isotope evolution of seawater during the early Miocene. Geology 23, 795-798.

Harris, N., Bickle, M., Chapman, H., Fairchild, I., Bunbury, J., 1998. The significance of Himalayan rivers for silicate weathering rates: evidence from the Bhote Kosi tributary. Chemical Geology 144, 205-220.

Heroy, D.C., 2000. Sand- and clay-size mineralogy of the Ganges and Brahmaputra rivers: records of river switching and Late Quaternary climate change. Masters Thesis, William and Mary, Virginia Institute of Marine Science, Gloucester Point, VA, 65pp.

Heroy, D.C., Kuehl, S.A., Goodbred Jr., S.L., 2003. Mineralogy of the Ganges and Brahmaputra Rivers: implications for river switching and Late Quaternary climate change. Sedimentary Geology 155, 343-359.

Huggan, R.D., 2005. Co-evolution of rice and humans. GeoJournal 35, 262-265.

Huizing, H.G.J., 1971. A reconnaissance study of the mineralogy of sand fractions from East Pakistan sediments and soils. Geoderma 6, 109-133.

Jaboyedoff, M., Bussy, F., Kübler, B., Thelen, Ph., 2001. Illite "crystallinity" revisited. Clays and Clay Minerals 49, 156-167.

Jacobson, A.D., Blum, J.D., Walter, L.M., 2002a. Reconciling the elemental and Sr isotope composition of Himalayan weathering: Insights from the carbonate geochemistry of stream waters. Geochimica et Cosmochimica Acta 66, 3417-3429.

Jacobson, A.D., Blum, J.D., Chamberlain, C.P., Poage, M.A., Sloan, V. F., 2002b. Ca/Sr and Sr isotope systematics of a Himalayan glacial chronosequence: Carbonate versus silicate weathering rates as a function of landscape surface age. Geochimica et Cosmochimica Acta 66, 13-27.

Krishnaswami, S., Trivedi, J.R., Sarin, M.M., Ramesh, R., Sharma, K.K., 1992. Strontium isotopes and rubidium in the Ganga-Brahmaputra river system: Weathering in the Himalaya, fluxes to the Bay of Bengal and contributions to the evolution of oceanic $^{87}Sr/^{86}Sr$. Earth and Planetary Science Letters 109, 243-253.

McLennan, S.M., 1993. Weathering and Global Denudation. The Journal of Geology 101, 295-303.

McLennan, S. M., Hemming, S., McDaniel, D. K., Hanson, G. N., 1993. Geochemical approaches to sedimentation, provenance and tectonics. In: M. J. Johnsson and A. Basu (Eds.) Processes controlling the composition of clastic sediments. Geological Society of America Special Paper 284, 21-40.

McLennan, S.M., Bock, B., Hemming, S.R., Hurowitz, J.A., Lev, S.M., McDaniel, D.K., 2003. The roles of provenance and sedimentary processes in the geochemistry of sedimentary rocks. In Lentz, D.R., ed., Geochemistry of Sediments and Sedimentary Rocks: Evolutionary Considerations to Mineral Deposit-Forming Environments: Geological Association of Canada, GeoText 4, 7-38.

Nesbitt, H.W., Markovics, G., Price, R.C., 1980. Chemical processes affecting alkalis and alkaline earths during continental weathering. Geochimica et Cosmochimica Acta 44, 1659-1666.

Nesbitt, H.W., Young, G.M., 1984. Prediction of some weathering trends of plutonic and volcanic rocks based on thermodynamic and kinetic considerations. Geochimica et Cosmochimica Acta 48, 1523-1534.

Nesbitt, H.W., Markovics, G., 1997. Weathering of granodioritic crust, long-term storage of elements in weathering profiles, and petrogenesis of siliciclastic sediments. Geochimica et Cosmochimica Acta 61, 1653-1670.

Ohta, T., Arai, H., 2007. Statistical empirical index of chemical weathering in igneous rocks: A new tool for evaluating the degree of weathering. Chemical Geology 240, 280-297.

Palmer, M.R., Edmond, J.M., 1992. Controls over the strontium isotope composition of river water. Geochimica et Cosmochimica Acta 56, 2099-2111.

Price, J.R., Velbel, M.A., 2003. Chemical weathering indices applied to weathering profiles developed on heterogeneous felsic metamorphic parent rocks. Chemical Geology 202, 397-416.

Sarin, M.M., Krishnaswami, S., Dilli, K., Somayajulu, B.L.K., Moore, W.S., 1989. Major ion chemistry of the Ganges-Brahmaputra river system: Weathering processes and fluxes to the Bay of Bengal. Geochimica et Cosmochimica Acta 53, 997-109.

Singer, A., 1984. The paleoclimatic Interpretation of Clay Minerals in Sediments – A Review. Earth Science Reviews 21, 251-293.

Singh, M., Sharma, M., Tobschall, H.J., 2005. Weathering of the Ganga alluvial plain, northern India: Implications from fluvial geochemistry of the Gomati River. Applied Geochemistry 20, 1-21.

Singh, P., 2009. Major, trace and REE geochemistry of the Ganga River sediments: Influence of provenance and sedimentary processes. Chemical Geology 266, 251-264.

Singh, P., 2010. Geochemistry and provenance of stream sediments of the Ganga River and its major tributaries in the Himalayan region, India. Chemical Geology 269, 220-236.

Singh, S.K., France-Lanord, C., 2002. Tracing the distribution of erosion in the Brahmaputra watershed from isotopic compositions of stream sediments. Earth and Planetary Science Letters 6341, 1-18.

Singh, S.K., Sarin, M.M., France-Lanord, C., 2005. Chemical erosion in the eastern Himalaya: Major ion composition of the Brahmaputra and $\delta^{13}C$ of dissolved inorganic carbon. Geochimica et Cosmochimica Acta 69, 3573-3588.

Singh, S.K., Kumar, A., France-Lanord, C., 2006. Sr and $^{87}Sr/^{86}Sr$ in waters and sediments of the Brahmaputra river system: Silicate weathering, CO_2 consumption and Sr flux. Chemical Geology 234, 308-320.

Singh, S.K., 2006. Spatial variability in erosion in the Brahmaputra basin: causes and impacts. Current Science 90, 1272-1276.

Singh, S.K., Santosh, K.R., Krishnaswami, S., 2008. Sr and Nd isotopes in river sediments from the Ganga Basin: Sediment provenance and spatial variability in physical erosion. Journal of Geophysical Research 113, F03006, 18pp.

Tennant, E., 2005. Late Quaternary climate and provenance signals of the Ganges-Brahmaputra Delta Plain, Bangladesh. Honors Thesis, William and Mary, Williamsburg, VA.

vanGeen, A., Zheng, Y., Goodbred Jr., S., Horneman, A., Aziz, Z., Cheng, Z., Stute, M., Mailloux, B., Weinman, B., Hoque, M.A., Seddique, A.A., Hossain, M.S., Chowdhury, S.H., Ahmed, K.M., 2008. Flushing history as a hydrogeological control on the regional distribution of arsenic in shallow groundwater of the Bengal Basin. Environmental Science and Technology 42, 2283-2288.

Yokoyama, K., Amano, K., Taira, A., Saito, Y., 1990. Mineralogy of silts from the Bengal Fan. In: Cochran, J.R., Stow, D.A.V., et al., *Proc. ODP, Sci. Results,* 116: College Station, TX (Ocean Drilling Program), 59–73.

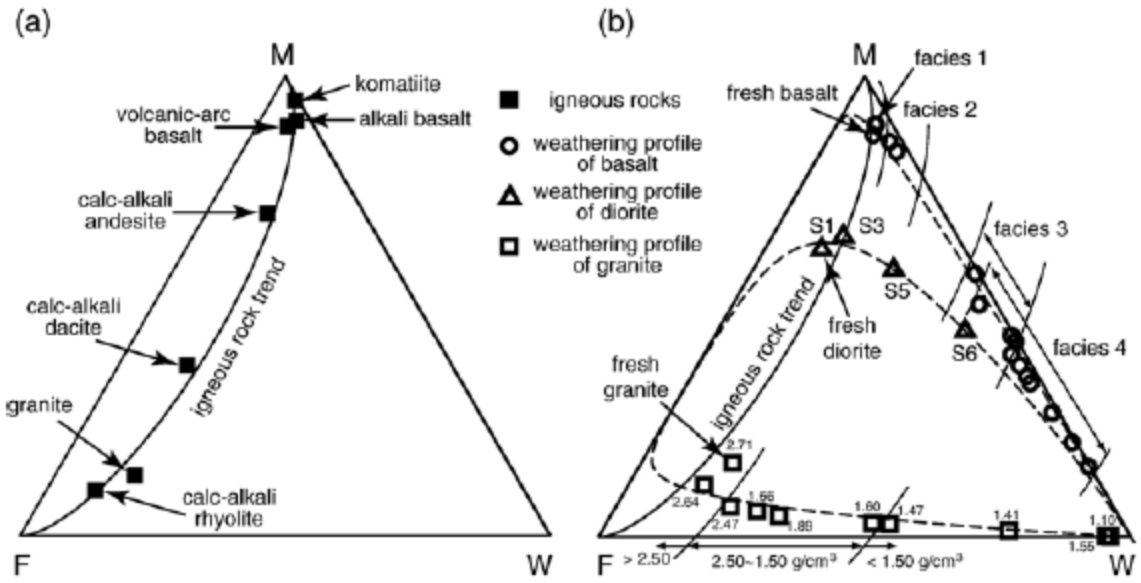

Figure 1. From Ohta and Arai (2007). Weathering paths of several fresh igneous rock types on the MFW diagram: (a) a variety of fresh rock types; (b) linear trend of weathering profiles for some rock types.

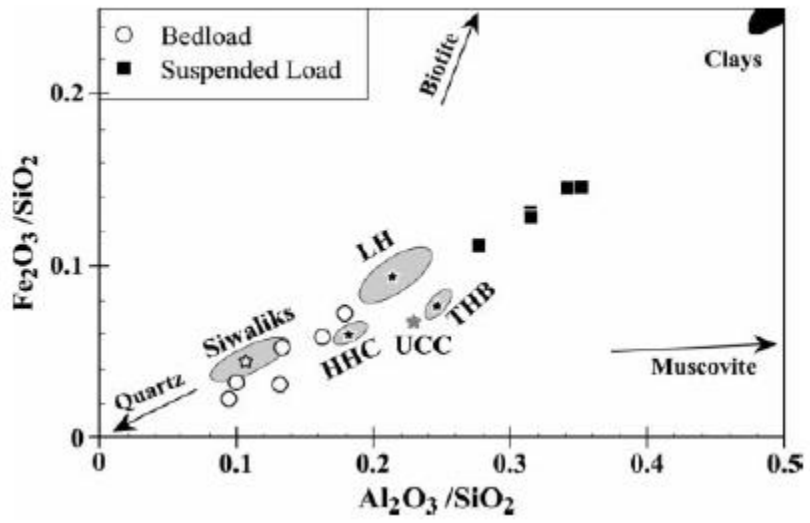

Figure 2. From Galy and France-Lanord (2001). Partitioning of elements among different grain-size classes and expected trends of mineralogical sorting on bulk sediment elemental ratios. Iron concentrations are relatively higher in finer-grained material. In addition, the enrichment of Fe in biotite and enrichment of Al in muscovite are demonstrated.

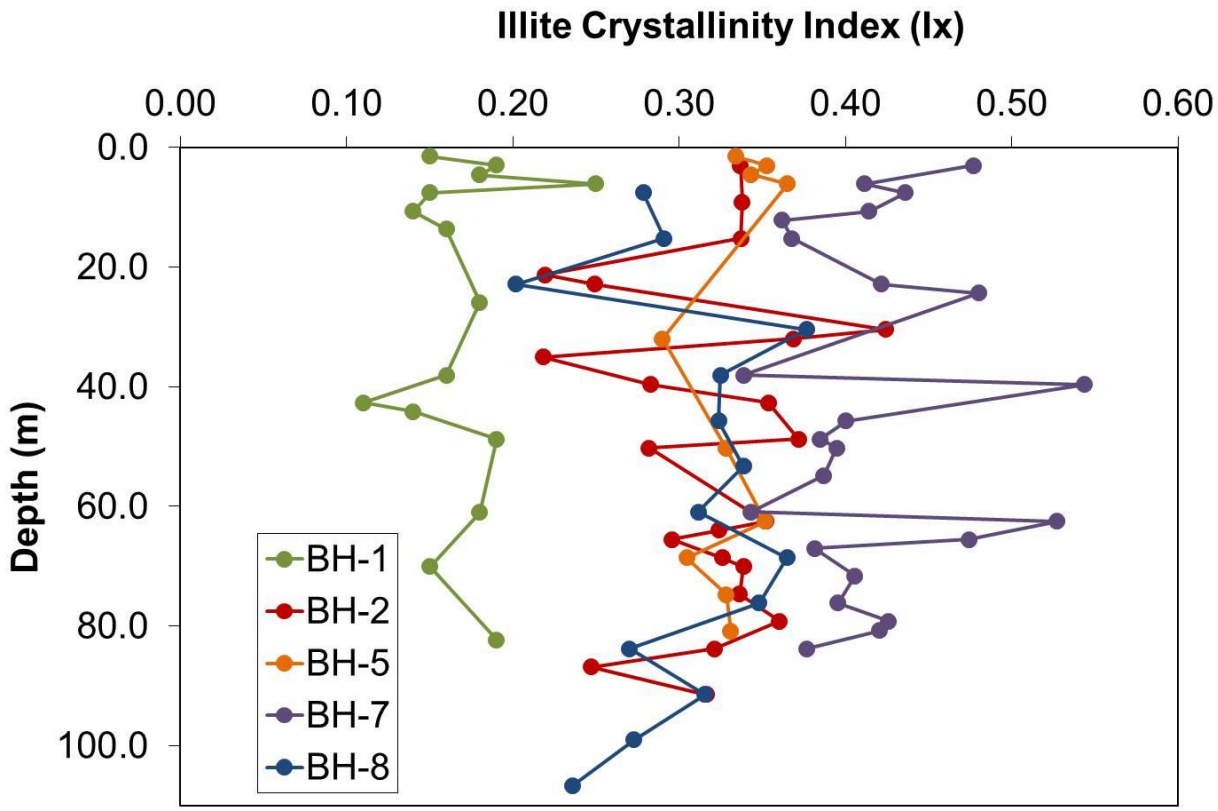

Figure 3. Profiles of illite crystallinity index (Ix) with depth for the boreholes used in this study. Note that Ix for BH-1 was calculated using different parameters which explains the offset from the other boreholes.

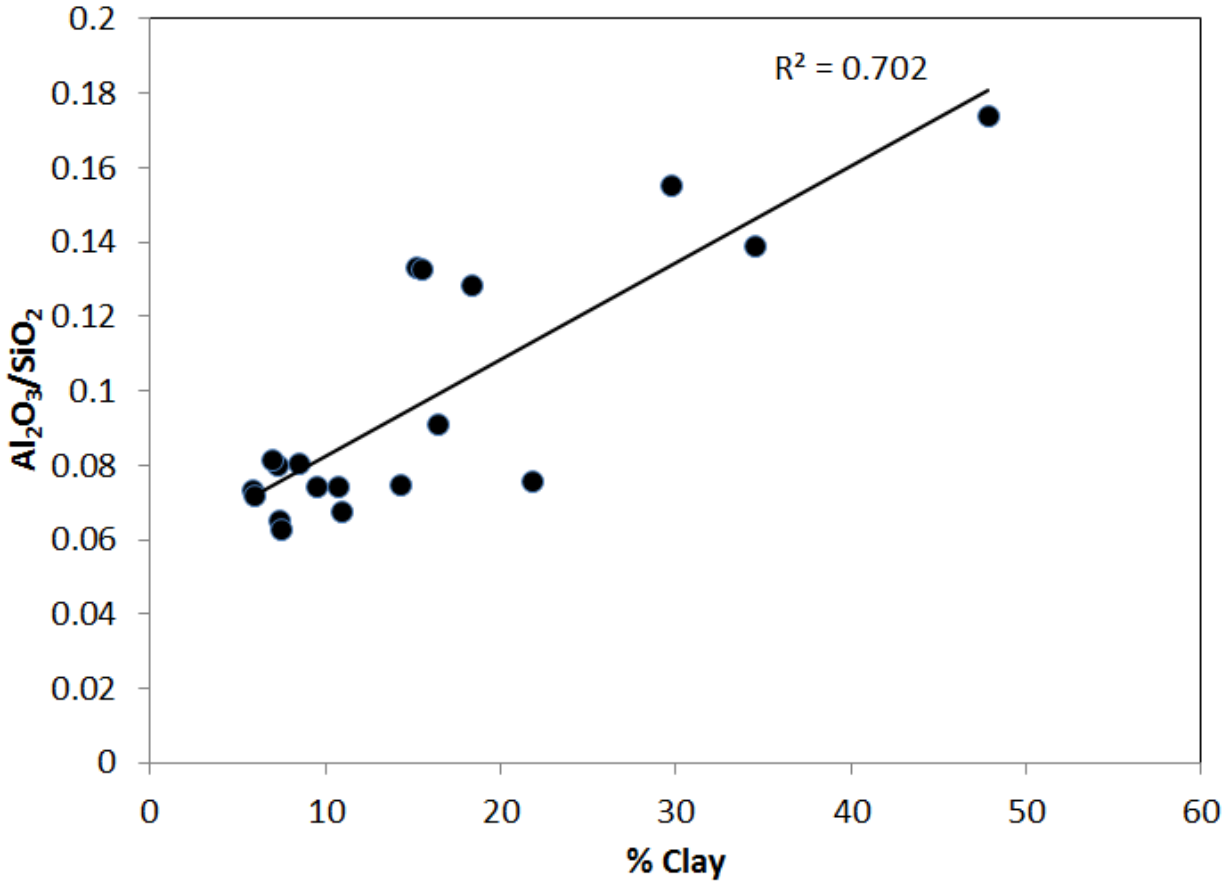

Figure 4. Correlation of clay content with Al_2O_3/SiO_2 of bulk sample shows that Al_2O_3/SiO_2 is a good cheochemical approximate for sample texture with higher Al_2O_3/SiO_2 indicating more clay content or overall finer grain size.

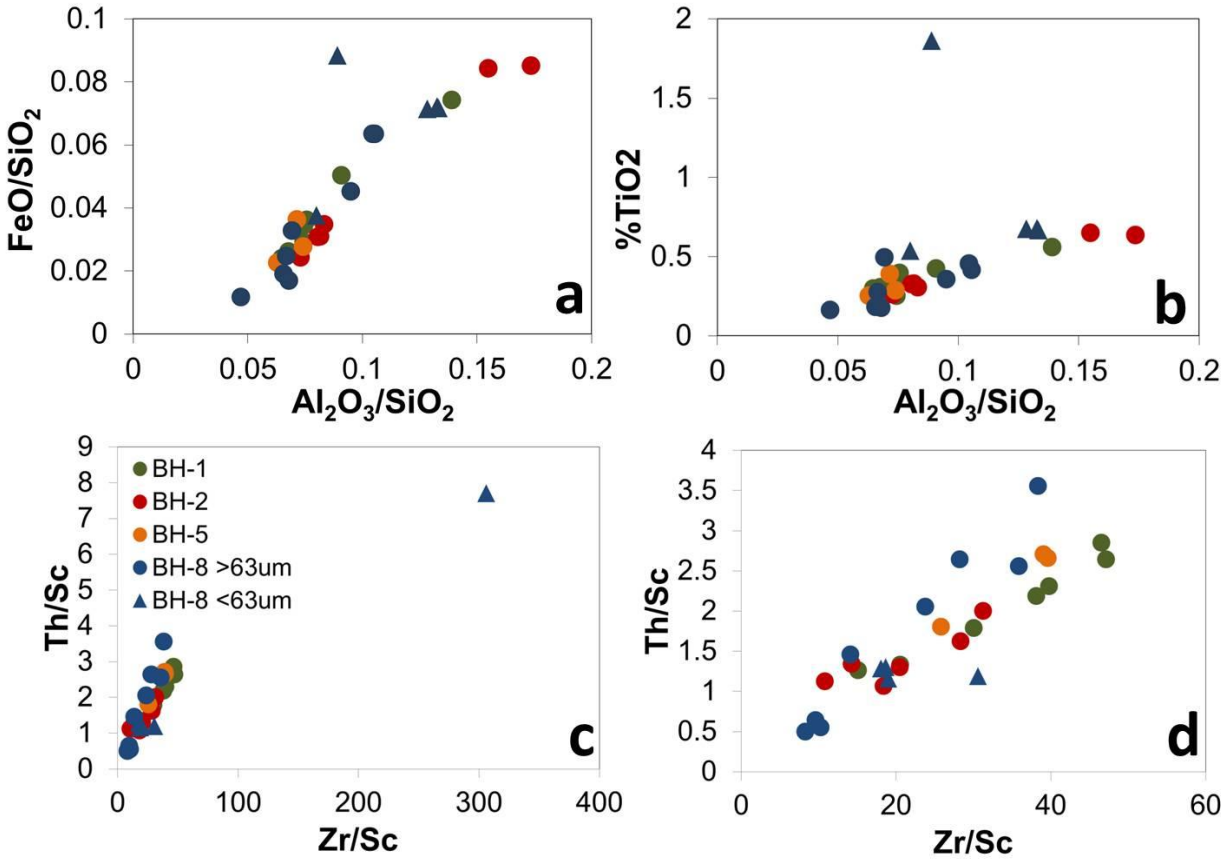

Figure 5. Plots of important major and trace elemental ratios for depiction of mineralogical sorting. In (a) and (b) increasing concentrations of heavy metals with increasing relative Al indicates enrichment of heavy minerals in the finer-grained (more weathered) fraction. Enrichment or depletion in FeO or TiO_2 indicates enrichment in biotite due to mineralogical sorting or preferential dissolution of biotite respectively, (a), (b). Th/Sc vs. Zr/Sc are also used to identify heavy mineral enrichment (c). Data with the outlier removed shown in (d). The sample outlier showing enrichment in FeO, TiO_2, and Zr appears to be the result of non-homogeneous sampling in the lab and is not a reflection of true bulk sediment geochemistry.

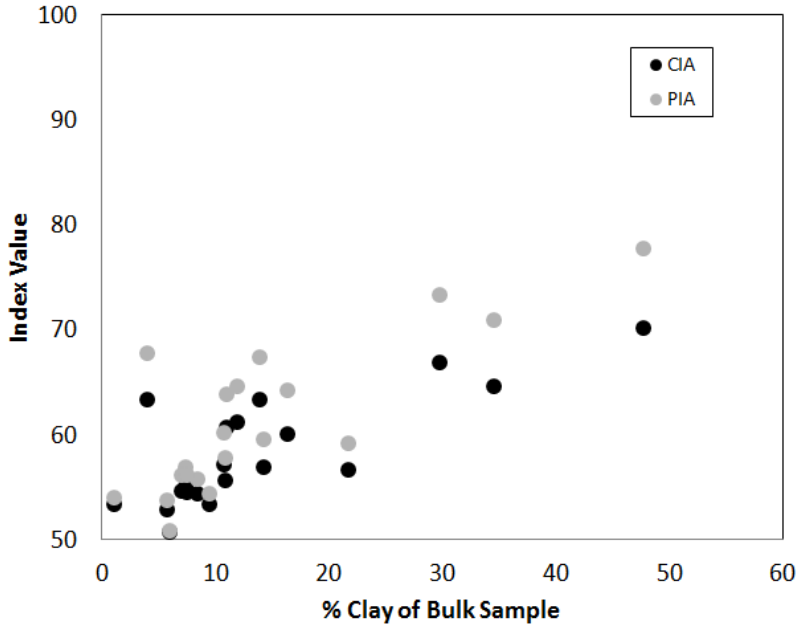

Figure 6. Plot of two weathering indices, PIA and CIA with % clay illustrating the control of grain-size on overall weathering signature.

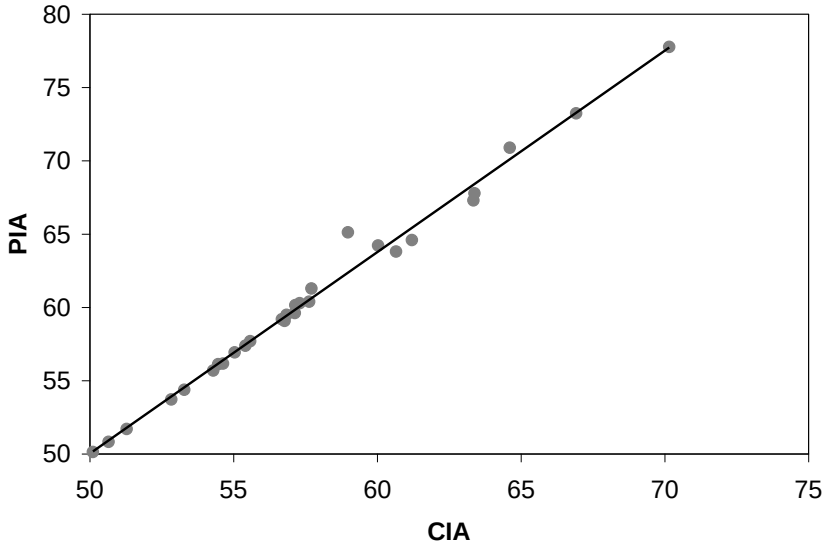

Figure 7. Plot of PIA (plagioclase index of alteration) vs. CIA (chemical index of alteration) used to identify samples that have undergone preferential dissolution of plagioclase with respect to total feldspars. Only one sample (61 m depth in BH-8) deviates from the trend.

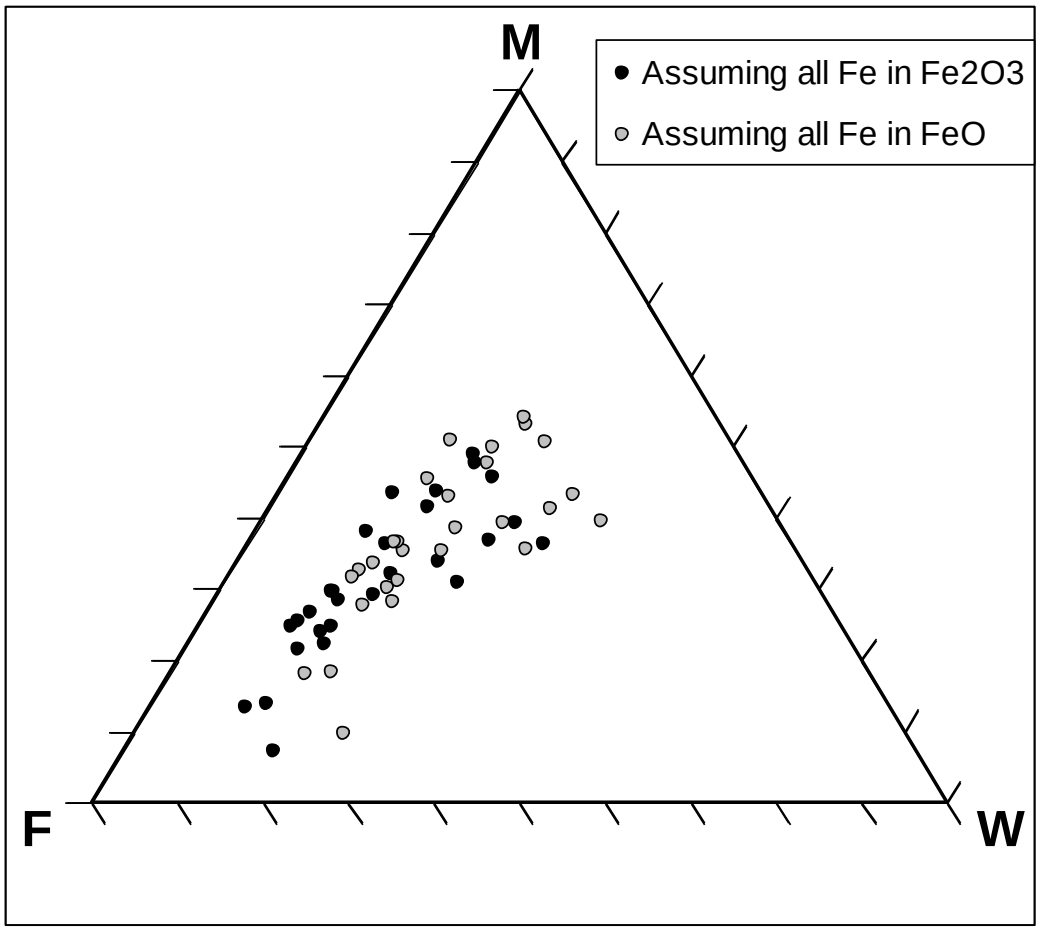

Figure 8. An MFW plot of all samples analyzed in this study addressing the effect of oxidation state of iron on the W index. Assuming all iron in FeO makes samples appear more mafic and slightly more weathered than Fe_2O_3, however differences are minimal enough not to have an effect on the outcomes of this study.

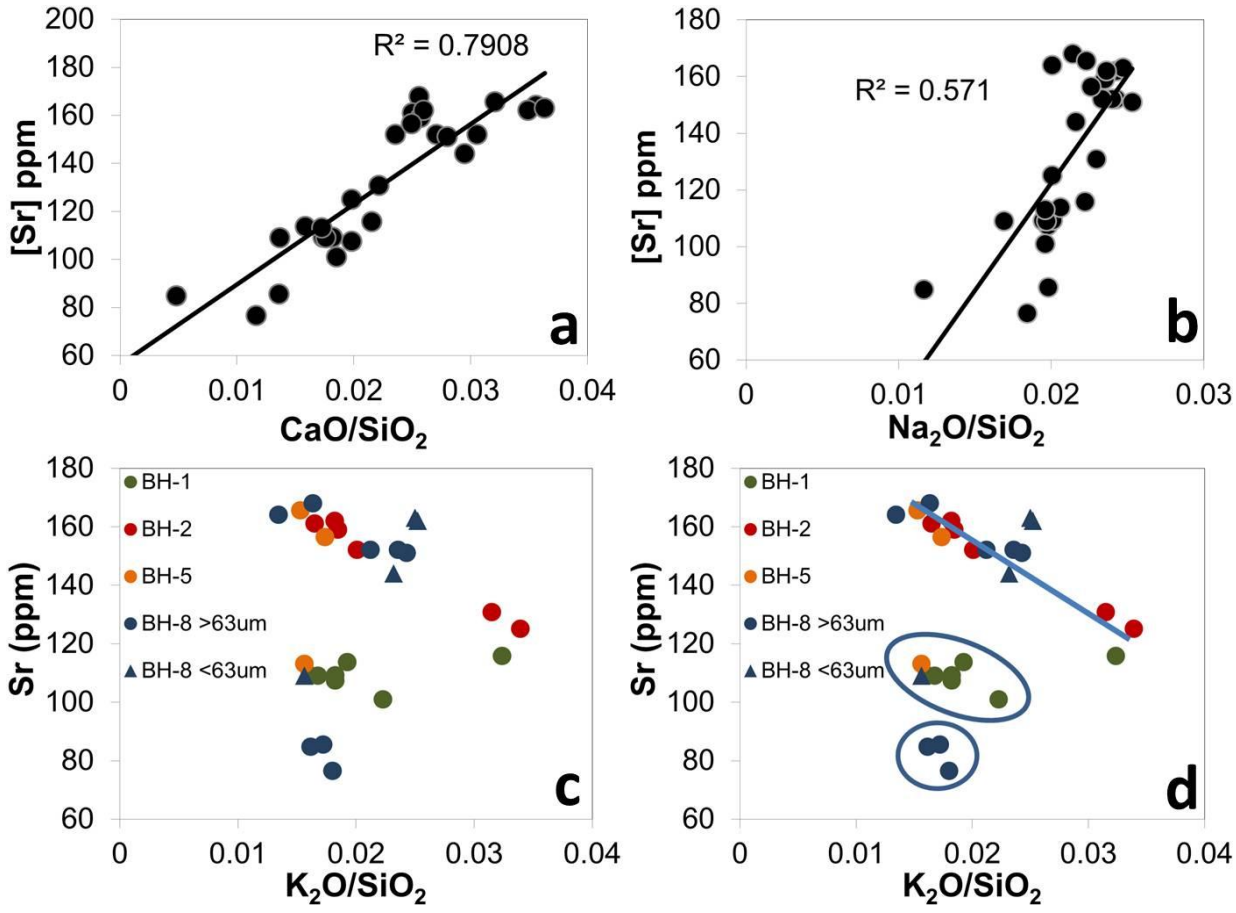

Figure 9. Elemental correlations with Sr: (a) CaO, (b) Na_2O, (c) K_2O, (d) K_2O with trends outlined. Sr displays the strongest correlation with Ca showing that most Sr is most associated with Ca-bearing minerals such as anorthite. Correlation is weaker with Na and K, however sediments to seem to be partitioned and some weak trends emerge (d) suggesting mineralogy is not the primary control in these relationships.

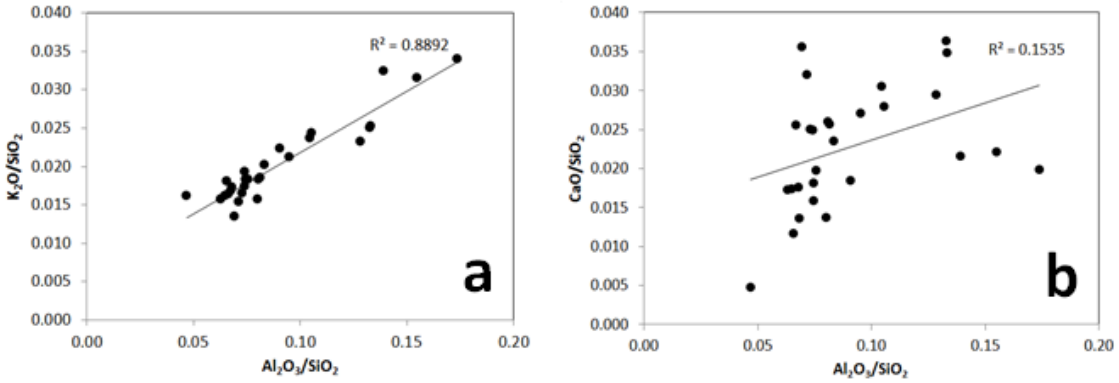

Figure 10. (a) Effect of grain-size sorting on K distribution in deltaic sediments. Good correlation between K_2O and Al_2O_3/SiO_2 indicates that K is more concentrated in finer-grained samples and therefore mineralogical sorting processes are affecting K distribution in sediments. (b) Lack of correlation between Ca and Al_2O_3/SiO_2 reveals no effects of weathering or sorting on Ca distribution among sediments.

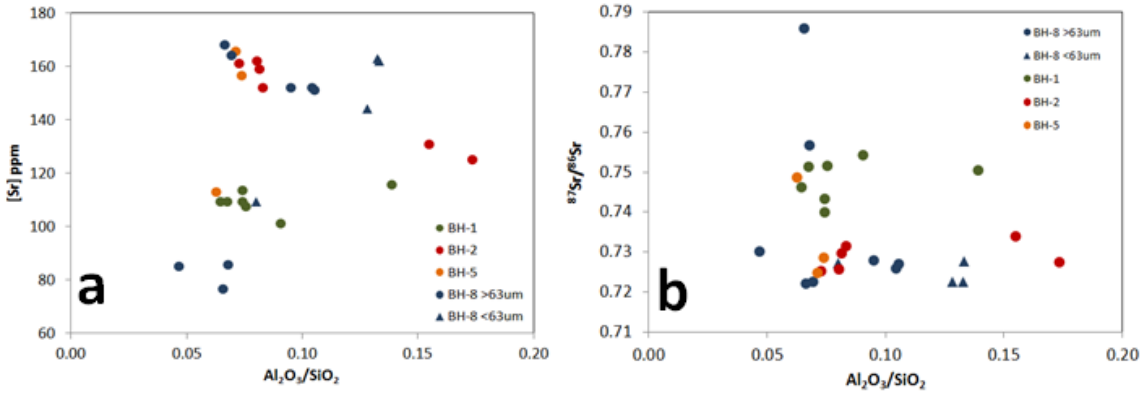

Figure 11. Effects of grain-size sorting on [Sr] and $^{87}Sr/^{86}Sr$. Some Sr depletion is evident in the finest grained samples, yet provenance signals remain preserved. There is no correlation between $^{87}Sr/^{86}Sr$ and Al_2O_3/SiO_2 revealing that grain-size sorting does not affect Sr isotopic signatures.

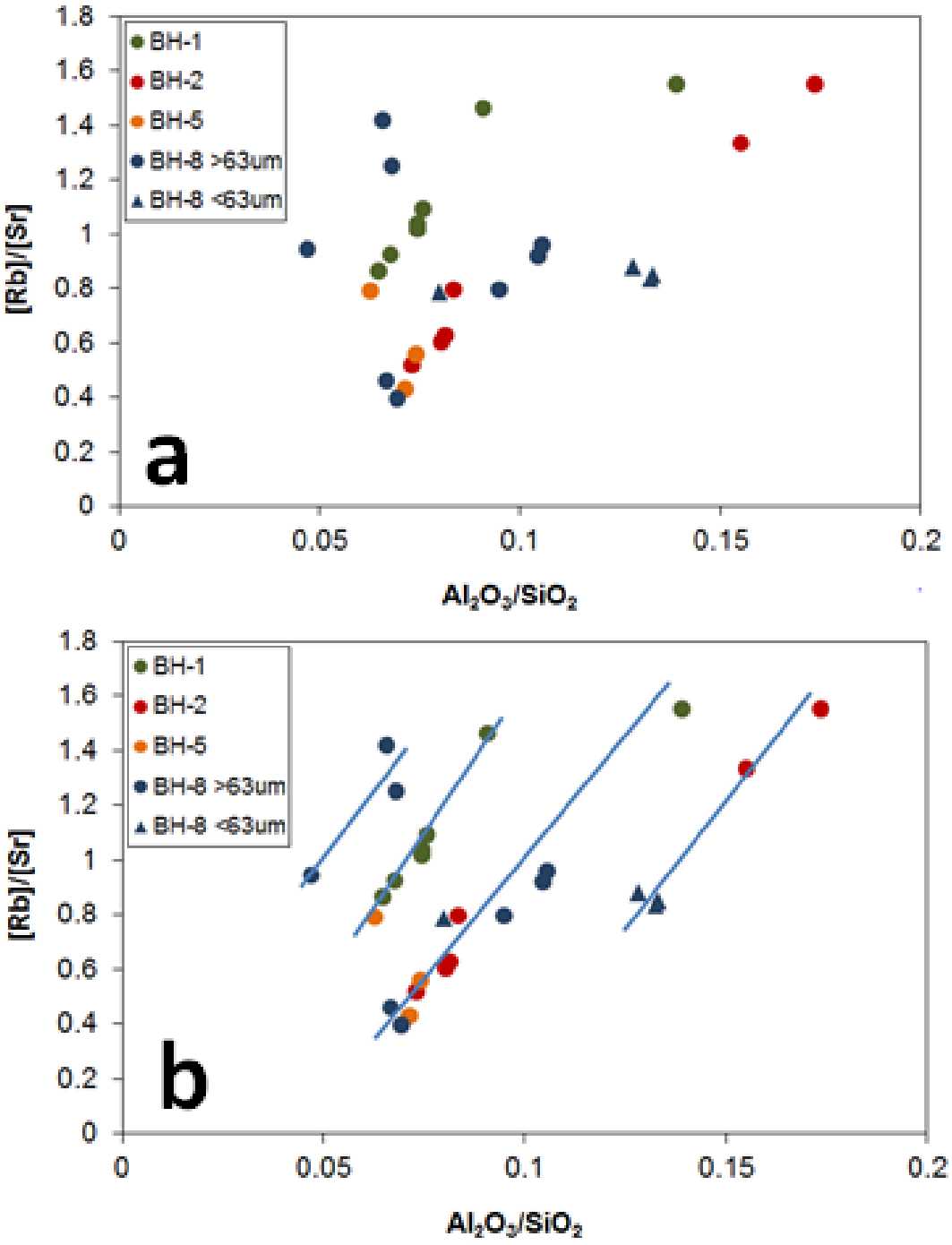

Figure 12. Positive correlation reveals the control of mineralogical sorting and possibly weathering on Rb/Sr ratio, but separation of data points into several separate trends illustrates significant overprinting of provenance signature.

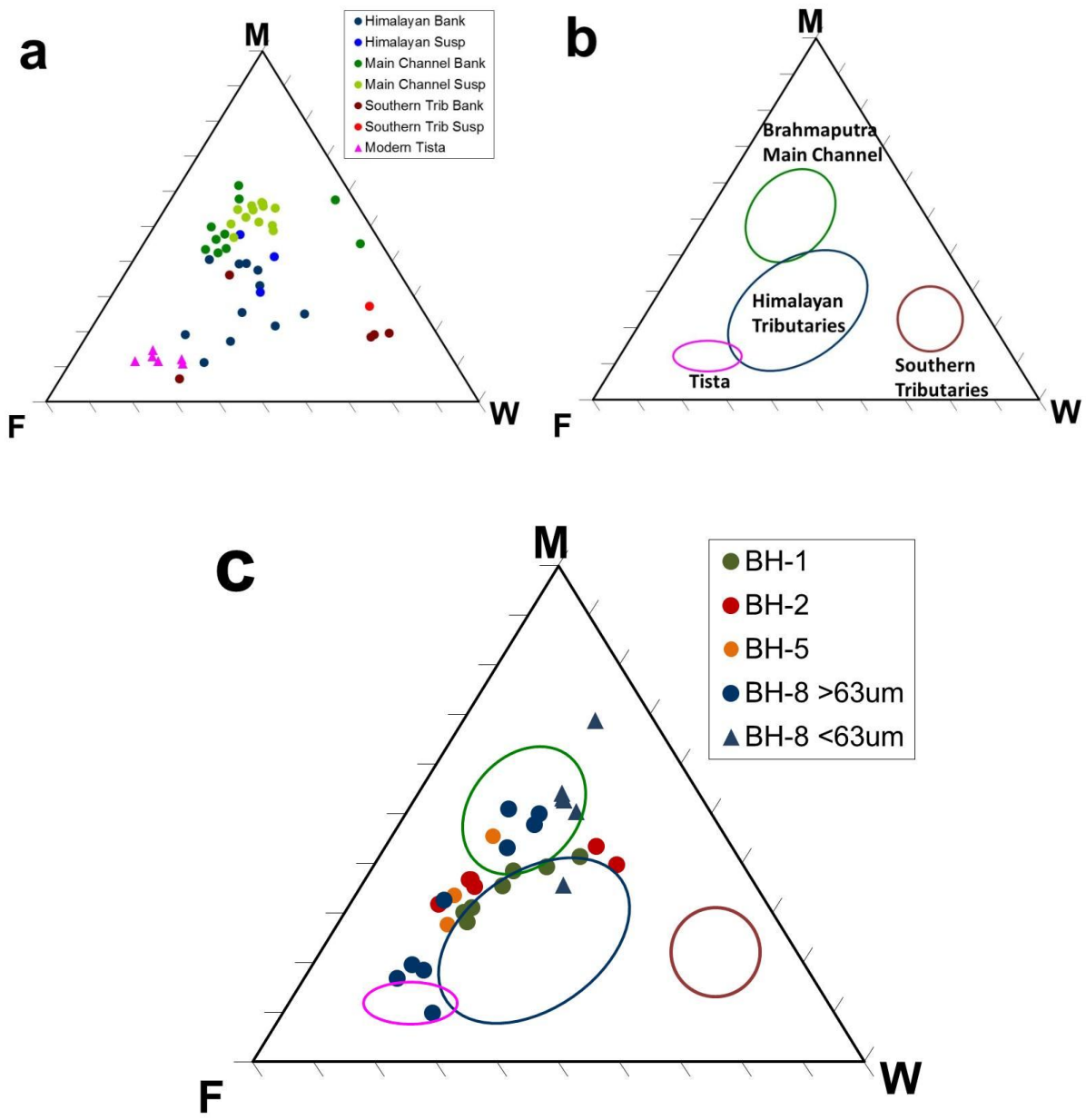

Figure 13. (a) Compiled data from Singh and France-Lanord, 2002 and vanGeen et al., 2008 showing how modern Brahmaputra and tributary sediments plot on an MFW diagram (from Ohta and Arai, 2007). (b) Borehole data from this study.

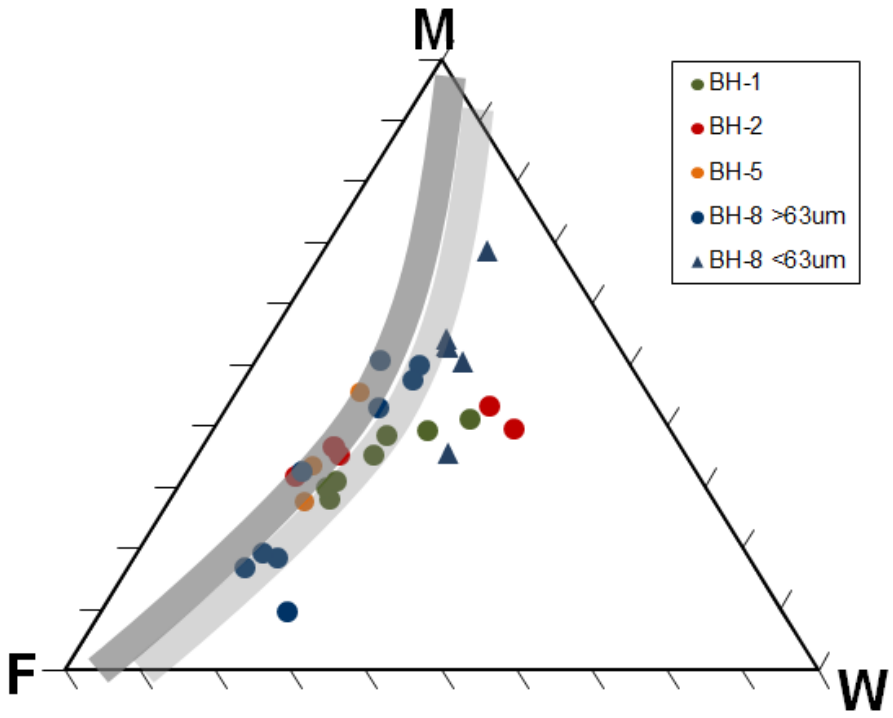

Figure 14. Data from this study presented on an MFW diagram (from Ohta and Arai, 2007). Darker shaded area denotes regions of fresh, unweathered rock signatures. Lighter shading denotes the zone of incipient weathering. Samples with W values beyond the shaded areas have undergone slight to moderate chemical alteration. All samples falling outside the shaded areas contain greater than 15% clay content.

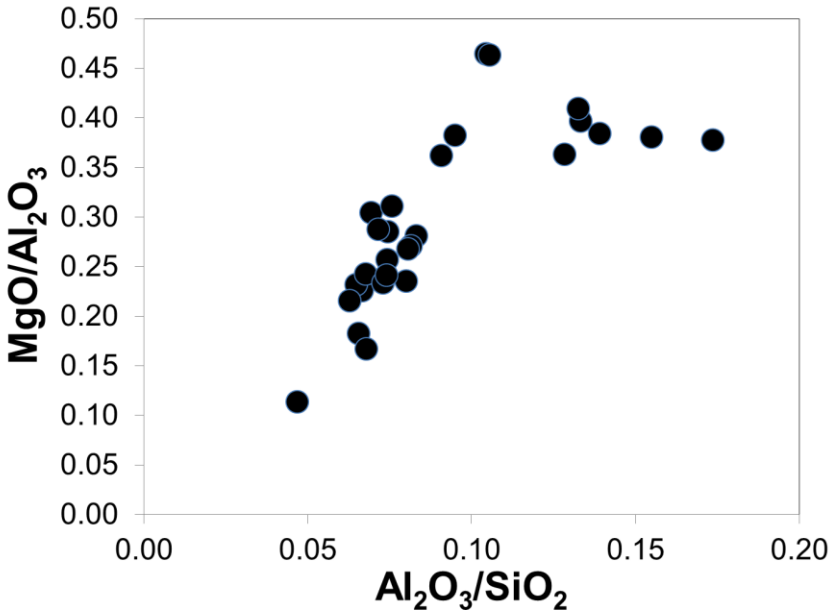

Figure 15. Partitioning of Mg with grain-size. Direct correlation indicates concentration of Mg in finer grain sizes, while finest grained samples (Al_2O_3/SiO_2 >0.11) show Mg-depletion suggesting evidence for biotite dissolution.

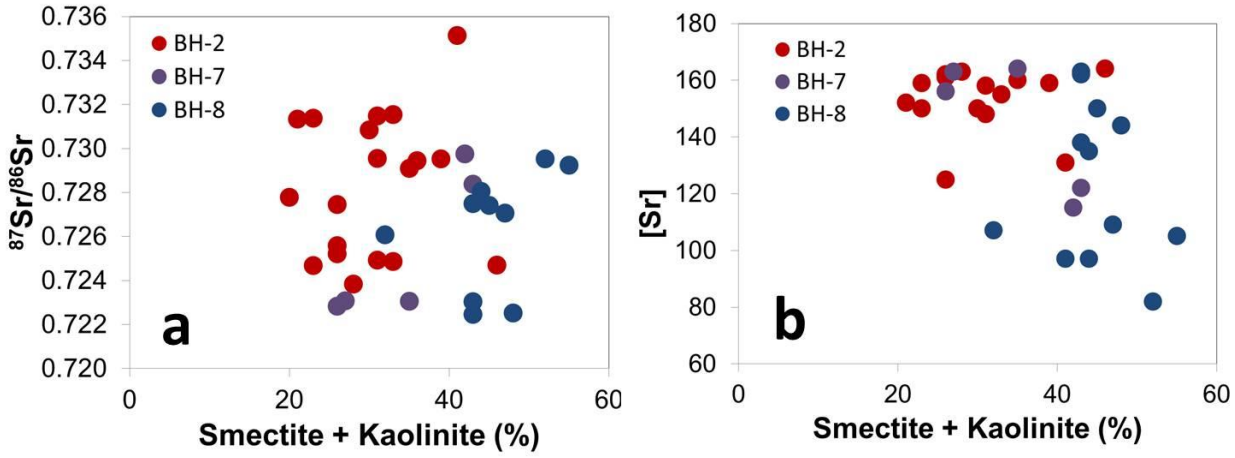

Figure 16. Effects of smectite+kaolinite on (a) $^{87}Sr/^{86}Sr$ and (b) Sr concentrations (ppm). Lack of trend in either figure indicates that neither $^{87}Sr/^{86}Sr$ nor [Sr] is impacted when clays exhibit a more weathered signature (higher S+K). Note that Pleistocene samples in BH-8 are excluded.

	Depth (m)	%S	%K	%I	%C
BH-1	1.5	8	26	59	5
	3.0	15	23	56	4
	4.6	10	24	58	5
	6.1	15	23	56	5
	7.6	5	23	71	1
	10.7	3	22	68	5
	13.7	12	22	58	6
	25.9	6	15	72	5
	38.1	7	20	66	6
	42.7	5	23	67	4
	44.2	5	22	67	5
	48.8	4	20	68	7
	61.0	2	14	75	9
	70.1	4	18	73	4
	82.3	5	15	69	9
BH-2	3.0	4	37	58	1
	9.1	5	21	61	12
	21.3	4	22	63	12
	22.9	0	20	68	12
	30.5	7	24	65	4
	32.0	6	24	61	9
	35.1	5	23	64	9
	39.6	0	21	68	10
	42.7	7	24	62	7
	50.3	4	29	65	3
	62.5	4	31	64	1
	64.0	4	29	64	3
	65.5	2	34	61	3
	68.6	7	32	59	2
	70.1	4	19	66	11
	74.7	6	17	66	11
	83.8	3	23	64	10
	86.9	7	24	69	0
	91.4	11	35	54	0
BH-5	1.5	17	17	66	0
	3.0	10	16	74	0
	4.6	8	18	74	0
	6.1	21	12	67	0
	15.2	7	23	69	3
	24.4	3	23	74	2
	32.0	9	21	70	1
	50.3	13	18	68	1
	62.5	6	22	71	1
	68.6	7	23	69	1
	74.7	4	19	73	5
	80.8	21	21	56	2

	Depth (m)	%S	%K	%I	%C
BH-7	3.0	13	30	55	2
	6.4	1	15	82	2
	7.6	0	28	67	5
	10.7	1	35	63	2
	12.2	1	61	28	10
	13.7	5	9	81	6
	16.8	1	29	68	2
	18.3	3	43	50	4
	19.8	0	35	64	2
	22.9	1	33	63	3
	24.4	2	37	58	3
	25.9	0	10	85	5
	27.4	2	49	45	5
	29.0	0	27	69	3
	30.5	0	27	66	7
	32.0	0	39	61	0
	35.1	12	56	32	0
	38.1	0	29	64	7
	39.6	4	30	63	2
	41.2	0	45	52	3
	42.7	0	42	52	7
	45.7	3	35	60	3
	47.3	0	25	72	3
	48.8	0	34	62	4
	50.3	0	33	65	2
	51.8	0	26	72	2
	53.4	0	29	70	2
	54.9	0	36	63	1
	56.4	0	29	67	4
	57.9	0	27	70	3
	61.0	3	33	58	5
	62.5	0	30	66	4
	64.0	0	63	30	7
	65.5	0	31	65	3
	67.1	2	27	66	5
	68.6	0	26	69	5
	70.1	0	54	39	7
	71.6	0	32	66	3
	73.2	4	45	47	4
	74.7	0	33	64	3
	76.2	0	21	74	5
	77.7	0	23	71	6
	79.3	0	29	67	4
	82.3	0	27	66	7
	83.8	0	28	68	4
	85.4	0	29	60	12
	86.9	0	30	65	4

	Depth (m)	%S	%K	%I	%C
BH-8	7.6	6	38	56	0
	15.2	7	36	57	0
	22.9	2	43	55	0
	30.5	11	37	50	2
	38.1	6	37	57	0
	45.7	8	35	57	1
	53.4	12	43	45	0
	61.0	10	42	48	0
	68.6	0	32	67	1
	76.2	12	35	53	0
	83.8	0	36	64	0
	91.4	0	27	59	14
	99.1	0	41	59	0
	106.7	4	40	56	1

Table 1. Compilation of relative clay mineral abundance data from Heroy et al (2003) and Tennant (2005). S = smectite, K = kaolinite, I = illite, C = chlorite.

	Depth (m)	Ix
BH-1	1.5	0.15
	3.0	0.19
	4.6	0.18
	6.1	0.25
	7.6	0.15
	10.7	0.14
	13.7	0.16
	25.9	0.18
	38.1	0.16
	42.7	0.11
	44.2	0.14
	48.8	0.19
	61.0	0.18
	70.1	0.15
	82.3	0.19
BH-2	3.0	0.34
	9.1	0.34
	15.2	0.34
	21.3	0.22
	22.9	0.25
	30.5	0.42
	32.0	0.37
	35.1	0.22
	39.6	0.28
	42.7	0.35
	48.8	0.37
	50.3	0.28
	62.5	0.35
	64.0	0.32
	65.5	0.30
	68.6	0.33
	70.1	0.34
	74.7	0.34
	79.2	0.36
	83.8	0.32
	86.9	0.25
	91.4	0.32

	Depth (m)	Ix
BH-5	1.5	0.33
	3.1	0.35
	4.6	0.34
	6.1	0.37
	32.0	0.29
	50.3	0.33
	62.5	0.35
	68.6	0.30
	74.7	0.33
	80.8	0.33
BH-7	3.0	0.48
	6.1	0.41
	7.6	0.44
	10.7	0.41
	12.2	0.36
	15.2	0.37
	22.9	0.42
	24.4	0.48
	38.1	0.34
	39.6	0.54
	45.7	0.40
	48.8	0.38
	50.3	0.39
	54.9	0.39
	61.0	0.34
	62.5	0.53
	65.5	0.47
	67.1	0.38
	71.6	0.41
	76.2	0.40
	79.2	0.43
	80.8	0.42
	83.8	0.38

	Depth (m)	Ix
BH-8	7.6	0.28
	15.2	0.29
	22.9	0.20
	30.5	0.38
	38.1	0.32
	45.7	0.32
	53.3	0.34
	61.0	0.31
	68.6	0.36
	76.2	0.35
	83.8	0.27
	91.4	0.32
	99.1	0.27
	106.7	0.24

Table 2. Illite crystallinity (Ix) for boreholes used in this study calculated from original data files collected by Heroy et al (2003) and Tennant (2005).

		Major Elements (mole %)							
Boreholes	**Depth (m)**	**SiO_2**	**Al_2O_3**	**TiO_2**	**FeO***	**CaO**	**MgO**	**K_2O**	**Na_2O**
BH-1	9.1	83.5	6.3	0.40	3.02	1.65	1.96	1.53	1.65
	18.3	84.0	6.3	0.36	2.89	1.53	1.78	1.53	1.69
	24.4	84.7	6.3	0.25	2.47	1.34	1.62	1.63	1.74
	36.6	80.7	7.3	0.42	4.06	1.50	2.65	1.80	1.58
	51.8	74.0	10.3	0.56	5.50	1.60	3.96	2.40	1.65
	64.0	86.2	5.6	0.30	2.06	1.50	1.30	1.39	1.68
	76.2	85.6	5.8	0.31	2.24	1.51	1.40	1.44	1.69
BH-2	9.1	71.1	12.3	0.64	6.05	1.41	4.66	2.41	1.43
	13.7	72.3	11.2	0.65	6.09	1.60	4.26	2.28	1.66
	21.3	84.6	6.2	0.26	2.05	2.12	1.44	1.40	2.00
	39.6	82.5	6.9	0.31	2.86	1.95	1.93	1.66	1.93
	68.6	82.9	6.8	0.33	2.57	2.13	1.83	1.53	1.95
	83.8	83.0	6.7	0.32	2.56	2.16	1.79	1.51	1.96
BH-5	19.8	86.6	5.4	0.25	1.96	1.50	1.17	1.36	1.70
	39.6	83.1	5.9	0.39	3.02	2.67	1.71	1.27	1.85
	79.3	84.2	6.2	0.29	2.33	2.10	1.51	1.46	1.90
BH-8	15.2	74.0	9.9	0.67	5.30	2.58	3.91	1.87	1.80
(<63um)	30.5	75.2	9.7	0.67	5.37	2.22	3.51	1.74	1.63
	45.7	73.8	9.8	0.68	5.32	2.68	4.01	1.85	1.83
	76.2	84.1	6.7	0.54	3.17	1.15	1.59	1.32	1.42
	80.8	76.5	6.8	1.86	6.76	3.53	2.09	1.03	1.39
BH-8	15.2	76.9	8.0	0.45	4.88	2.35	3.73	1.81	1.87
(>63um)	30.5	79.8	7.6	0.36	3.61	2.16	2.90	1.69	1.92
	45.7	76.9	8.1	0.42	4.88	2.15	3.76	1.87	1.95
	61.0	91.0	4.3	0.16	1.06	0.44	0.49	1.47	1.06
	83.8	83.4	5.8	0.50	2.73	2.97	1.76	1.12	1.67
	91.5	85.2	5.7	0.28	2.11	2.18	1.28	1.40	1.83
	99.1	87.2	5.7	0.18	1.66	1.02	1.04	1.57	1.61
	106.7	87.0	5.9	0.18	1.47	1.19	0.99	1.50	1.73

Table 3. Major elemental data collected for this study and converted to mole % for use in calculating weathering proxies. FeO* combines Fe measured in both FeO and Fe_2O_3 oxide states.

Borehole	Depth (m)	Ni	Cr	Sc	V	Ba	Rb	Sr	Zr	Y	Nb	Ga	Cu	Zn	Pb	La	Ce	Th	Nd	U	Cs
BH-1	9.1	16	44	9	54	355	118	107	350	34	12	12	8	42	18	48	98	20	39	4	7
	18.3	16	42	9	52	357	111	109	332	31	10	12	11	51	19	46	87	19	36	3	5
	24.4	14	34	7	46	370	118	114	150	20	7	12	5	38	20	25	50	10	22	2	8
	36.6	23	53	10	69	406	148	101	286	30	13	15	15	64	22	43	83	17	36	4	9
	51.8	39	83	14	104	538	180	116	215	33	15	20	33	86	25	42	90	18	36	4	14
	64.0	8	35	7	39	324	95	109	316	30	8	10	3	38	18	40	82	18	36	5	5
	76.2	10	34	7	46	340	101	109	307	30	9	11	5	42	19	43	83	19	38	3	6
BH-2	9.1	63	116	16	136	505	194	125	173	34	17	23	44	101	31	52	94	18			
	13.7	54	108	16	118	476	175	131	224	36	16	22	38	92	28	47	98	21	41	4	12
	21.3	17	37	8	35	339	84	161	227	26	8	14	3	27	16	32	61	13			
	39.6	23	42	10	49	385	121	152	205	23	9	14	5	46	20	32	57	13			
	68.6	21	49	8	52	375	100	159	250	28	10	13	5	35	15	37	83	16			
	83.8	20	44	15	52	362	98	162	276	31	9	10	7	39	18	45	87	16			
BH-5	19.8	8	33	6	39	310	89	113	227	25	8	10	3	42	18	34	65	16	29	2	4
	39.6	10	60	9	62	303	72	166	372	39	10	11	2	45	20	58	117	25	47	2	1
	79.3	10	45	8	51	345	88	156	212	24	7	11	5	33	19	33	70	15	28	3	3
BH-8	15.2	54	108	20	118	455	138	162	352	45	18	19	31	82	24	57	125	25			
(<63um)	30.5	55	113	19	118	420	127	144	361	44	17	18	23	76	23	52	108	22			
	45.7	54	106	20	119	461	136	163	374	45	18	20	31	82	30	62	119	26			
	76.2	38	100	16	71	315	86	109	490	38	14	13	10	48	16	39	87	19			
	80.8	16	110	12	74	279	63	161	865	54	15	10	3	34	16	73	146	34	61	4	1
BH-8	15.2	43	79	20	78	423	140	152	206	26	13	17	20	71	18	22	54	11			
(>63um)	30.5	32	59	14	80	413	121	152	116	21	10	14	8	60	16	27	51	7			
	45.7	43	69	14	88	436	145	151	135	22	12	17	19	76	17	29	44	9			
	61.0	16	24	4	24	377	80	85	52	9	4	8	4	18	17	6	26	5	8	0	3
	83.8	20	80	9	68	274	65	164	323	43	14	11	2	31	12	57	112	23			
	91.5	9	46	8	46	327	78	168	178	25	7	11	1	25	17	32	68	15	27	3	2
	99.1	4	24	5	28	331	109	77	141	23	6	11	2	24	23	28	51	13	23	2	4
	106.7	9	15	5	23	333	107	86	173	27	6	10	1	22	20	36	81	16			

Table 4. Concentration of trace elements in parts per million collected for this study. Values left blank were not measured for.

Borehole	Depth	CIA	PIA	M%	F%	W%
BH-1	9.2	57	59	38	38	24
	18.3	57	59	35	41	23
	24.4	57	60	28	51	21
	36.6	60	64	39	32	29
	51.9	65	71	41	26	33
	64.1	55	57	30	50	20
	76.3	56	58	31	49	20
BH-2	9.2	70	78	40	21	40
	13.7	67	73	43	22	35
	21.4	53	54	32	54	15
	39.7	55	57	35	46	19
	68.6	55	56	37	46	18
	83.9	54	56	37	46	17
BH-5	19.8	54	56	28	54	18
	39.7	51	51	45	38	17
	79.3	53	54	33	50	16
BH-8 >63µm	15.3	57	60	50	28	22
	30.5	57	59	43	37	20
	45.8	58	60	48	30	22
	61.0	59	65	10	66	25
	83.9	50	50	51	33	17
	91.5	51	52	32	52	15
	99.1	58	61	18	63	19
	106.8	57	60	18	66	16
BH-8 <63µm	15.3	61	65	53	23	24
	30.5	63	67	50	22	28
	45.8	61	64	54	22	24
	76.3	63	68	36	31	33

Table 5. Calculated weathering indices for samples used in this study, including M and F for ternary plotting on the MFW diagram.

Chapter 3: Provenance of Late Quaternary deposits from the Ganges-Brahmaputra delta, Bangladesh using Sr geochemistry

I. Introduction

The different mineralogical and petrologic histories of each source lithology (presented in Chapter 1 of this dissertation) allow for unique bulk geochemical signatures in the sediments they yield. That the Ganges and Brahmaputra rivers each drain distinct portions of the Himalayan mountain range allows for uniqueness in the geochemical character of their sediment loads to persist such that sediment deposits in the G-B delta and ultimately the Bengal Fan may be traced back to not only the original rocks that produced them, but the river that is responsible for their deposition as well. The different paths taken by the individual rivers through the G-B basin is presented in detail in Chapter 1. In this chapter, the specific geochemical differences between the different source areas and their effect on the bulk geochemical nature of fluvial sediments are presented. Sr and Nd radioisotopic analyses are tools that have proved useful in tracing sediments deposited away from the G-B erosional basins to their source (Kessarkar et al. 2005, Colin et al. 1999, Derry and France-Lanord 1996, and others). Strontium isotopes have been used in this study for direct comparison, and in the absence of Nd isotope data, $^{87}Sr/^{86}Sr$ has been combined with [Sr] to delineate distinct geochemical character of the source regions that can be traced to deltaic deposits. The Sr concentration and isotope data are supported by major elemental data as well. While the provenance of Bengal Fan sediments has been widely studied, little is known about the sourcing and deposition of sediments in the G-B delta, and if they reflect the same processes responsible for the Fan deposits. Comprehensive source-to-sink studies are vital in understanding the nature of sediment dispersal and margin development. Until now, the G-B delta has been a poorly understood link in this source-to-sink chain, especially in terms of the propagation of provenance signatures and whether or not any sorting or attenuation of these signals occurs as sediments pass through such a large and climatically and tectonically dynamic basin. By characterizing the sourcing of sediments in the delta, this chapter takes a first step toward further unraveling the complexities of G-B delta development.

II. Background

With such high sediment loads carried by both the Ganges and Brahmaputra rivers (>1 Gt combined), it is evident that physical processes dominate Himalayan erosion. Physical erosion is a major player in the basin with only about 9% of the total erosive flux coming from chemical erosion (Galy and France-Lanord, 2001). While sediment loads are high in the modern, they have been up to 2.5 times greater in the past, associated with climatic shifts such as the early Holocene peak in southwest monsoon intensity (Goodbred and Kuehl, 2000b). Understanding the sources of sediments and what changes they have undergone along their path to the margin not only illuminates some specifics of delta and margin development, but can also reveal how provenance signals are propagated to the deep sea where interpretation of Bengal Fan deposits are used to unravel the longer history of Himalayan uplift and erosion.

Sediment budgets of the Ganges and Brahmaputra rivers based on the dissolved and suspended loads (with bedload contribution estimated) suggest that erosion in the Brahmaputra basin is nearly 1.5 times greater than in the Ganges (2.9 mm/yr vs. 2.1 mm/yr respectively) (Galy and France-Lanord, 2001). This has been attributed to greater precipitation in the eastern Himalayas and greater rates of uplift along the eastern syntaxis at Namche Barwa. This discrepancy in erosion rate combined with the unique combination of source lithologies drained by each river and their tributaries requires that the Ganges and Brahmaputra rivers be treated as two distinct fluvial systems.

2.1 Source lithologies

A map outlining the placement and surface expression of the major lithostratigraphic units of the entire Ganges-Brahmaputra basin is presented in Figure 1. Along the Indus-Tsangpo suture (ITS) are the Trans Himalayan Plutonic Belt (THB) and the Tibetan or Tethyan Sedimentary Series (TSS). The THB is sourced from the melted oceanic crust of the Tethys Sea as it was subducted during the India/Asia collision. The relatively short crustal history of these rocks (being derived from oceanic basalts) accounts for the low radiogenic Sr signature with a

range of 0.700-0.715 (Schärer et al, 1984; Debon et al., 1986; Singh et al, 2008). The TSS, formed from shallow Tethys Sea sedimentary deposits, also displays a relatively unradiogenic signature relative to the rest of the Himalayas with a range of 0.710-0.735 (Bickle et al., 2005; Bickel et al., 2003; Najman et al., 2000). Both of these lithologies are also characterized by high [Sr], commonly >200 ppm in both lithologies and >400ppm for some THB samples. In all cases discussed here, bulk rock geochemistry refers to the silicate fraction following carbonate removal.

Along the central axis of the Himalayan orogen, the lithology is dominated by High Himalayan Crystalline (HHC) rocks with locally interspersed TSS units. The HHC rocks are more radiogenic than the Tibetan lithologies, with a range of $^{87}Sr/^{86}Sr$ of 0.740-0.765, yet have a lower concentration of Sr with values ranging from ~70-120ppm (Ahmad et al., 2000; White, 2001). The last major lithologic unit, the Lesser Himalayas (LH), being derived from the oldest material relative to the other lithologic units displays the most radiogenic $^{87}Sr/^{86}Sr$ signature with values >0.780, commonly exceeding 0.800. The extensive crustal history of this unit has also depleted it in Sr overall, with concentrations typically less than 80ppm (Célérier et al., 2009; Ahmad et al., 2000). The Siwalik Hills or Siwaliks are the southernmost unit of the Himalayas composed primarily of reworked sedimentary material from the HHC and LH units. As a result of the limited aerial extent and low relief of this range, the sediment yield is insignificant to the overall loads of both the Ganges and Brahmaputra rivers (Sinha and Friend, 2004; Campbell et al., 2005), so its influence on the geochemical nature of sediments will not be considered further.

On the Indian subcontinent, the sediments supplied to the Ganges from southern tributaries are derived from the Deccan Trap basalts, Vindhyan sediments and the Archean basement of the Indian Shield. The Deccan flood basalts are young, having been formed between the upper Cretaceous and the Eocene, and therefore have a pretty unradiogenic $^{87}Sr/^{86}Sr$ signature with a range of 0.704-0.716 and high Sr concentrations >150ppm on average, and often exceeding 200ppm (Alexander and Paul, 1977; Peng et al., 1998; Singh et al., 2008). The Vindhyan sediments are slightly more radiogenic at ~0.720, and the ancient Archean craton is the most radiogenic, with $^{87}Sr/^{86}Sr$ values around 0.800 and noted by significantly depleted Sr concentrations typically <60ppm (Saha et al., 2004; Singh et al., 2008 and references therein).

In the eastern basin, the Sylhet region through which the Brahmaputra flows when it follows its eastern course is bounded by the Shillong Plateau in the north and by the Mishmi hills

and Tripura fold belt to the east. The plateau is composed primarily of Archean gneisses akin to the Indian Shield and orthoquartzite and phyllite of Proterozoic age, and is marked by several plutonic intrusions ranging between 450 and 700 Ma (Srivastava et al., 2005). Along the southern front of the plateau bordering Bangladesh are sedimentary rocks of Cretaceous-Tertiary age. Very little Sr data are available for the plateau, however data from bedload and suspended sediments collected from streams draining the north portion of the plateau into the main stem Brahmaputra in Assam reveal semi-radiogenic $^{87}Sr/^{86}Sr$ signatures ranging between 0.733 and 0.750 with depleted Sr concentrations measuring below 60ppm and as low as 32 ppm (Singh and France-Lanord, 2002). Estimates place the Shillong contribution to overall Brahmaputra sediment load at approximately 11% before the river reaches the G-B delta in Bangladesh (Garzanti et al., 2004; Singh and France-Lanord, 2002), but no previous work has been done to estimate the contribution of these sediments to the Sylhet basin.

2.2 Modern sediment provenance: Brahmaputra

The mainstem of the Brahmaputra through the Assam plains transports significant volumes of sediments from both Tibetan and Himalayan lithologies (Singh and France-Lanord, 2002; Garzanti et al., 2004; Stewart et al., 2008; Harris et al., 1998). Sediment supply in the Brahmaputra basin is characterized by a marked spatial variability in erosion rates due to differences in erodability of the lithostratigraphic units, local to regional precipitation gradients, and rapid incision and uplift around the eastern syntaxis (Galy and France-Lanord, 2001; Harris et al., 1998; Singh and France-Lanord, 2002; Garzanti et al., 2004; Stewart et al., 2008). Analysis of the Brahmaputra mainstem and its tributaries from its source to where it enters the G-B delta using sand mineralogy, Sr and Nd isotopes of the silicate fraction of bulk bedload samples and U-Pb dating of detrital zircons reveals that roughly half the sediments transported by the Brahmaputra are derived from Tibetan Lithologies (Singh and France-Lanord, 2002; Garzanti et al., 2004; Stewart et al., 2008; Harris et al., 1998). These studies show that the eastern syntaxis around Namche Barwa, characterized by THB lithology, contributes approximately 45% of the total Brahmaputra sediment supply, a region that covers only 2% of the total Brahmaputra drainage area (Stewart et al., 2008). Another 5% is derived from the Tsangpo, draining THB and TSS lithologies making Tibetan lithologies responsible for half of

the material carried to the G-B delta by the Brahmaputra. This prevalence of Tibetan influence is responsible for the relatively less radiogenic $^{87}Sr/^{86}Sr$ signature and relatively high strontium concentration that characterizes Brahmaputra sediments. The other half of sediments carried to the confluence with the Ganges are sourced from HHC and LH lithologies (40% combined) and the Mishmi Hills combined with other eastern tributaries (10%) (Singh and France-Lanord, 2002; Garzanti et al, 2004; Singh, 2006).

2.3 Modern and historical sediment provenance: Ganges

The modern Ganges River sediments are sourced primarily from a mixture of High Himalayan and Lesser Himalayan lithologies, with minor contributions from the peninsular rivers draining the Indian Shield and Deccan Traps (Singh et al., 2008). At Rajmahal, just before the Ganges enters Bangladesh, sediments are characterized by <4% influence from the TSS, <3% from the Siwaliks, and ~2.5% from peninsular rivers with the HHC supplying ~65% of the total load and the LH making up the rest (Singh et al., 2008). Like the Brahmaputra, there is considerable spatial variability in erosion within the Ganges basin, with several sub-basins exerting control on mainstem sediments at various points. For instance, the bedload of the Yamuna River, a major tributary to the Ganges is comprised of 30-40% of peninsular river sediments, a number that decreases to 15% after confluence with the Ganges and continues to decrease to 2.5% at the outflow into Bangladesh. This pattern of dilution is driven by large inputs of Himalayan sediments from several large tributaries feeding the Ganges downstream of the Yamuna. The two major Himalayan tributaries at the eastern portion of the basin, the Gandak and the Kosi contribute at least 60% of the total sediment load at Rajmahal while covering only 13% of the total basin area (Singh et al., 2008). In addition to providing a large quantity of sediment, the Gandak exerts considerable control on the Ganges bulk sediment geochemistry due to large volumes of less-radiogenic TSS input as compared with other Himalayan tributaries ($^{87}Sr/^{86}Sr$ =.747 vs. ~0.771 for upstream Himalayan tributaries). Further downstream the Kosi is the most radiogenic of the tributaries with $^{87}Sr/^{86}Sr$ of the bedload exceeding 0.800. Based on Nd isotopes, this is more likely the result of spatial variability in the HHC than greater influence from the LH (Singh et al., 2008).

Only one study has been published which addresses the historical provenance record of Ganges-derived sediments (Rahaman et al., 2009). The study site is located in Kanpur, India, approximately 200km upstream of the modern Ganges-Yamuna confluence at Allahabad and records approximately 100 kyr of Ganges sedimentation. Results from Sr and Nd isotope analysis reveal a clear correlation between changes in precipitation and the relative erosional contribution of different Himalayan lithologies. Specifically, during times of reduced monsoon intensity (associated with increased glacial cover as a result of lower solar insolation) there is a reduction in erosion and sediment supply from the Higher Himalaya and an increase in relative Lesser Himalayan influence on sedimentation (Rahaman et al., 2009). While the late Quaternary borehole at Kanpur provides information regarding the relative contribution of sediments between Himalayan lithologies, its presence upstream of the Yamuna confluence does not allow for analysis of the influence of peninsular rivers on mainstem sediment loads and how this may have varied relative to Himalayan influence throughout the late Pleistocene and Holocene periods. However, the clear relationship between short term (century-millennial-scale) climate change and variations in Himalayan erosion found in the Late Quaternary combined with the even shorter term inter-annual and seasonal variability in bedload geochemical character displayed in the modern (Singh et al., 2008; Singh 2010) suggests that variations in relative contribution of peninsular rivers to the mainstem bedload associated with short-term Quaternary climate shifts are a possibility and warrant further inspection both along the mainstem and in the deltaic deposits downstream

2.4 Modern and historical sediment provenance: the G-B delta

On the Ganges-Brahmaptura delta, bedload samples taken at the same location during the dry season one year apart show a range in $^{87}Sr/^{86}Sr$ of 0.769-0.774 for the Ganges and 0.721-0.735 for the Brahmaputra (Galy and France-Lanord, 2001). For the Brahmaputra, these samples were taken upon first entering Bangladesh, upstream of the Tista confluence which is significantly more radiogenic with an average $^{87}Sr/^{86}Sr$ of ~0.813 (Singh and France-Lanord, 2002). There is no data regarding what proportion of the total Brahmaputra bedload is supplied by the Tista river, so complete geochemical characterization of the Brahmaputra prior to the Ganges confluence is unavailable. This interannual variability in $^{87}Sr/^{86}Sr$ apparent in both rivers

underscores the spatial variability in erosion among the various river sub-basins and suggests that relative contributions to both river mainstems are not stable on very short time scales, perhaps due to variations in precipitation (e.g. Bookhagen et al., 2005a; Bookhagen et al., 2005b) or short-term catastrophic events such as floods or mass-wasting in individual tributary basins. This interannual variability is potentially further complicated by the timing of seasonal rainfall and snowmelt in the many lithologically distinct tributary sub-basins. During the monsoon, the dissolved load of the Brahmaputra exhibits reduced Sr concentrations but an increase in radiogenic signature due to greater influence of High Himalayan erosion over TSS in the basin during this time (Galy et al., 1999). The Ganges also sees an increase in Himalayan influence to the dissolved load during this monsoon, with the drier season providing a relatively more important input from the Indo-Gangetic plain and peninsular rivers compared to their importance during the monsoon (Galy and France-Lanord, 2001; M. Singh et al., 2007). If these relationships apply to the bedload as well, we would expect more radiogenic bedload signatures during the monsoon for the Brahmaputra, though this relationship could be complicated for the Ganges since the both the peninsular rivers and Lesser Himalayas carry rather radiogenic $^{87}Sr/^{86}Sr$ signatures (Singh et al., 2008; Singh and France-Lanord, 2002).

Information regarding the Sr signature of the combined flow of the two rivers is extremely limited, consisting of only two suspended load samples taken during a monsoon season. The first sample was taken within the Ganges and Brahmaputra confluence zone and with an $^{87}Sr/^{86}Sr$ of 0.753 and [Sr] of 113ppm reflects the mixing of the Sr systematics of the two rivers, while the other sample taken approximately 50km upstream of the mouth of the Meghna River has an $^{87}Sr/^{86}Sr$ of 0.738 and [Sr] of 135ppm (Galy and France-Lanord, 2001), significantly less radiogenic than the Ganges and Brahmaputra combined signatures alone and suggestive of more Brahmaputra influence than a simple 50-50 mix of the two rivers. In fact, satellite images suggest that waters from the two rivers remain relatively unmixed well downstream of the confluence (Figure 2), a phenomenon documented in other major river systems (e.g. Pereira et al., 1992). With only two data points, it is not possible to draw any strong conclusions regarding what characterizes the Sr signal of the combined river sediment loads, how the suspended load and bedload sediments compare in their geochemical signatures, or how much variability downstream would be expected. The variation in combined signature seen here is unlikely due to influence from less radiogenic Meghna-derived sediments as in the

modern, the Meghna discharges very little sediment. The variation could be attributed to variability in either the Ganges or Brahmaputra rivers individually, or in the degree of mixing between the waters and sediments of the distinct rivers as there are no data detailing how the geochemistry of the sediments evolves over a monsoon season or how the signals propagate downstream once they reach the delta.

The distinction in geochemical signature of the Ganges and Brahmaputra has persisted throughout the late Quaternary based on previous studies of deltaic boreholes using different proxies (Heroy et al., 2003; Pate, 2008; Allison et al., 2003; Huizing, 1971). Heroy et al. (2003) found distinctive mineralogical signatures between the two rivers in both the fine and coarse sediment fractions of several of the boreholes used also in this study. Specifically the ratio of epidote to garnet grains (E/G) in the sand fraction and relative clay mineralogy (smectite, kaolinite, illite and chlorite) of the <4um fraction were used to denote areas of the delta that were dominated by Ganges sedimentation, by Brahmaputra sedimentation and by a mixed input of the two rivers. The results of this study indicate that the Ganges has been responsible for the sediment supply to the western G-B delta and the Brahmaputra to the east as would be expected based on their modern courses, and that a combined, mixed signature of the two rivers is limited to a narrow margin that roughly follows the path of the modern Meghna river below the G-B confluence. Allison et al. (2003) expanded this work to the margin using the same clay mineralogical methods on the <4um sediments and developed a model of river location history that suggest that the Ganges and Brahmaputra rivers have only interacted directly over the past ~200 years. This model also suggests that the Brahmaputra has been of limited influence in supplying sediments to the progradational areas of the margin during the Holocene, thereby attributing most of the shoreline progradation to the Ganges River.

2.5 Selecting provenance tools for this study

While the previous sand and clay mineralogical study in the Holocene G-B deltaic deposits was successful in delineating Ganges and Brahmaputra signals to a certain degree (Heroy et al., 2003), these methods may not provide a good representation of bulk sediment provenance. Heavy minerals such as epidote and garnet are subject to hydrologic sorting which could overprint provenance signatures. In addition, it has been shown that abundance of these

two minerals varies considerably between different tributary basins in the Brahmaputra River (Garzanti et al., 2004), so temporal variations in sediment discharge in these tributaries could potentially change the Brahmaputra E/G ratios over time. With regards to clay mineralogy, while Chapter 2 of this thesis showed that overall sediments have not undergone a great degree of chemical alteration over this time period in the G-B basin that could drastically alter provenance signatures, many clays are still the products of chemical alteration and therefore introduce further complexity into provenance analysis. In addition, for many of the boreholes used in that study and in this one, the clay fraction is a small portion of the total bulk sediment (<15%) and subject to hydrologic sorting as well, and therefore may not be a good representation of bulk sediment provenance

Despite the seasonal and interannual variability in Sr isotopic character of the Ganges and Brahmaputra's individual bedloads, their $^{87}Sr/^{86}Sr$ signals remain distinct as they enter the delta due to their unique flow paths and most specifically, the significant effect of the less-radiogenic Tibetan contribution to the Brahmaputra. This distinction allows for $^{87}Sr/^{86}Sr$ to be a useful tool in tracking the history of each river's sedimentation in the delta. While Sr concentration signatures have the potential to be altered by chemical weathering processes, Chapter 2 of this thesis shows how this is not of concern for these samples.

Rare earth element (REE) profiles have been employed in the modern Ganges basin to track provenance (Singh, 2010) but little to no data is available for Brahmaputra sediments and the distinctions between different source areas are limited at best. Neodymium isotopes have been used extensively throughout the system from the source lithologies, the catchment basins and as far as the distal Bengal Fan in conjunction with $^{87}Sr/^{86}Sr$ (Galy et al., 1996; Derry and France-Lanord 1996; Singh et al., 2006; Singh et al., 2008; Singh and France-Lanord, 2002; Rahaman et al., 2009), however reliable εNd was not obtained for the samples in this study. In addition, the relatively narrow range in εNd between some Himalayan lithological units reduces its usefulness in calculating sediment budgets (Singh et al, 2008). Instead, recent work on late Quaternary G-B delta sediments revealed [Sr] to be a good indicator of provenance with higher concentrations (>155 ppm) reflecting Brahmaputra sourcing as a result of Tibetan and Eastern Syntaxis sediment flux, low concentrations provided by (<105 ppm) from Eastern Himalayan tributaries such as the Tista receiving sediments from the Lesser Himalayas, and intermediate concentrations (90-120 ppm) in sediments of Ganges origin (Pate, 2008). With this in mind,

Figure 3 has been constructed using the data from Galy and France-Lanord (2001), Singh and France-Lanord (2002), and Singh et al., (2008) and outlines distinct $^{87}Sr/^{86}Sr$ /[Sr] signatures for each of the major source areas and highlights the unique signatures of the Ganges and Brahmaputra rivers. The data presented in this study are characterized and discussed using these classification signatures.

2.6 Summary of previous research

The major Himalayan source lithologies that supply sediment to the Ganges and Brahmaputra rivers are geochemically distinct which allows for provenance signals to be traced relatively easily throughout the river basins. Variations in relative contributions of these lithologic units owing to river drainage and precipitation patterns results in distinct geochemical signatures of sediments carried by each river, signatures that have remained unique throughout the Late Quaternary. Both the Ganges and Brahmaputra rivers are marked by significant spatial variability in erosion which is reflected in mainstem sediment geochemistry. The catchment of each individual river has been examined in depth and the relative contribution of important tributary basins has been quantified. However, there is limited data available for the relative importance of each river in influencing both modern and historical deltaic sedimentation. The work that has been done has been limited by the extent of sample collection and potential limitations of mineralogical methods employed. The study presented here utilizes a robust methodology in tracking sediment provenance ($^{87}Sr/^{86}Sr$ and [Sr]) that is able to reveal more about Late Quaternary delta morphology than previous geochemical and mineralogical studies.

III. Methods

A description of sampling and analytical techniques employed in this study are discussed in detail in Chapter 1 of this dissertation.

IV. Results

4.1 BH-1

BH-1 is located along the central delta plain and comprises a thick lower sequence of channel fill sands deposited since the last sea level lowstand during early Holocene transgression (Figure 4 and Figure 5). The channel sands are overlain by a muddy coastal plain sequence of predominantly silt (~54%) and clay (~31%). Muddy sands deposited with the river-mouth estuary or adjacent tidal channels overlie the coastal plain muds, indicating channel migration or delta-lobe switching (Goodbred and Kuehl, 2000a).

$^{87}Sr/^{86}Sr$ values in BH1 range between 0.740 and 0.754 with an average of 0.749. These are the most radiogenic Holocene values measured in this study, and also yield the widest range of $^{87}Sr/^{86}Sr$. These data are less radiogenic than the modern Ganges average of 0.774, although data for the modern Ganges are highly variable (SD = 0.009) (Singh et al., 2008; Galy and France-Lanord, 2001). Average [Sr] in BH-1 is 108ppm with a range of 101 to 116ppm, which is significantly higher than modern Ganges averages of 79 ppm (Singh et al., 2008) and 82ppm (Galy and France-Lanord, 2001) in Bangladesh. In both $^{87}Sr/^{86}Sr$ and [Sr], there is significant variation throughout the borehole indicating a temporal complexity to the story. The most radiogenic $^{87}Sr/^{86}Sr$ value of 0.754 is found at 36m depth, overlain by progressively less radiogenic sediments until the minimum of 0.740 at 18m is reached. There is a second minimum that is more radiogenic than the first at 64m with a value of 0.746. In both cases, the lower spike is located near the top of a fine sand deposit indicating active channel deposition.

4.2 BH-8

BH-8 is located in the eastern Sylhet basin and is dominated by silt deposition indicative of flood plain sedimentation. The base of the borehole is also noted by a significant coarsening of the sediments, with predominately sandy deposits between 82m and 95m, coarsening to coarse sands at the very bottom (95-107m). These sandy sediments have not been accurately dated, but shallower dates in the borehole indicate that they predate the Holocene, and are referred to as late Pleistocene deposits (Goodbred and Kuehl, 2000a). Holocene deposits in BH-8 (between 0 and

81.5m depths) have an average $^{87}Sr/^{86}Sr$ of 0.726 in the combined silt and clay fraction and 0.727 in the sand fraction. The range of values is 0.720-0.731 in the sand fraction and 0.723-0.730 in the finer grains, a narrower range of values than in BH-1. The concentration of Sr in the sediments averages 130ppm in the silt and clay fraction, and 133ppm in the sand fraction. An exception is noted at 61m depth where [Sr] reaches a low of 82ppm in the fine fraction and 85ppm in the coarse fraction while $^{87}Sr/^{86}Sr$ remains within the range of the rest of the Holocene sediments.

Most notable in BH-8 is the highly radiogenic signature at the base of the core in Late Pleistocene deposits (Figure 6). The basal sand deposits are where the most radiogenic $^{87}Sr/^{86}Sr$ values (up to 0.802) and lowest Sr concentrations (as low as 77ppm) are recorded. Though the sands directly above this highly radiogenic signature are still considered late Pleistocene in age, $^{87}Sr/^{86}Sr$ values are much more typical of modern and Holocene Brahmaputra sediments, with values of 0.722 and an average [Sr] of 166ppm in the coarse fraction. Data is not available for the silt+clay fraction here. The sample at 83.8m has been excluded as an outlier based on mineralogical sorting (see chapter 2), and there was not enough sample recovered at 91.4m for analysis.

4.3 BH-7

BH-7 is located approximately 30km west of BH-8 in closer proximity to the Old Brahmaputra channel. The deposits are comprised primarily of fine and medium channel fill sands that fine upwards to be capped by 3-5m think muddy floodplain sequences. The site preserves a record of deposition and avulsion of the Brahmaputra as it changes between its eastern and western courses (Goodbred and Kuehl, 2000a). The average $^{87}Sr/^{86}Sr$ of the sand units is 0.723 with an average concentration of 161 ppm. The muds are slightly more radiogenic with an average $^{87}Sr/^{86}Sr$ of 0.729, while the [Sr] is lower with an average of 119 ppm (Figure 6). Analysis of Sylhet sediments in Chapter 2 of this thesis suggests that it is unlikely that the Sr depletion in these muddy deposits is a result of chemical weathering and instead the Sr geochemical variation is a result of varying provenance.

4.4 BH-9

Holocene deposits in BH-9 are the most fine-grained of the three Sylhet boreholes, owing to its location furthest from the old Brahmaputra course, which has been presumed to be the main source of sediments to the Sylhet basin (Goodbred and Kuehl, 2000a). BH-9 is located ~10km from the Surma River, which drains the Manipur Hills of eastern India and within 30 km of the Baulai River draining the Shillong Plateau. The Holocene sediments are mostly silt and clay with some fine sands between 11 and 31m depth. The average $^{87}Sr/^{86}Sr$ for these sediments is 0.729 with an average [Sr] of 122ppm (Figure 6). A coarse sand facies is found below 67m that is channel fill deposited during the last sea level lowstand and early transgression (Goodbred and Kuehl 2000a). This sandy sequence is comparable to the deep sandy sequence in BH-8 in age and grain-size, but the one sample analyzed in this unit (82m) has a $^{87}Sr/^{86}Sr$ value of 0.728118, much less radiogenic than the high of 0.802 in BH8. However, [Sr] is low in this sample (83 ppm) and for another sample at 45m depth (95ppm), which falls within the range of values for the Shillong Plateau (Singh and France-Lanord, 2002).

4.5 BH-5

BH-5 is located approximately 20km south of the current Ganges-Brahmaputra confluence, and previous work has suggested that the borehole comprises alternating and/or combined Ganges- and Brahmaputra-sourced sediment (Heroy et al., 2003). The core lithology is primarily sand (>77%) with the exception of a silt-dominated mud layer in the uppermost 7m. Beginning at the base of the borehole, medium sands make up 10-20% of the deposits, decreasing upward to 0% at ~30m where a slight increase in silt is noted. The deeper, sandier portion of the core has an average $^{87}Sr/^{86}Sr$ of 0.726 with an average bulk sediment Sr concentration of 162ppm (Figure 7). The sample taken in the finer sand portion at 20m depth is much more radiogenic with a $^{87}Sr/^{86}Sr$ value of 0.748 and a [Sr] of 113ppm. There is no perceptible effect of grain-size or sorting on Sr geochemistry of sediments in this region in the Holocene (Chapter 2 this thesis), so variations in $^{87}Sr/^{86}Sr$ and [Sr] are attributed to variations in provenance.

4.6 BH-2

BH-2 is located in the lower delta plain, along the northern edge of tidally influenced distributary channels and westward of the modern Meghna River. This site has been suggested to represent a location of combined Ganges and Brahmaputra sedimentation throughout the Holocene (Heroy et al., 2003). At depths greater than 20m, sediments are primarily fine sand (69% on average) channel fill with silt making up approximately 20% of the composition. The upper 20m of the borehole are characterized by muddy overbank deposits composed of 63% silt and 37% clay on average. In the sandy portion of the borehole the average $^{87}Sr/^{86}Sr$ is 0.728 and average [Sr] is 157ppm, and both parameters are marked by frequent oscillations (Figure 7). The average $^{87}Sr/^{86}Sr$ for thick mud cap is higher with a value of 0.733 and the average [Sr] of 129ppm is lower than the sand-dominated deposits.

V. Discussion

5.1 Holocene eastern delta and Sylhet Basin

BH-7, the westernmost of the Sylhet boreholes used in this study and the coarsest-grained is most likely a result of direct channel deposition when the Brahmaputra flowed into the Sylhet basin (Goodbred and Kuehl, 2000a). The sandiest samples display low $^{87}Sr/^{86}Sr$ values and high Sr concentrations typical of the modern Brahmaputra main channel and suggest that the Sr geochemistry of the Brahmaputra has remained relatively stable throughout the Holocene (Figure 6). Boreholes 8 and 9 are characterized by silty deposits that while not displaying as low $^{87}Sr/^{86}Sr$ or as high [Sr] signature as the sandy deposits in BH-7 still fall well within the range of modern Brahmaputra Sr geochemical signatures (Figure 8) and support the hypothesis that these values have not varied much through several thousand years of deposition. Therefore, modern Brahmaputra Sr signatures may be used as an analog for Brahmaputra sediment geochemistry throughout the Holocene

In BH-7, two finer-grained sedimentary deposits at 3m and 43m depth (Figure 6) exhibit depleted [Sr] and increased $^{87}Sr/^{86}Sr$. Major elemental data is only available for BH-8 in these region, but reveals that shifts in $^{87}Sr/^{86}Sr$ and [Sr] values are not a result of chemical weathering or mineralogical sorting (Chapter 2, this thesis), therefore this depletion in [Sr] is representative of a provenance signal. The silt and clay deposits suggest that active channel deposition is not occurring in the region and the Brahmaputra is likely following its western course during these periods of deposition. The Sr signatures of these fine-grained deposits are not indicative of exclusive sediment derivation from the more local basinal sources, however the Sr geochemistry could be explained by mixing with a more radiogenic, Sr-depleted source such as the Shillong Plateau. A mixing curve based on the limited data reveal an estimated Shillong influence of 35% - 40% for these finer grained deposits (Figure 9). The silt-dominated deposits of BH-8 and BH-9 contain even greater amounts of Shillong-derived material, up to 67% in some samples. This suggests that while contribution to the overall Brahmaputra mainstem sediment load before the delta may be of minor geochemical significance, sediments from the Shillong Plateau exert a more significant influence in a localized subsiding basin such as the Sylhet and will need to be considered in calculating sediment budgets along the Eastern portion of the delta.

5.2 Holocene western delta

The strontium geochemical signature of BH-1 is one that is significantly less radiogenic and with higher Sr concentrations than modern Ganges bedload in Bangladesh (Derry and France-Lanord, 2001). If modern values are an analog for early Holocene Ganges values in this region, then BH-1 could be the result of mixed inputs from Ganges and a less radiogenic source. While it is possible that Ganges Sr geochemistry may have varied throughout the Holocene as a result of variability in sediment supply from its distinct sub-basins such as increased input from the Deccan traps which carries a low $^{87}Sr/^{86}Sr$ and high [Sr] signature, recent data from Ullah (2010) from four different boreholes west of BH-1 on the G-B delta show that the Ganges Sr signature was similar to the modern throughout the last several thousand years of deposition. Therefore the less radiogenic sediments are likely being supplied from within the delta or another source not within the Ganges catchment. The variability in both $^{87}Sr/^{86}Sr$ and [Sr] are not directly correlated with major textural changes in BH-1, and are not attributed to weathering

(Chapter 2 this thesis) so the variations in Sr geochemistry are not a result of changes in river migration or depositional regime. Further, the variations in [Sr] are not aligned with $^{87}Sr/^{86}Sr$ variations. The lowest Sr concentration of 101 ppm (found at both 36 and 41m depth) is associated with the most radiogenic $^{87}Sr/^{86}Sr$ values. More radiogenic, less concentrated signatures are typically associated with Himalayan tributaries, however these [Sr] values are greater than those found in modern Himalayan tributaries and suggest some influence of higher concentration sources such as Tibetan sediments.

The Sr geochemistry of Brahmaputra sediments during this time is now well-constrained, with a signature that is less radiogenic with higher Sr concentrations than the BH-1 sediments, therefore it is unlikely that the Brahmaputra is the sole source for these sediments. The most plausible explanation is a mixing of Brahmaputra- and Ganges-derived sediments. A two endmember mixing model for Ganges and Brahmaputra influence on BH-1 sediment geochemistry estimates that the Brahmaputra supplies 30% - 50% of the sediments to these deposits (Figure 11). This finding contrasts with the previously held assumptions that the Ganges and Brahmaputra maintained separate courses throughout the late Quaternary with only a narrow zone of mixing in the vicinity of the current Meghna channel (Heroy et al., 2003; Allison et al., 2003, Goodbred and Kuehl, 2000a). With Brahmaputra influence being recorded farther westward than previous models have suggested, sediment budgets for the delta as well as for each individual river must be reconsidered. Budgets based on facies and volumetric analyses alone are not sufficient as displayed by these results, since stratigraphically it is not always clear which river carried the sediments in a given deposit or to what degree mixing may have taken place.

5.3 Holocene central delta and river mixing

In BH-5, the $^{87}Sr/^{86}Sr$ values appear to come from two distinct sources. The less radiogenic source in the samples from the 40-80m depth range is within the range of modern Brahmaputra sediments and the Holocene sediments from the Sylhet Basin analyzed here, and is therefore interpreted as Brahmaputra channel fill (Figure 8). The shallower sample at 20m depth is more radiogenic than the sediments below, and falls within the range of $^{87}Sr/^{86}Sr$ and [Sr] observed in BH-1 indicating that this sample is derived from a mix of Ganges and Brahmaputra

influence. This suggests that Ganges influence in this region of the delta is fairly recent, and that the Brahmaputra dominated sedimentation in the central delta throughout the early- and mid-Holocene. The Sr geochemistry of this sample suggest a mix of ~55% Ganges and ~45% Brahmaputra sediments (Figure 10) which indicates that the confluence of these two rivers has likely been relatively stable in this region throughout this depositional time period.

Farther downstream of the modern confluence, BH-2 sediment $^{87}Sr/^{86}Sr$ and [Sr] values fall within the range of modern Brahmaputra values (Figure 8), with samples on the whole being slightly more radiogenic than Holocene $^{87}Sr/^{86}Sr$ values in the Sylhet basin. Below 20m depth, the sediments are clearly dominated by Brahmaputra influence. The slightly more radiogenic and somewhat Sr-depleted nature of the sediments in the upper 20m of the borehole gives the appearance of increased Ganges influence in these most recently deposited sediments, perhaps as much as 35% (Figure 10). While it has been shown that grain-size sorting does not have a significant effect on the Sr geochemistry of these deltaic sediments (Chapter 2 this thesis), the prolonged period of overbank flood deposition in the absence of direct influence from a main river channel allows for an increased probability that these sediments have been reworked and may not represent a true measurement of the mix of Ganges and Brahmaputra influence downstream of the confluence. What is clear is that as seen further upstream, the early and mid-Holocene deposits are derived from Brahmaputra sedimentation, with the Ganges contributing sediments only relatively recently.

Both of these centralized boreholes reveal the importance of Brahmaputra sedimentation throughout the middle portions of the delta during the early and middle Holocene. Previous models suggested that this region of mixing had been relatively stable (Goodbred and Kuehl, 2000a; Allison et al., 2003, Heroy et al., 2003), with the Brahmaputra being confined primarily to the Sylhet basin and a narrow region west of the Madhupur terrace. However, Sr geochemistry has revealed that the Brahmaputra is responsible for sedimentation over a broad swath of the central delta (in addition to dominating eastern delta sedimentation) with potential for influence beyond these points westward. Indeed, recent work has revealed that Brahmaputra influence extends into the Western delta for parts of the Holocene (Ullah, 2010). These findings could have implications for developing individual Brahmaputra and Ganges sediment budgets through the Holocene.

5.4 Late Pleistocene eastern delta and Sylhet Basin

Samples from the basal coarse sands in BH-8 (below 91m), presumably latest Pleistocene in age, display extremely radiogenic $^{87}Sr/^{86}Sr$ and depleted [Sr] signatures (Figure 6). These samples plot well within the range of Himalayan Tributaries, and suggest that during this time period there was little to no input of sediment from Tibet or around the syntaxis region. The coarse grain size and highly radiogenic nature of the sediments indicates that an active river channel was present in the Sylhet basin at the time these sediments were deposited, as there must be significant stream velocity to carry such coarse sands, and the geochemical signature is more radiogenic than sediments sourced more proximal to the basin such as the Shillong Plateau. Though micas are easily detected upon visual inspection of the samples, there is no geochemical indication of enrichment in biotite that could lead to an anomalously radiogenic signal (Chapter 2, this thesis). In order for there to be such an increase in Himalayan influence on bedload sediments, there would have to be a significant or complete reduction in sediment input from the Tsangpo portion of the Brahmaputra. This could be achieved through ice damming and the formation of high altitude glacial lakes in this portion of the basin (e.g. Montgomery et al., 2004). As a result, the primary sediment input would be from the Himalayan tributaries. The only major tributary with $^{87}Sr/^{86}Sr$ values radiogenic enough to supply sediments with the signature seen at 99m is the Tista River with $^{87}Sr/^{86}Sr$ between 0.810 and 0.825 (Singh and France-Lanord, 2002). The similarity of these samples with the modern Tista values suggests that not only was Tsangpo influence cut off to this region at this time, but that the Tista River itself may have actually flowed through Sylhet.

VI. Conclusions

The unique Sr geochemical signatures of the Ganges and Brahmaputra rivers have remained distinct throughout the Holocene and allow for the spatial reconstruction of their depositional history throughout this time period on the Ganges-Brahmaputra delta. The data presented here reveal that not only has the Brahmaputra River been responsible for deposition in

the eastern delta and Sylhet Basin as previous expected, but that the river has deposited sediments much farther westward than previously modeled. In sediments previously believed to have been derived solely from Ganges input a mix of up to 50% Brahmaputra sediments has been found suggesting the possibility for Brahmaputra deposition in even the westernmost portions of the delta. This expansive reach of Brahmaputra sedimentation needs to be considered when calculating Holocene sediment budgets for the two rivers.

In the region of the modern Ganges-Brahmaputra confluence it is apparent that influence from Ganges sedimentation is relatively recent. Downstream of the modern confluence, Ganges sedimentary influence is even less significant, further underscoring the importance of the Brahmaputra in delivering sediment to the margin throughout the Holocene. This would suggest that even during times of rapid subsidence and infilling of the Sylhet basin, at least a portion of the Brahmaputra sediment load was reaching the margin.

The Sr data reveal a more complex depositional history in the Sylhet Basin as well. When the Brahmaputra is following its western course (as in the modern example) local sediment sources such as the Shillong Plateau and possibly the Mishmi Hills supply sediments in broad deposits several meters thick. This suggests that these minor sources play a more significant role in the infilling of the Sylhet basin than previously expected and need to be taken into account when calculating sediment budgets. Sr geochemistry of late Pleistocene sediments in the Sylhet basin reveals that glacial damming in the Tsangpo portion of the Brahmaputra River impacts sedimentation patterns downstream resulting in deposits that are clearly Himalayan in origin. The depleted [Sr] and highly radiogenic $^{87}Sr/^{86}Sr$ signature of these basal sands indicates direct derivation from the Tista River which also carries implications for re-routing and avulsions of major tributaries. In order to clarify the input of other Himalayan sources and the routing of the Tista, more focused work needs to take place upstream.

References

Ahmad, T., Harris, N., Bickle, M., Chapman, H., Bunbury, J., Prince, C., 2000. Isotopic constraints on the structural relationships between the Lesser Himalayan Series and the High Himalayan Crystalline Series, Garhwal Himalaya. GSA Bulletin 112, 467-477.

Alexander, P.O., Paul, D.K., 1977. Geochemistry and strontium isotopic composition of basalts from the Eastern Deccan volcanic province, India. Mineralogical Magazine 41, 165-172.

Allison, M.A., Khan, S.R., Goodbred Jr., S.L., Kuehl, S.A., 2003. Stratigraphic evolution of the late Holocene Ganges-Brahmaputra lower delta plain. Sedimentary Geology 155, 317-342.

Bickle, M.J., Bunbury, J., Chapman, H.J., Harris, N.B.W., Fairchild, I.J., Ahmad, T., 2003. Fluxes of Sr into the headwaters of the Ganges. Geochimica et Cosmochimica Acta 67, 2567-2584.

Bickle, M.J., Chapman, H.J., Bunbury, J., Harris, N.B.W., Fairchild, I., Ahmad, T., Pomiès, C., 2005. Relative contributions of silicate and carbonate rocks to riverine Sr fluxes in the headwaters of the Ganges. Geochimica et Cosmochimica Acta 69, 2221-2240.

Bookhagen, B., Thiede, R.C., Strecker, M.R., 2005a. Late Quaternary intensified monsoon phases control landscape evolution in the northwest Himalaya. Geology 33, 149-152.

Bookhagen, B., Thiede, R.C., Strecker, M.R., 2005b. Abnormal Monsoon years and their control on erosion and sediment flux in the high, arid northwest Himalaya. Earth and Planetary Science Letters 231, 131-146.

Campbell, I.H., Reiners, P.W., Allen, C.M., Nicolescu, S., Upadhyay, R., 2005. He-Pb double dating of detrital zircons from the Ganges and Indus Rivers: Implication for quantifying sediment recycling and provenance studies. Earth and Planetary Science Letters 237, 402-432.

Célérier, J., Harrison, T.M., Webb, A.A.G., Yin, A., 2009. The Kuman and Garwhal Lesser Himalaya, India: Part 1. Structure and Stratigraphy. GSA Bulletin 121, 1262-1280.

Colin, C., Turpin, L., Bertaux, J., Desprairies, A., Kissel, C., 1999. Erosional history of the Himalayan and Burman ranges during the last two glacial-interglacial cycles. Earth and Planetary Science Letters 171, 647-660.

Debon, F., Le Fort, P., Sheppard, S.M.F., Sonet, J., 1986. The Four Plutonic Belts of the Transhimalaya-Himalaya: a Chemical, Mineralogical, Isotopic, and Chronological Synthesis along a Tibet-Nepal Section. Journal of Petrology 27, 219-250.

Derry, L.A., France-Lanord, C., 1996. Neogene Himalayan weathering history and river $^{87}Sr/^{86}Sr$: impact on the marine Sr record. Earth and Planetary Science Letters 142, 59-74.

Galy, A, France-Lanord, C, Derry, L.A., 1996. The Late Oligocene-Early Miocene Himalayan belt Constraints deduced from isotopic compositions of Early Miocene turbidites in the Bengal Fan. Tectonophysics 260, 109-118.

Galy, A., France-Lanord, C., Derry, L.A., 1999. The strontium isotopic budget of Himalayan Rivers in Nepal and Bangladesh. Geochimica et Cosmochimica Acta 63, 1905-1925.

Galy, A., France-Lanord, C., 2001. Higher erosion rates in the Himalaya: Geochemical constraints on riverine fluxes. Geology 29, 23-26.

Garzanti, E., Vezzoli, G., Andò, S., France-Lanord, C., Singh, S.K., Foster, G., 2004. Sand petrology and focused erosion in collision orogens: the Brahmaputra case. Earth and Planetary Science Letters 230, 157-174.

Goodbred Jr., S.L., Kuehl, S.A., 2000a. The significance of large sediment supply, active tectonism, and eustasy on margin sequence development: Late Quaternary stratigraphy and evolution of the Ganges-Brahmaputra delta. Sedimentary Geology 133, 227-248.

Goodbred Jr., S.L., Kuehl, S.A., 2000b. Enormous Ganges-Brahmaputra sediment discharge during strengthened early Holocene monsoon. Geology 28, 1083-1086.

Harris, N., Bickle, M., Chapman, H., Fairchild, I., Bunbury, J., 1998. The significance of Himalayan rivers for silicate weathering rates: evidence from the Bhote Kosi tributary. Chemical Geology 144, 205-220.

Heroy, D.C., Kuehl, S.A., Goodbred Jr., S.L., 2003. Mineralogy of the Ganges and Brahmaputra Rivers: implications for river switching and Late Quaternary climate change. Sedimentary Geology 155, 343-359.

Huizing, H.G.J., 1971. A reconnaissance study of the mineralogy of sand fractions from East Pakistan sediments and soils. Geoderma 6, 109-133.

Kessarkar, P.M., Rao, V.P., Ahmad, S.M., Patil, S.K., Kumar, A.A., Babu, G.A., Chakraborty, S., Rajan, R.S., 2005. Changing sedimentary environment during the Late Quaternary: Sedimentological and isotopic evidence from the distal Bengal Fan. Deep-Sea Research I 52, 1591-1615.

Montgomery, D.R., Hallet, B., Yuping, L., Finnegan, N., Anders, A., Gillespie, A., Greenberg, H., 2004. Evidence for Holocene megafloods down the Tsangpo River gorge, southeastern Tibet. Quaternary Research 62, 201-207.

Najman, Y., Bickle, M.J., Chapman, H.J., 2000. Early Himalayan exhumation: Isotopic constraints from the Indian foredeep basin. Terra Nova 12, 28-34.

Najman, Y., 2006. The detrital record of orogenesis: A review of approaches and techniques used in the Himalayan sedimentary basin. Earth-Science Reviews 74, 1-72.

Pate, R.D., 2008. Multiple-proxy records of delta evolution and dispersal system behavior: Fluvial and coastal borehole evidence from the Bengal Basin, Bangladesh. Masters Thesis, Vanderbilt University, Nashville, TN, 112pp.

Peng, Z.X., Mahoney, J.J., Hooper, P.R., MacDougal, J.D., Krishnamurthy, P., 1998. Basalts of the northeaster Deccan traps, India: Isotopic and elemental geochemistry and relation to southwestern Deccan stratigraphy. Journal of Geophysical Research 103, 29843-29865.

Pereira, W.E., Rostad, C.E., Leiker, T.J., 1992. Synthetic organic agrochemicals in the lower Mississippi River and its major tributaries: Distribution, transport and fate. Journal of Contaminant Hydrology 9, 175-188.

Rahaman, W., Singh, S.K., Sinha, R., Tandon, S.K., 2009. Climate control on erosion distribution over the Himalaya during the past ~100 ka. Geology 37, 559-562.

Saha, A., Basu, A.R., Garzione, C.N., Bandyopadhyay, P.K., Chakrabarti, A., 2004. Geochemical and petrological evidence for subduction-accretion processes in the Archaen Eastern Indian Craton. Earth and Planetary Science Letters 220, 91-106.

Schärer, U., Hamet, J., Allègre, C.J., 1984. The Transhimalaya (Gangdese) plutonism in the Ladakh region: a U-Pb and Rb-Sr study. Earth and Planetary Science Letters 67, 327-339.

Singh, P., 2009. Major, trace and REE geochemistry of the Ganga River sediments: Influence of provenance and sedimentary processes. Chemical Geology 266, 251-264.

Singh, P., 2010. Geochemistry and provenance of stream sediments of the Ganga River and its major tributaries in the Himalayan region, India. Chemical Geology 269, 220-236.

Singh, S.K., France-Lanord, C., 2002. Tracing the distribution of erosion in the Brahmaputra watershed from isotopic compositions of stream sediments. Earth and Planetary Science Letters 6341, 1-18.

Singh, S.K., Kumar, A., France-Lanord, C., 2006. Sr and $^{87}Sr/^{86}Sr$ in waters and sediments of the Brahmaputra river system: Silicate weathering, CO_2 consumption and Sr flux. Chemical Geology 234, 308-320.

Singh, S.K., Santosh, K.R., Krishnaswami, S., 2008. Sr and Nd isotopes in river sediments from the Ganga Basin: Sediment provenance and spatial variability in physical erosion. Journal of Geophysical Research 113, F03006, 18pp.

Singh, S.K., 2006. Spatial variability in erosion in the Brahmaputra basin: causes and impacts. Current Science 90, 1272-1276.

Sinha, R., Friend, P.F., 1994. River systems and their sediment flux, Indo-Gangetic Plains, Northern Bihar, India. Sedimentology 41, 825-845.

Srivastava, R.K., Heaman, L.M., Sinha, A.K., Shihua, S., 2005. Emplacement age and isotope geochemistry of Sung Valley alkaline-carbonatite complex, Shillong Plateau, northeastern India: Implications for primary carbonate melt and genesis of the associated silicate rocks. Lithos 81, 33-54.

Stewart, R.J., Hallet, B., Zeitler, P.K., Malloy, M.A., Allen, C.M., Trippett, D., 2008. Brahmaputra sediment flux dominated by highly localized rapid erosion from the easternmost Himalaya. Geology 36, 711-714.

Ullah, M., 2010. Provenance analysis of Late Quaternary sediments from the Ganges-Brahmaputra delta, Bangladesh. Masters Thesis, Vanderbilt University, Nashville, TN, 95pp.

White, N.M., Parrish, R.R., Bickle, M.J., Najman, Y.M.R., Burbank, D., Maithani, A., 2001. Metamorphism and exhumation of the NW Himalaya constrained by U-Th-Pb analyses of detrital monazite grains from early foreland basin sediments. Journal of the Geological Society (London) 158, 625-635.

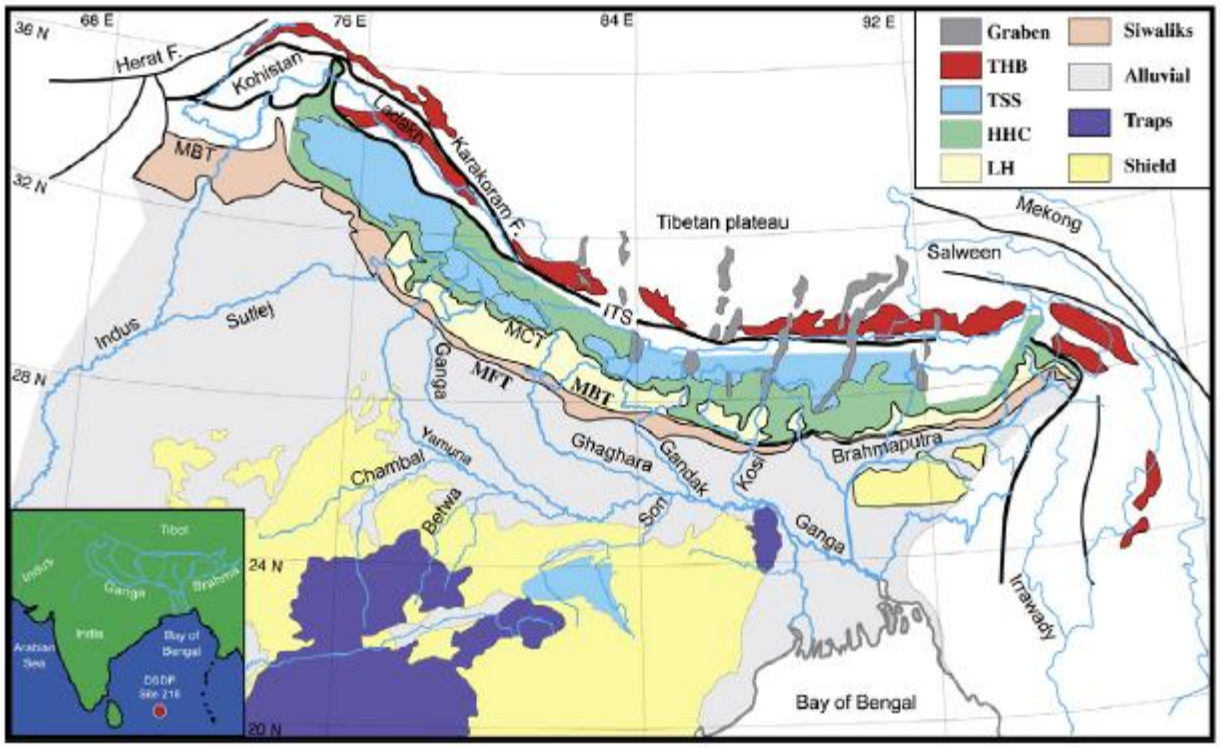

Figure 1. Map of major Himalayan lithologic untils that supply sediments to the Ganges and Brahmaputra rivers (taken from Galy et al., 2010).

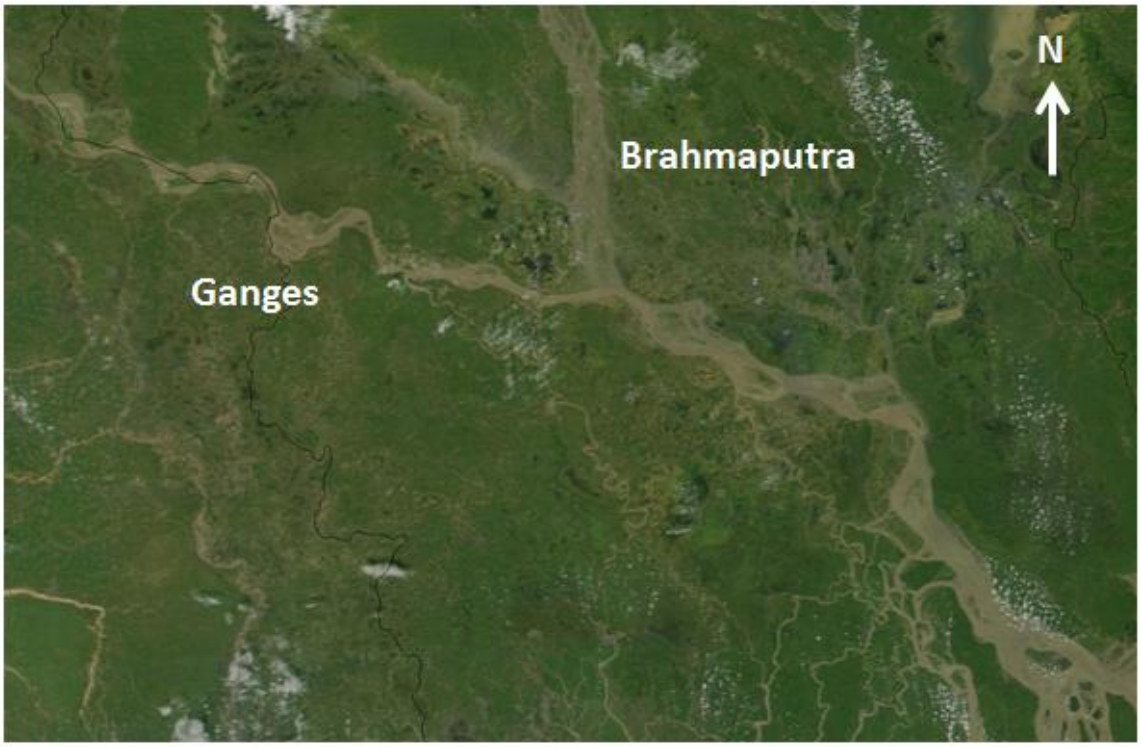

Figure 2. Satellite image showing how sediments from the Ganges and Brahmaputra rivers remain unmixed well downstream of their confluence (image from NASA earth observatory http://earthobservatory.nasa.gov/IOTD/view.php?id=1937).

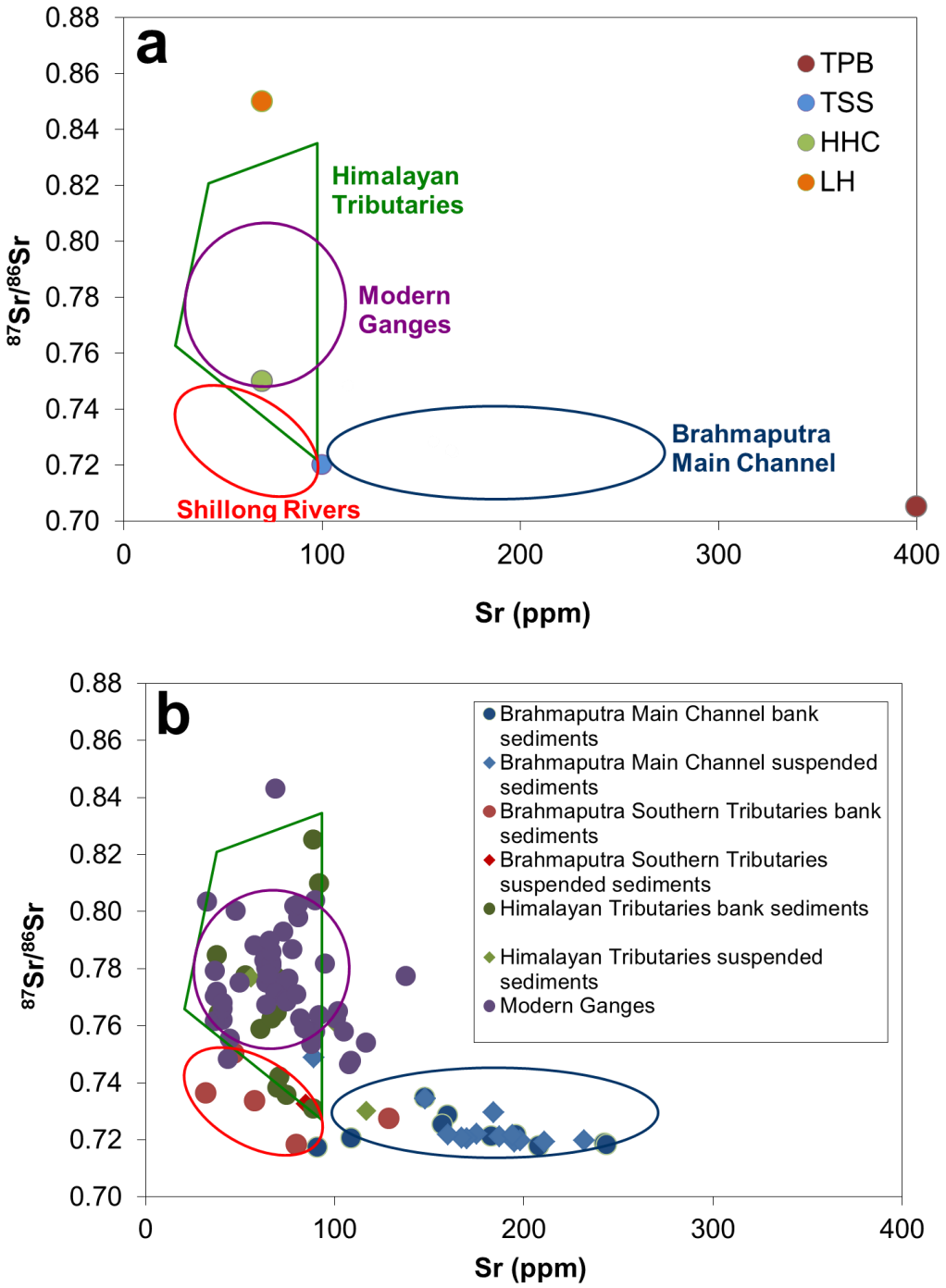

Figure 3. (a) $^{87}Sr/^{86}Sr$ vs. Sr plot outlining modern geochemical signatures of the primary sediment sources to the Ganges and Brahmaputra rivers, along with endmember geochemical signatures for the major Himalayan lithologies (Singh and France-Lanord, 2002; Galy and France-Lanord, 2001; Singh et al., 2008). (b) Plot of source area data (Singh and France-Lanord, 2002; Galy and France-Lanord, 2001; Singh et al., 2008).

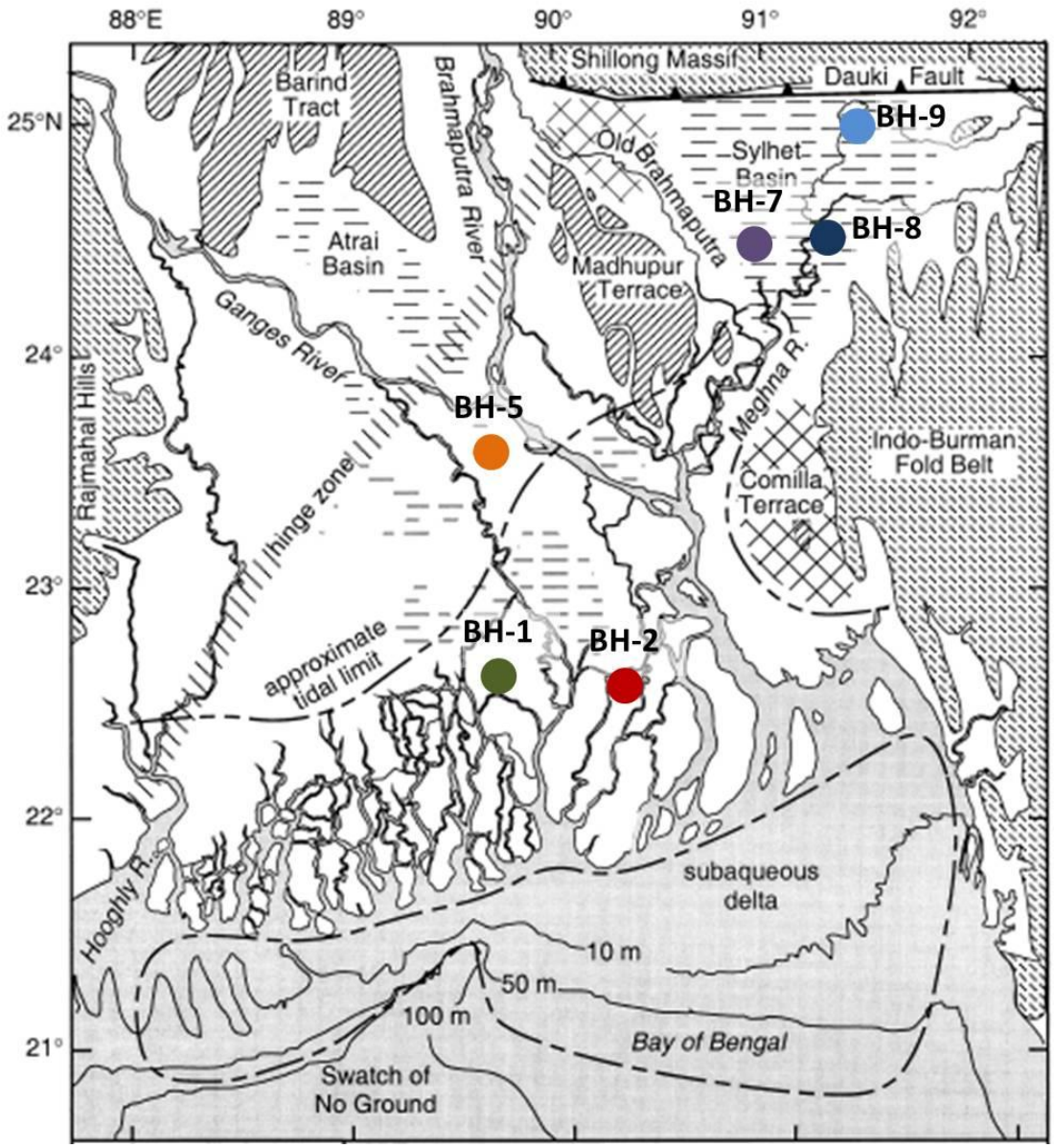

Figure 4. Locations of the boreholes used in this study on a generalized geologic map of the Ganges-Brahmaputra delta (adapted from Goodbred and Kuehl, 2000a).

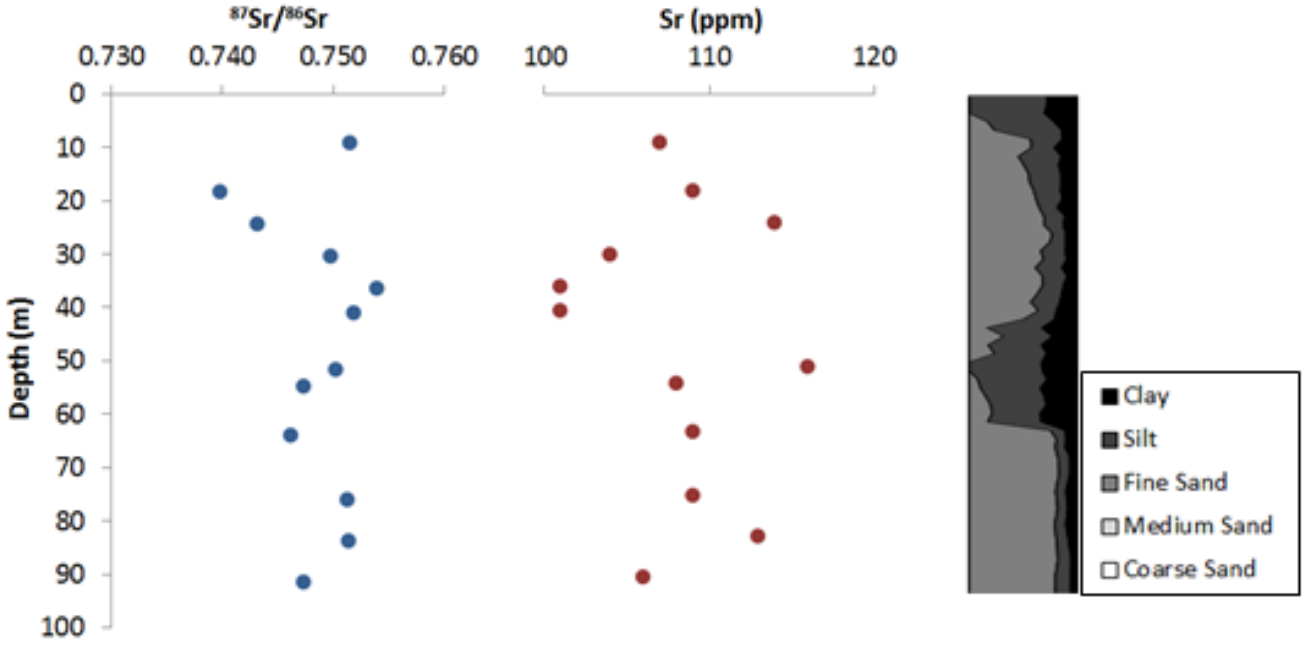

Figure 5. $^{87}Sr/^{86}Sr$ and Sr concentration profiles for BH-1 with relative grain-size shown for comparison.

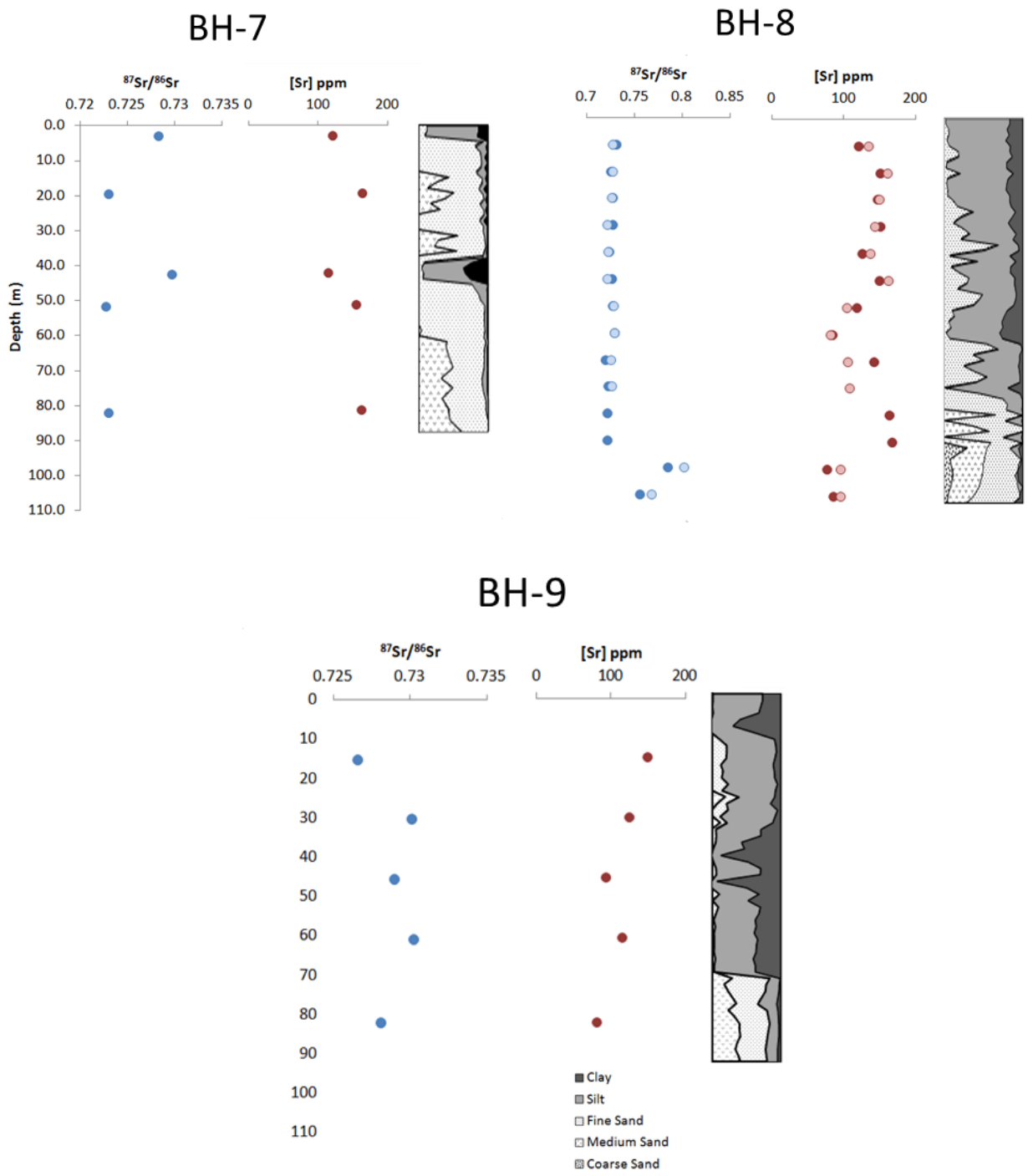

Figure 6. $^{87}Sr/^{86}Sr$ and Sr concentration profiles for the three Sylhet Basin (eastern delta) boreholes used in this study. Note the different x-axis scales between the different boreholes.

BH-2

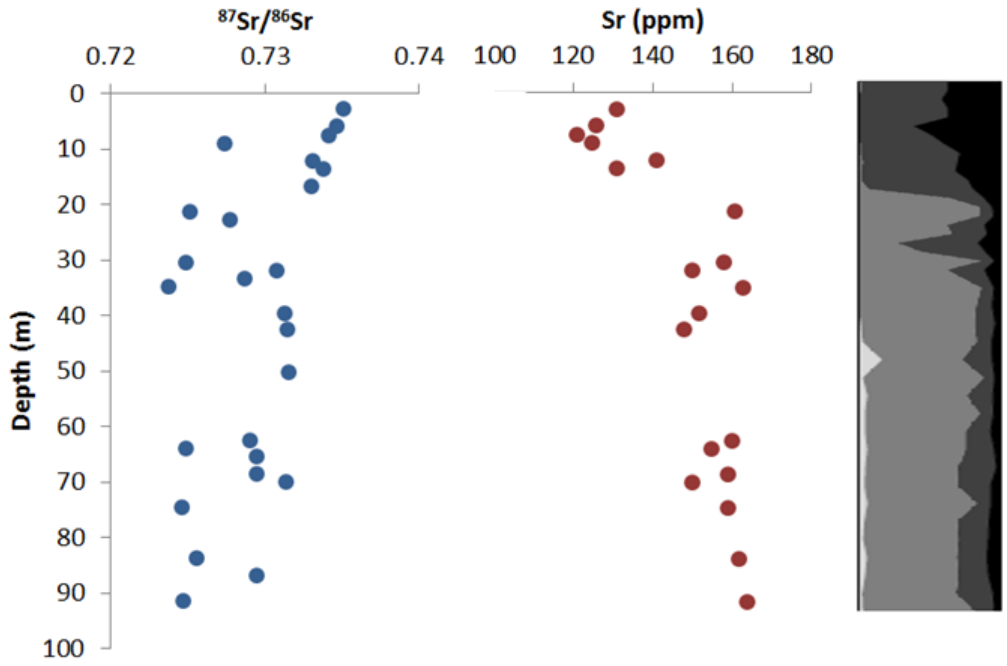

BH-5

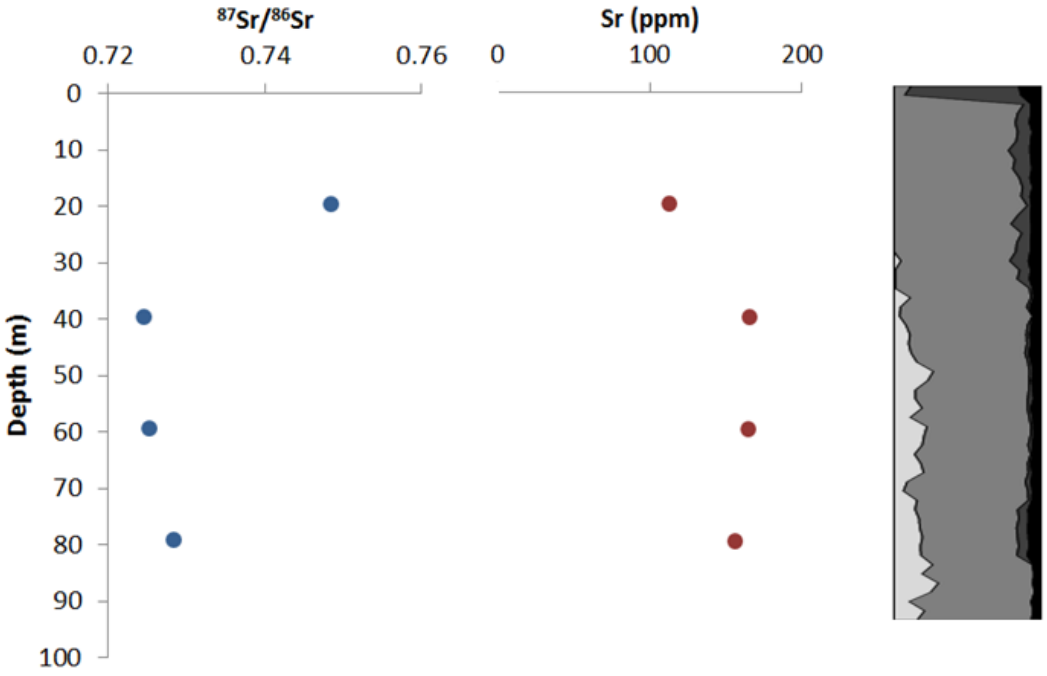

Figure 7. Sr geochemistry of central deltaic boreholes, BH-2 and BH-5.

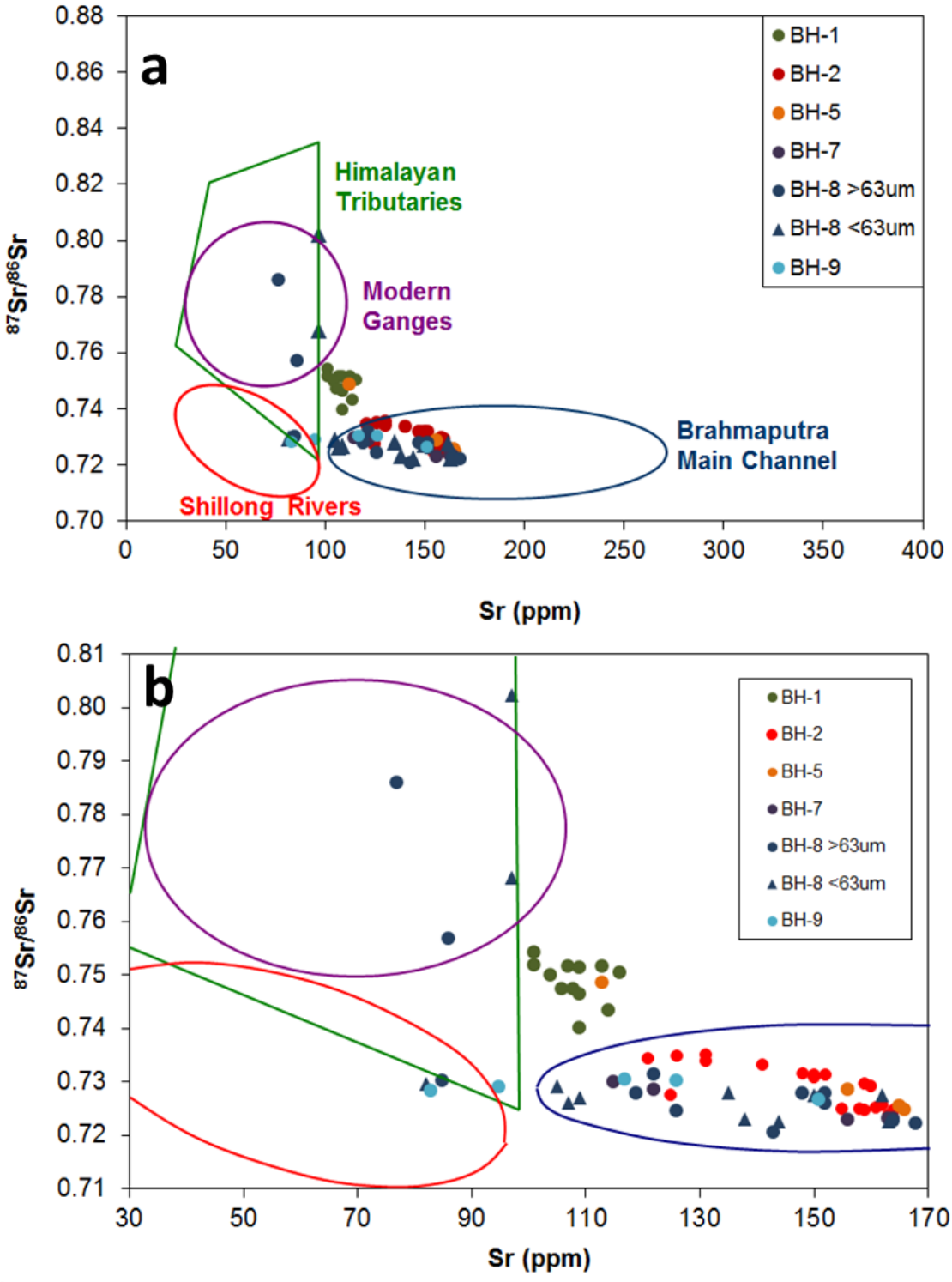

Figure 8. (a) Provenance of borehole samples in light of primary river and tributary sources. (b) Blow-up of (a) to reveal interrelationships between boreholes. BH-1 is a mix of Ganges and Brahmaputra sediments, and BH-7, BH-8, and BH-9 reveal influence from Shillong sedimentation.

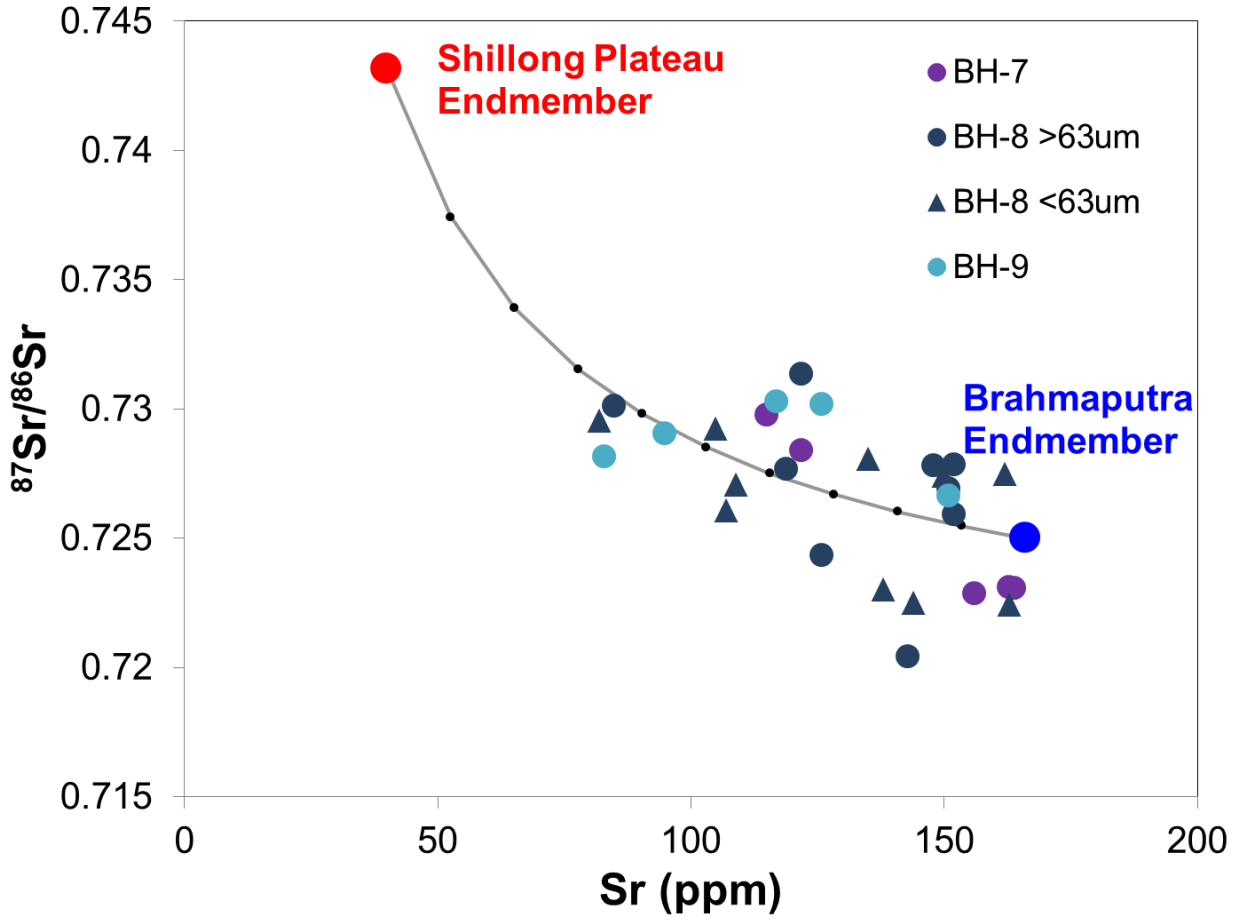

Figure 9. Mixing curve for Sylhet basin (eastern delta) boreholes illustrating greater influence of Shillong sedimentation for some samples. Mixing line calculated at 10% intervals.

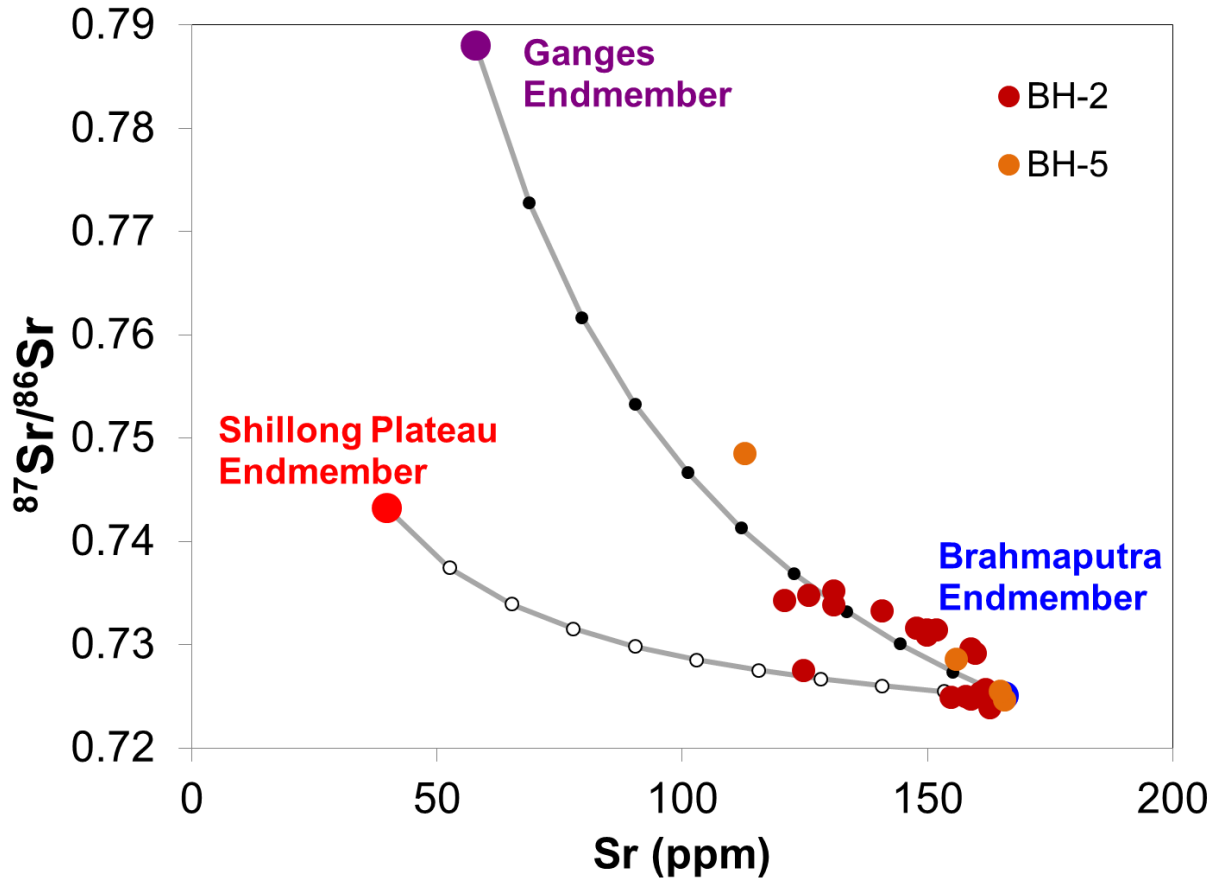

Figure 10. Mixing curves for central delta boreholes. Sediments are primarily derived from the Ganges and Brahmaputra, however the dominance of Brahmaputra-derived sedimentation in BH-2 also reveals influcen from the Shillong Plateau. Mixing line calculated at 10% intervals.

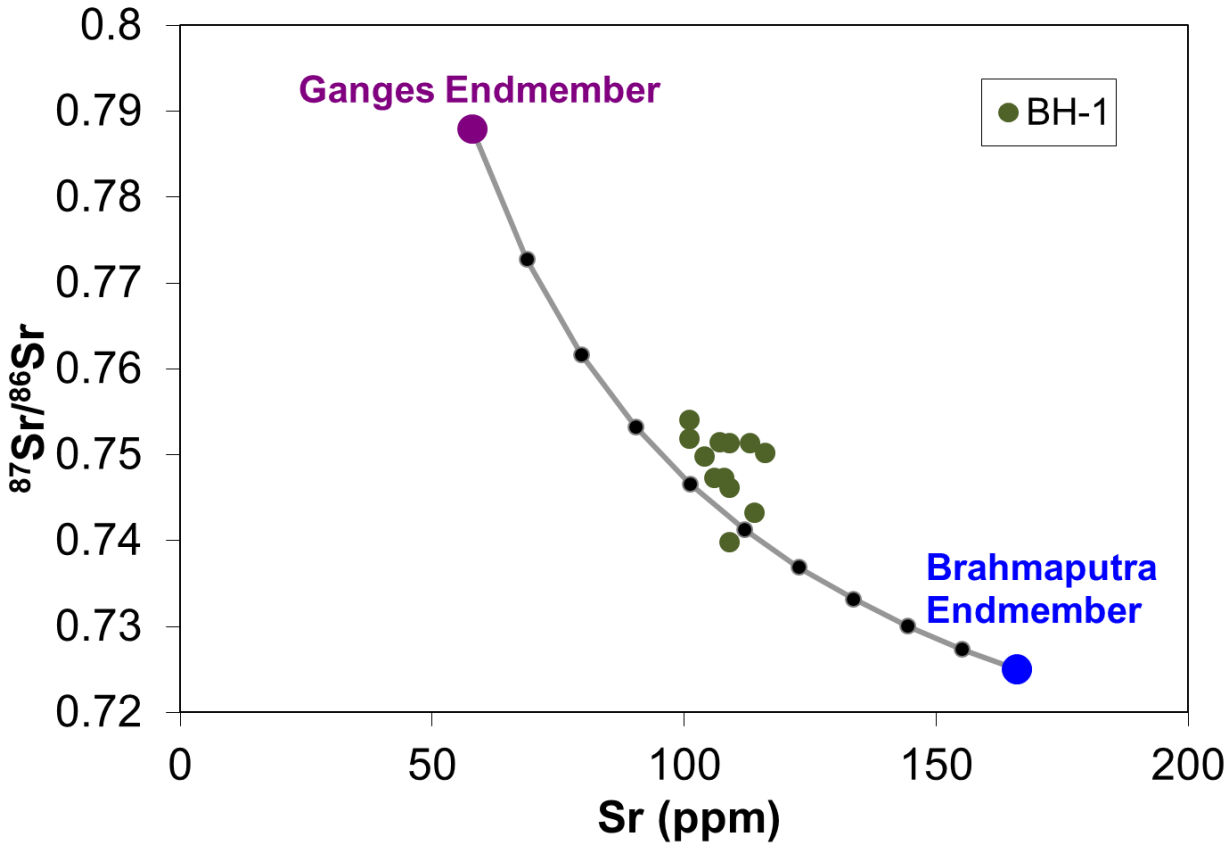

Figure 11. Mixing curve for the western delta. Mixing line calculated at 10% intervals. Sediments are a clear mix of Brahmaputra and Ganges inputs revealing much less Ganges influence than previously suspected based on clay mineralogy and heavy mineral assemblages.

Chapter 4: Conclusions, Implications, and Directions for Future Study

The dissertation research presented here reveals some surprising results regarding the development of the G-B delta and the sedimentary records deposited by the two primary river influences, the Ganges and the Brahmaputra. Most noteworthy regarding the Holocene development of the delta is that the Brahmaputra is responsible for vast sedimentary deposits spanning a much larger area of the delta than previously recognized. To this point, it has been presumed that the Brahmaputra was responsible for the infilling of the Sylhet basin during times of rapid subsidence with little of its load bypassing the eastern portion of the delta. However, we now see that even during times of rapid infilling of the Sylhet basin, Brahmaputra sediments were reaching the margin (as evidenced by the dominance of Brahmaputra-derived sedimentation in BH-2). Further, when the Brahmaputra followed its western course (west of the Madhupur Terrace) it deposited sediments not just along a narrow mixing zone in the central delta, but far into the western delta, only there mixing with Ganges sediments. Without a full mapping of the extent of Brahmaputra influence throughout Holocene deltaic deposits, we cannot calculate a budget at this time to estimate the relative volume of sediment deposited by the individual rivers, but the provenance tools presented here, $^{87}Sr/^{86}Sr$ and [Sr], will allow for this goal to be achieved with future research.

One question that arises from these findings is the potential partitioning of sediment from different river sources between the sub-aerial and sub-aqueous deltas. Are Brahmaputra sediments being preferentially sequestered on the sub-aerial delta with a larger proportion of Ganges sediments moving offshore to the sub-aqueous delta? This is one direction where future work will be directed. Sr geochemistry should provide insight into the sourcing of off-shore Late Quaternary deposits. In addition, it will be important to have a better understanding of the modern system with this regard. Currently there is very little data available for the fate of sediments downstream of the confluence with regard to their geochemical character, mixing and partitioning. Future work will be focused in this direction as well.

Concerning the weathering of deltaic deposits, it was surprising to find no general trends that can be directly attributed to climate change throughout the Holocene and even into the latest Pleistocene deposits analyzed in the Sylhet Basin. Late Quaternary Bengal Fan deposits display a clear trend of increased weathering signatures during increased monsoon intensity (Colin et al.,

1999; Kessarkar et al., 2005), but this trend is absent on the delta. It is possible that due to the increased discharge and sediment loads at this time (Goodbred and Kuehl, 2000) these weathering signals were just not preserved on the delta. This is an important finding especially with respect to source-to-sink research. Weathering trends with short-term climate change are noted in the catchment as well as the ultimate sink for this system, the Bengal Fan, but are absent in the intermediary portion, the delta. In addition, we find that almost no additional chemical alteration takes place as sediments pass through the delta meaning that in a system such as this with incredibly high sediment loads, the delta seems to be more of a conduit for the propagation of weathering signals from source to sink. However, as discussed above, there may be some evidence for preferential sequestration of Brahmaputra sands on the delta which could impact provenance analyses of fan deposits.

Further implications of this work are that these results may help with understanding the heterogeneous nature of As contamination in Holocene and Pleistocene aquifers in Bangladesh. Recent work has shown that both modern and historical river morphological patterns exert some control on Arsenic distribution in shallow aquifers. In addition, evidence shows that provenance of aquifer sands is related to the As geochemistry as well (Weinman, 2010; Weinman et al., 2008). The research presented here is a first step in beginning to map out a complete Holocene provenance history of the delta which may assist in the discovery of clean drinking water resources for the people of Bangladesh.

The work presented here also shows the value of $^{87}Sr/^{86}Sr$ and [Sr] as powerful tools for unraveling provenance signatures. We have shown that $^{87}Sr/^{86}Sr$ values are not altered even in sediments with highly weathered signatures where preferential dissolution of biotite is occurring. While [Sr] may be altered to some degree in bulk samples containing high clay content due to a higher overall weathering signature, the provenance signals are still preserved. The demonstration of the robust nature of these signatures in deltaic deposits will allow for their use in addressing a variety of future questions in onshore deposits, offshore deposits, and even modern river mixing dynamics.

References

Clift, P.D., Giosan, L., Blusztajn, J., Campbell, I.H., Allen, C., Pringle, M., Tabrez, A.R., Danish, M., Rabbani, M.M., Alizai, An., Carter, A., Lückge, A., 2008. Holocene erosion of the Lesser Himalaya triggered by intensified summer monsoon. Geology 36, 79-82.

Colin, C., Turpin, L., Bertaux, J., Desprairies, A., Kissel, C., 1999. Erosional history of the Himalayan and Burman ranges during the last two glacial-interglacial cycles. Earth and Planetary Science Letters 171, 647-660.

Goodbred Jr., S.L., Kuehl, S.A., 2000b. Enormous Ganges-Brahmaputra sediment discharge during strengthened early Holocene monsoon. Geology 28, 1083-1086.

Kessarkar, P.M., Rao, V.P., Ahmad, S.M., Patil, S.K., Kumar, A.A., Babu, G.A., Chakraborty, S., Rajan, R.S., 2005. Changing sedimentary environment during the Late Quaternary: Sedimentological and isotopic evidence from the distal Bengal Fan. Deep-Sea Research I 52, 1591-1615.

Weinman, B., Goodbred, S.L., Zheng, Y., van Geen, A., Aziz, Z., Singhvi, A., Steckler, M., 2008. Controls of Floodplain evolution on shallow aquifer development and the resulting distribution of groundwater arsenic: Araihazar, Bangladesh. GSA Bulletin 120, 1567-1580.

Weinman, B., 2010. The evolution of aquifers and arsenic in Asia: A study of the fluvio-deltaic processes leading to aquifer formation and arsenic cycling and heterogeneity in Bangladesh, Vietnam, and Nepal. Ph.D. Dissertation, Vanderbilt University, Nashville, TN, 220pp.

Complete list of references for this dissertation

Ahmad, T., Harris, N., Bickle, M., Chapman, H., Bunbury, J., Prince, C., 2000. Isotopic constraints on the structural relationships between the Lesser Himalayan Series and the High Himalayan Crystalline Series, Garhwal Himalaya. GSA Bulletin 112, 467-477.

Alam, M., 1996. Subsidence of the Ganges-Brahmaputra delta of Bangladesh and associated drainage, sedimentation, and salinity problems. In: Milliman, J.D., Haq, B.U. (Eds). Sea-Level Rise and Coastal Subsidence. Kluwer Academic Publishers, Dordrecht, 169-192.

Alam., M., Alam, M.M., Curray, J.R., Chowdhury, M.L.R., Gani, M.R., 2003. An overview of the sedimentary geology of the Bengal Basin in relation to the regional tectonic framework and basin-fill history. Sedimentary Geology 155, 179-208.

Alexander, P.O., Paul, D.K., 1977. Geochemistry and strontium isotopic composition of basalts from the Eastern Deccan volcanic province, India. Mineralogical Magazine 41, 165-172.

Allison, M.A., Khan, S.R., Goodbred Jr., S.L., Kuehl, S.A., 2003. Stratigraphic evolution of the late Holocene Ganges-Brahmaputra lower delta plain. Sedimentary Geology 155, 317-342.

Bickle, M.J., Bunbury, J., Chapman, H.J., Harris, N.B.W., Fairchild, I.J., Ahmad, T., 2003. Fluxes of Sr into the headwaters of the Ganges. Geochimica et Cosmochimica Acta 67, 2567-2584.

Bickle, M.J., Chapman, H.J., Bunbury, J., Harris, N.B.W., Fairchild, I., Ahmad, T., Pomiès, C., 2005. Relative contributions of silicate and carbonate rocks to riverine Sr fluxes in the headwaters of the Ganges. Geochimica et Cosmochimica Acta 69, 2221-2240.

Blum, J.D., Erel, Y., 1997. Rb-Sr isotope systematics of a granitic soil chronosequence: The importance of biotite weathering. Geochimica et Cosmochimica Acta 61, 3193-3204.

Bookhagen, B., Thiede, R.C., Strecker, M.R., 2005a. Late Quaternary intensified monsoon phases control landscape evolution in the northwest Himalaya. Geology 33, 149-152.

Bookhagen, B., Thiede, R.C., Strecker, M.R., 2005b. Abnormal Monsoon years and their control on erosion and sediment flux in the high, arid northwest Himalaya. Earth and Planetary Science Letters 231, 131-146.

Bouquillon, A., France-Lanord, C., Michard, A., Tiercelin, J.J.,1990. Sedimentology and isotopic chemistry of the Bengal Fan sediments: the denudation of the Himalaya. Proceedings of the Ocean Drilling Program. Scientific Results, vol. 116, 43– 58.

Brammer, H., 1996. The Geography of the Soils of Bangladesh. University Press, Ltd. Dhaka, 287 pp.

Bristow, C.S., 1999. Gradual avulsion, river metamorphosis and reworking by underfit streams: a modern example from the Brahmaputra River in Bangladesh and possible ancient example in the Spanish Pyrenees. In: Smith, N., Rogers, J., (Eds.), Fluvial Sedimentology VI. Special Publication of International Association of Sedimentologists, vol. 28, 221-230.

Campbell, I.H., Reiners, P.W., Allen, C.M., Nicolescu, S., Upadhyay, R., 2005. He-Pb double dating of detrital zircons from the Ganges and Indus Rivers: Implication for quantifying sediment recycling and provenance studies. Earth and Planetary Science Letters 237, 402-432.

Célérier, J., Harrison, T.M., Webb, A.A.G., Yin, A., 2009. The Kuman and Garwhal Lesser Himalaya, India: Part 1. Structure and Stratigraphy. GSA Bulletin 121, 1262-1280.

Clift, P.D., Giosan, L., Blusztajn, J., Campbell, I.H., Allen, C., Pringle, M., Tabrez, A.R., Danish, M., Rabbani, M.M., Alizai, An., Carter, A., Lückge, A., 2008. Holocene erosion of the Lesser Himalaya triggered by intensified summer monsoon. Geology 36, 79-82.

Coleman, J.M., 1969. Brahmaputra river: channel processes and sedimentation. Sedimentary Geology 3, 129-239.

Colin, C., Turpin, L., Bertaux, J., Desprairies, A., Kissel, C., 1999. Erosional history of the Himalayan and Burman ranges during the last two glacial-interglacial cycles. Earth and Planetary Science Letters 171, 647-660.

Curtis, C.D., 1990. Aspects of climate influence on the clay mineralogy and geochemistry of soils, paleosols and clastic sedimentary rocks. Journal of the Geological Society, London 147, 351-357.

Dasch, E.J., 1969. Strontium isotopes in weathering profiles, deep-sea sediments, and sedimentary rocks. Geochimica et Cosmochimica Acta 33, 1521-1552.

Datta, D.K., Subramanian, V., 1997. Texture and mineralogy of sediments from the Ganges-Brahmaputra-Meghna river system in the Bengal Basin, Bangladesh and their environmental implications. Environmental Geology 30, 181-188.

Debon, F., Le Fort, P., Sheppard, S.M.F., Sonet, J., 1986. The Four Plutonic Belts of the Transhimalaya-Himalaya: a Chemical, Mineralogical, Isotopic, and Chronological Synthesis along a Tibet-Nepal Section. Journal of Petrology 27, 219-250.

Derry, L.A., France-Lanord, C., 1996. Neogene Himalayan weathering history and river $^{87}Sr/^{86}Sr$: impact on the marine Sr record. Earth and Planetary Science Letters 142, 59-74.

Edmond, J.M., 1992. Himalayan Tectonics, Weathering Processes, and the Strontium Isotope Record in Marine Limestones. Science 258, 1594-1597.

Egashira, K., Aramaki, K., Yoshimasa, M., Takeda, A., Yamasaki, S., 2004. Rare earth elements and clay minerals of the soils of the floodplains of three major rivers in Bangladesh. Geoderma 120, 7-15.

Eisenhauer, A., Meyer, H., Rachold, V., Tuetken, T., Wiegand, B., Hansen, B.T., Spielhagen, R.F., Lindemann, F., Kassesn, H., 1999. Grain size separation and sediment mixing in Arctic Ocean sediments: evidence from the strontium isotope systematic. Chemical Geology 158, 173-188.

English, N.B., Quade, J., DeCelles, P.G., Garzione, C.N., 2000. Geologic control of Sr and major elemental chemistry in Himalayan Rivers, Nepal. Geochimica et Cosmochimica Acta 64, 2549-2566.

Evans, L.J., 1992. Alteration products at the earth's surface – the clay minerals. In: Martini, I.P., Chesworth, W., (Eds.) Weathering, Soils, and Paleosols (Developments in Earth Surface Processes). Elsevier Science, 107-125.

Faure, G., Powell, J.L., 1972. Strontium isotope geology. Springer-Verlag, New York, 197 pp.

Fedo, C.M., Nesbitt, H.W., Young, Grant, M., 1995. Unraveling the effects of potassium metasomatism in sedimentary rocks and paleosols, with implications for paleoweathering conditions and provenance. Geology 23, 921-924.

Finlayson, D.P., Montgomery, D.R., Hallet, B., 2002. Spatial coincidence of rapid inferred erosion with young metamorphic massifs in the Himalayas. Geology 30, 219-222.

France-Lanord C., Derry L.A. and Michard A. (1993). Evolution of the Himalaya since Miocene time: Isotopic and sedimentologic evidence from the Bengal Fan. In: Treloar, P.J., Searle, M. (Eds) Himalayan Tectonics, Geological Society of London Special Publication 74, 605-623.

France-Lanord, C., Derry, L.A., 1994. $\delta^{13}C$ of organic carbon in the Bengal fan: source evolution and transport of C3 and C4 plant carbon to marine sediments. Geochimica et Cosmochimica Acta 58, 4809-4814.

Galy, A, France-Lanord, C, Derry, L.A., 1996. The Late Oligocene-Early Miocene Himalayan belt Constraints deduced from isotopic compositions of Early Miocene turbidites in the Bengal Fan. Tectonophysics 260, 109-118.

Galy, A., France-Lanord, C., Derry, L.A., 1999. The strontium isotopic budget of Himalayan Rivers in Nepal and Bangladesh. Geochimica et Cosmochimica Acta 63, 1905-1925.

Galy, A., France-Lanord, C., 2001. Higher erosion rates in the Himalaya: Geochemical constraints on riverine fluxes. Geology 29, 23-26.

Galy, V., France-Lanord, C., Peucker-Ehrenbrink, B., Huyghe, P., 2010. Sr-Nd-Os evidence for a stable erosion regime in the Himalaya during the past 12 Myr. Earth and Planetary Science Letters 290, 474-480.

Gardner, R., Walsh, N., 1996. Chemical weathering of metamorphic rocks from low elevations in the southern Himalaya. Chemical Geology 127, 161-176.

Garzanti, E., Vezzoli, G., Andò, S., France-Lanord, C., Singh, S.K., Foster, G., 2004. Sand petrology and focused erosion in collision orogens: the Brahmaputra case. Earth and Planetary Science Letters 230, 157-174.

Goodbred Jr., S.L., Kuehl, S.A., 1998. Floodplain processes in the Bengal Basin and the storage of Ganges-Brahmaputra river sediment: an accretion study using ^{137}Cs and ^{210}Pb geochronology. Sedimentary Geology 121, 239-258.

Goodbred Jr., S.L., Kuehl, S.A., 1999. Holocene and modern sediment budgets for the Ganges-Brahmaputra river system: Evidence for highstand dispersal to flood-plain, shelf, and deep-sea depocenters. Geology 27, 559-562.

Goodbred Jr., S.L., Kuehl, S.A., 2000a. The significance of large sediment supply, active tectonism, and eustasy on margin sequence development: Late Quaternary stratigraphy and evolution of the Ganges-Brahmaputra delta. Sedimentary Geology 133, 227-248.

Goodbred Jr., S.L., Kuehl, S.A., 2000b. Enormous Ganges-Brahmaputra sediment discharge during strengthened early Holocene monsoon. Geology 28, 1083-1086.

Goodbred, Jr., S.L., Kuehl, S.A., Steckler, M., and Sarker, M.H., 2003. Controls on facies distribution and stratigraphic preservation in the Ganges-Brahmaputra delta sequence. Sedimentary Geology 155, 301-316.

Harris, N., 1995. Significance of weathering Himalayan metasedimentary rocks and leucogranites for the Sr isotope evolution of seawater during the early Miocene. Geology 23, 795-798.

Harris, N., Bickle, M., Chapman, H., Fairchild, I., Bunbury, J., 1998. The significance of Himalayan rivers for silicate weathering rates: evidence from the Bhote Kosi tributary. Chemical Geology 144, 205-220.

Hay, W.W., 1998. Detrital sediment fluxes from continents to oceans. Chemical Geology 145, 287-323.

Heroy, D.C., Kuehl, S.A., Goodbred Jr., S.L., 2003. Mineralogy of the Ganges and Brahmaputra Rivers: implications for river switching and Late Quaternary climate change. Sedimentary Geology 155, 343-359.

Höhndorf, A., Kudrass, H.R., France-Lanord, C., 2003. Transfer of the Sr isotopic signature of the Himalayas to the Bay of Bengal. Deep-Sea research II 50, 951-960.

Huggan, R.D., 2005. Co-evolution of rice and humans. GeoJournal 35, 262-265.

Huizing, H.G.J., 1971. A reconnaissance study of the mineralogy of sand fractions from East Pakistan sediments and soils. Geoderma 6, 109-133.

Jaboyedoff, M., Bussy, F., Kübler, B., Thelen, Ph., 2001. Illite "crystallinity" revisited. Clays and Clay Minerals 49, 156-167.

Jacobson, A.D., Blum, J.D., Walter, L.M., 2002a. Reconciling the elemental and Sr isotope composition of Himalayan weathering: Insights from the carbonate geochemistry of stream waters. Geochimica et Cosmochimica Acta 66, 3417-3429.

Jacobson, A.D., Blum, J.D., Chamberlain, C.P., Poage, M.A., Sloan, V. F., 2002b. Ca/Sr and Sr isotope systematics of a Himalayan glacial chronosequence: Carbonate versus silicate weathering rates as a function of landscape surface age. Geochimica et Cosmochimica Acta 66, 13-27.

Johnson, A.Y., Alam, A.M.N., 1991. Sedimentation and tectonics of the Sylhet trough, Bangladesh. Geological Society of America Bulletin 103, 1513-1527.

Kessarkar, P.M., Rao, V.P., Ahmad, S.M., Patil, S.K., Kumar, A.A., Babu, G.A., Chakraborty, S., Rajan, R.S., 2005. Changing sedimentary environment during the Late Quaternary: Sedimentological and isotopic evidence from the distal Bengal Fan. Deep-Sea Research I 52, 1591-1615.

Krishnaswami, S., Trivedi, J.R., Sarin, M.M., Ramesh, R., Sharma, K.K., 1992. Strontium isotopes and rubidium in the Ganga-Brahmaputra river system: Weathering in the Himalaya, fluxes to the Bay of Bengal and contributions to the evolution of oceanic $^{87}Sr/^{86}Sr$. Earth and Planetary Science Letters 109, 243-253.

Lindsay, J.F., Holiday, D.W., Hulbert, A.G., 1991. Sequence stratigraphy and the evolution of the Ganges-Brahmaputra complex. American Association of Petroleum Geologists Bulletin 75, 1233-1254.

McLennan, S.M., 1993. Weathering and Global Denudation. The Journal of Geology 101, 295-303.

McLennan, S. M., Hemming, S., McDaniel, D. K., Hanson, G. N., 1993. Geochemical approaches to sedimentation, provenance and tectonics. In: M. J. Johnsson and A. Basu (Eds.) Processes controlling the composition of clastic sediments. Geological Society of America Special Paper 284, 21-40.

McLennan, S.M., Bock, B., Hemming, S.R., Hurowitz, J.A., Lev, S.M., McDaniel, D.K., 2003. The roles of provenance and sedimentary processes in the geochemistry of sedimentary rocks. In Lentz, D.R., ed., Geochemistry of Sediments and Sedimentary Rocks: Evolutionary Considerations to Mineral Deposit-Forming Environments: Geological Association of Canada, GeoText 4, 7-38.

Milliman, J.D., Syvitski, J.P.M., 1992. Geomorphic/tectonic control of sediment discharge to the ocean: The importance of small mountainous rivers. Journal of Geology 100, 525-544.

Montgomery, D.R., Hallet, B., Yuping, L., Finnegan, N., Anders, A., Gillespie, A., Greenberg, H., 2004. Evidence for Holocene megafloods down the Tsangpo River gorge, southeastern Tibet. Quaternary Research 62, 201-207.

Morgan, J.P., McIntire, W.G., 1959. Quaternary geology of the Bengal basin, East Pakistan and India. Geological Society of America Bulletin 70, 319-342.

Najman, Y., Bickle, M.J., Chapman, H.J., 2000. Early Himalayan exhumation: Isotopic constraints from the Indian foredeep basin. Terra Nova 12, 28-34.

Najman, Y., 2006. The detrital record of orogenesis: A review of approaches and techniques used in the Himalayan sedimentary basin. Earth-Science Reviews 74, 1-72.

Nesbitt, H.W., Young, G.M., 1984. Prediction of some weathering trends of plutonic and volcanic rocks based on thermodynamic and kinetic considerations. Geochimica et Cosmochimica Acta 48, 1523-1534.

Nesbitt, H.W., Markovics, G., 1997. Weathering of granodioritic crust, long-term storage of elements in weathering profiles, and petrogenesis of siliciclastic sediments. Geochimica et Cosmochimica Acta 61, 1653-1670.

Ohta, T., Arai, H., 2007. Statistical empirical index of chemical weathering in igneous rocks: A new tool for evaluating the degree of weathering. Chemical Geology 240, 280-297.

Palmer, M.R., Edmond, J.M., 1992. Controls over the strontium isotope composition of river water. Geochimica et Cosmochimica Acta 56, 2099-2111.

Pate, R.D., 2008. Multiple-proxy records of delta evolution and dispersal system behavior: Fluvial and coastal borehole evidence from the Bengal Basin, Bangladesh. Masters Thesis, Vanderbilt University, Nashville, TN, 112pp.

Peng, Z.X., Mahoney, J.J., Hooper, P.R., MacDougal, J.D., Krishnamurthy, P., 1998. Basalts of the northeaster Deccan traps, India: Isotopic and elemental geochemistry and relation to southwestern Deccan stratigraphy. Journal of Geophysical Research 103, 29843-29865.

Pereira, W.E., Rostad, C.E., Leiker, T.J., 1992. Synthetic organic agrochemicals in the lower Mississippi River and its major tributaries: Distribution, transport and fate. Journal of Contaminant Hydrology 9, 175-188.

Price, J.R., Velbel, M.A., 2003. Chemical weathering indices applied to weathering profiles developed on heterogeneous felsic metamorphic parent rocks. Chemical Geology 202, 397-416.

Rahaman, W., Singh, S.K., Sinha, R., Tandon, S.K., 2009. Climate control on erosion distribution over the Himalaya during the past ~100 ka. Geology 37, 559-562.

Raymo, M.E., Ruddiman, W.F., 1992. Tectonic forcing of late Cenozoic climate. Nature 359, 117-122.

Saha, A., Basu, A.R., Garzione, C.N., Bandyopadhyay, P.K., Chakrabarti, A., 2004. Geochemical and petrological evidence for subduction-accretion processes in the Archaen Eastern Indian Craton. Earth and Planetary Science Letters 220, 91-106.

Sarin, M.M., Krishnaswami, S., Dilli, K., Somayajulu, B.L.K., Moore, W.S., 1989. Major ion chemistry of the Ganges-Brahmaputra river system: Weathering processes and fluxes to the Bay of Bengal. Geochimica et Cosmochimica Acta 53, 997-109.

Schärer, U., Hamet, J., Allègre, C.J., 1984. The Transhimalaya (Gangdese) plutonism in the Ladakh region: a U-Pb and Rb-Sr study. Earth and Planetary Science Letters 67, 327-339.

Segall, M.P., Kuehl, S.A., 1992. Sedimentary processes on the Bengal shelf as revealed by clay-size mineralogy. Continental Shelf Research 12, 517-541.

Singer, A., 1984. The paleoclimatic Interpretation of Clay Minerals in Sediments – A Review. Earth Science Reviews 21, 251-293.

Singh, M., Sharma, M., Tobschall, H.J., 2005. Weathering of the Ganga alluvial plain, northern India: Implications from fluvial geochemistry of the Gomati River. Applied Geochemistry 20, 1-21.

Singh, M., Singh, I.R., Müller, G., 2007. Sediment characteristics and transportation dynamics of the Ganga River. Geomorphology 86, 144-175.

Singh, P., 2009. Major, trace and REE geochemistry of the Ganga River sediments: Influence of provenance and sedimentary processes. Chemical Geology 266, 251-264.

Singh, P., 2010. Geochemistry and provenance of stream sediments of the Ganga River and its major tributaries in the Himalayan region, India. Chemical Geology 269, 220-236.

Singh, S.K., France-Lanord, C., 2002. Tracing the distribution of erosion in the Brahmaputra watershed from isotopic compositions of stream sediments. Earth and Planetary Science Letters 6341, 1-18.

Singh, S.K., Sarin, M.M., France-Lanord, C., 2005. Chemical erosion in the eastern Himalaya: Major ion composition of the Brahmaputra and $\delta^{13}C$ of dissolved inorganic carbon. Geochimica et Cosmochimica Acta 69, 3573-3588.

Singh, S.K., Kumar, A., France-Lanord, C., 2006. Sr and $^{87}Sr/^{86}Sr$ in waters and sediments of the Brahmaputra river system: Silicate weathering, CO_2 consumption and Sr flux. Chemical Geology 234, 308-320.

Singh, S.K., 2006. Spatial variability in erosion in the Brahmaputra basin: causes and impacts. Current Science 90, 1272-1276.

Singh, S.K., Santosh, K.R., Krishnaswami, S., 2008. Sr and Nd isotopes in river sediments from the Ganga Basin: Sediment provenance and spatial variability in physical erosion. Journal of Geophysical Research 113, F03006, 18pp.

Sinha, R., Tandon, S.K., Gibling, M.R., Bhattacharjee, P.S., Dasgupta, A.S., 2005. Late Quaternary geology and alluvial stratigraphy of the Ganga basin. Himalayan Geology 26, 223-240.

Srivastava, R.K., Heaman, L.M., Sinha, A.K., Shihua, S., 2005. Emplacement age and isotope geochemistry of Sung Valley alkaline-carbonatite complex, Shillong Plateau, northeastern India: Implications for primary carbonate melt and genesis of the associated silicate rocks. Lithos 81, 33-54.

Stewart, R.J., Hallet, B., Zeitler, P.K., Malloy, M.A., Allen, C.M., Trippett, D., 2008. Brahmaputra sediment flux dominated by highly localized rapid erosion from the easternmost Himalaya. Geology 36, 711-714.

Tennant, E., 2005. Late Quaternary climate and provenance signals of the Ganges-Brahmaputra Delta Plain, Bangladesh. Honors Thesis, William and Mary, Williamsburg, VA.

Ullah, M., 2010. Provenance analysis of Late Quaternary sediments from the Ganges-Brahmaputra delta, Bangladesh. Masters Thesis, Vanderbilt University, Nashville, TN, 95pp.

vanGeen, A., Zheng, Y., Goodbred Jr., S., Horneman, A., Aziz, Z., Cheng, Z., Stute, M., Mailloux, B., Weinman, B., Hoque, M.A., Seddique, A.A., Hossain, M.S., Chowdhury, S.H., Ahmed, K.M., 2008. Flushing history as a hydrogeological control on the regional distribution of arsenic in shallow groundwater of the Bengal Basin. Environmental Science and Technology 42, 2283-2288.

Wasson, R.J., 2003. A sediment budget for the Ganga-Brahmaputra catchment. Current Science 84, 1041-1047.

Weinman, B., Goodbred, S.L., Zheng, Y., van Geen, A., Aziz, Z., Singhvi, A., Steckler, M., 2008. Controls of Floodplain evolution on shallow aquifer development and the resulting distribution of groundwater arsenic: Araihazar, Bangladesh. GSA Bulletin 120, 1567-1580.

Weinman, B., 2010. The evolution of aquifers and arsenic in Asia: A study of the fluvio-deltaic processes leading to aquifer formation and arsenic cycling and heterogeneity in Bangladesh, Vietnam, and Nepal. Ph.D. Dissertation, Vanderbilt University, Nashville, TN, 220pp.

White, N.M., Parrish, R.R., Bickle, M.J., Najman, Y.M.R., Burbank, D., Maithani, A., 2001. Metamorphism and exhumation of the NW Himalaya constrained by U-Th-Pb analyses of detrital monazite grains from early foreland basin sediments. Journal of the Geological Society (London) 158, 625-635.

Yokoyama, K., Amano, K., Taira, A., Saito, Y., 1990. Mineralogy of silts from the Bengal Fan. In: Cochran, J.R., Stow, D.A.V., et al., *Proc. ODP, Sci. Results,* 116: College Station, TX (Ocean Drilling Program), 59–73.